Doctoral theses at NTNU, 2017:179

Mladen Veletic

On the Neural Communication for Data Transmission in Nano-Networks

Doctoral thesis

ISBN 978-82-326-2430-0 (printed ver.)
ISBN 978-82-326-2431-7 (electronic ver.)
ISSN 1503-8181

NTNU
Norwegian University of
Science and Technology

NTNU

Norwegian University of Science and Technology
Thesis for the Degree of
Philosophiae Doctor
Faculty of Information Technology and Electrical
Engineering
Department of Electronic Systems

Doctoral theses at NTNU, 2017:179

NTNU

NTNU
Norwegian University of
Science and Technology

Mladen Veletic

On the Neural Communication for Data Transmission in Nano-Networks

Thesis for the Degree of Philosophiae Doctor

Trondheim, June 2017

Norwegian University of Science and Technology
Faculty of Information Technology and Electrical Engineering
Department of Electronic Systems

NTNU
Norwegian University of
Science and Technology

NTNU
Norwegian University of Science and Technology

Thesis for the Degree of Philosophiae Doctor

Faculty of Information Technology and Electrical Engineering
Department of Electronic Systems

ISBN 978-82-326-2430-0 (printed ver.)
ISBN 978-82-326-2431-7 (electronic ver.)
ISSN 1503-8181

Doctoral theses at NTNU, 2017:179

Printed by NTNU Grafisk senter

On the Neural Communication for Data Transmission in Nano-Networks

Mladen Veletić

Doctoral Thesis

Submitted for the Partial Fulfilment of the Requirements for the Degree of

philosophiae doctor

Department of Electronic Systems
Faculty of Information Technology and Electrical Engineering
Norwegian University of Science and Technology

Faculty of Electrical Engineering
University of Banja Luka

and in collaboration with Intervention Center, Oslo University Hospital

This thesis stems from the project “Norwegian, Bosnian, and Serbian cooperation platform for university and industry ICT R&D – NORBAS”

June 13, 2017

To Jelena, Nada and Branko
for their love and support

Abstract

Nano-networks are engineered systems for performing communication at the nano-scale. They are achieved through physical mechanisms suitable at this scale, including electromagnetism and electrochemical transport. From the communication and information engineering perspective, a challenging issue in nanotechnology involves interfacing between nano-scale components, and between nano-scale and macro-scale networks. A potential cutting-edge strategy is to use molecular communication and fine-tune the natural systems like muscular, cardiovascular, endocrine and nervous systems that have been engineered by evolution to transmit information. For intra-body communication, molecular communication has advantages over alternative electromagnetic nano communications in propagation gain and energy consumption, which motivates understanding and engineering intra-body molecular communication systems to send, transport, and receive artificial information. Among others, the neural nano-network which effectively communicates and rules other intra-body nano-networks is aimed to be understood to engineer solutions for useful problems in communications technology and medicine.

The focus of the thesis is to develop and analyze a theoretical framework for the neural communication in engineered neural-like nano-networks. First, a solid mathematical framework linked with relevant molecular segments in the electrochemical and molecular communication pathways including propagation modeling is developed. The neural communication is inspected through the concepts of electrochemical- and molecular communication, which are referred to as the intra- and inter-neuronal communication, respectively. In the analysis, the chemical and ionic processes are represented with signals, whereas the biological mechanisms are modeled as input-output systems. Second, the information transfer in neural communication is inspected by introducing analogies between the neural communication system and the optical communications system to apply results from optical Poisson channels in deriving theoretical upper bounds on the information capacity of neural synapses. The efficacy of information transfer is analyzed under different synaptic set-ups with progressive complexity, and is shown to depend on the peak rate of the communicated spiking sequence and neurotransmitter (spontaneous) release, neurotransmitter propagation, and neurotransmitter binding.

The presented research contribution promises in understanding the performance of the neural communication paradigm as a candidate for future nano-networks, and having an impact to the emerging area of molecular communication, as well as the fields of biotechnology and nanotechnology. Creating man-made neural-like communications systems can indubitably lead to new solutions in information and data transfer in nano-networks or, alternatively, to novel therapeutic methods for the neurodegenerative diseases.

Preface

This thesis is submitted to the Norwegian University of Science and Technology (NTNU) for partial fulfilment of the requirements for the degree of *Philosophiae Doctor* (Ph.D.), and to the University of Banja Luka (UNIBL) for partial fulfilment of the requirements for the degree of *Doktor nauka* (dr), under supervision of Professor Ilangko Balasingham from the Department of Electronic Systems, NTNU, and co-supervision of Professor Zdenka Babić from the Faculty of Electrical Engineering, UNIBL.

Besides the research activities, the Ph.D. work also included compulsory course studies at the NTNU and UNIBL, and teaching assistantship duties. This work was conducted in the period of Jan. 2013 – Dec. 2016.

The Ph.D. research was funded by the HERD/ICT NORBAS Project under reference 2011/1383 supported by the Norwegian Ministry of Foreign Affairs. The teaching assistantship was funded by the UNIBL.

Acknowledgements

I would like to express my sincere gratitude to my main advisor Prof. Ilangko Balasingham. He has been an exceptional advisor. Having innumerable Skype calls and discussions during my stay in Norway, he has taught me better ways of doing research and shaping my work and life. I appreciate all his contributions of willingness, time and travel. The energy and enthusiasm he has for work and research was contagious and motivational for me. It has been an honor and pleasure to have worked with him.

Many thanks go to my co-advisor Prof. Zdenka Babić for all the support and help during these years, including the proofreading of this thesis. Her determination and commitment to work have enabled the realization of my research.

My thanks also go to Dr. Pål Anders Floor for all the discussions and consultations during these years. His knowledge in the field of communication and information theory is exemplary. I also want to thank to Dr. Fabio Mesiti and Dr. Youssef Chahibi for being great colleagues. I have enjoyed working with all of them. Special thanks go the respected committee members, Prof. Özgür B. Akan, Dr. Sasitharan Balasubramaniam, Prof. Angela Sara Cacciapuoti, Prof. Lars Magne Lundheim, and Prof. Tatjana Pešić-Brđanin, for their time and review of this work.

Last, but not least, I want to thank colleagues at the Department of Electronic Systems, NTNU for the nice and friendly working environment I have enjoyed during my stays in Norway, and friends and colleagues from the Faculty of Electrical Engineering, UNIBL for their support. Special thanks go to NORBAS team members and administrative officers from NTNU and UNIBL for practical arrangements of my work.

Mladen Veletić
June 2017

Contents

List of Tables

List of Figures

Abbreviations

IP_3 Inositol 1,4,5-Triphosphate.

AM Adjacency Matrix.

AMPA α-Amino-3-Hydroxy-5-Methyl-4-Isoxazole Propionic Acid.

ANN Artificial Neural Network.

AP Action Potential.

ARP Absolute Refractory Period.

ATP Adenosine Triphosphate.

BANN Body Area Nano-Network.

BIS Biological Integrated System.

CA *Cornu Ammonis*.

CaG Calcium Gateway.

CICR Calcium-Induced Calcium-Release.

CNS Central Nervous System.

CSI Channel State Information.

EEG Electroencephalography.

EPSC Excitatory Post-Synaptic Current.

EPSP Excitatory Post-Synaptic Potential.

ER Endoplasmic Reticula.

fMRI Functional Magnetic Resonance Imaging.

GABA γ-Aminobutyric Acid.

IBC Intra-Body Communications.

IBSAN In-Body Sensor Actuator Network.

ICT Information and Communication Technology.

IPSC Inhibitory Post-Synaptic Current.

IPSP Inhibitory Post-Synaptic Potential.

LTD Long Term Depression.

LTI Linear Time-Invariant.

LTP Long Term Potentiation.

MEG Magnetoencephalography.

mGluR Metabotropic Glutamate Receptor.

MTx Molecular Transmitter.

NMDA N-Methyl-D-Aspartate.

PNS Peripheral Nervous System.

PSTH Peri-Stimulus Time Histogram.

RP Refractory Period.

RQ Research Question.

RRP Relative Refractory Period.

SERCA Sarco/Endoplasmic Reticulum Ca^{2+}-ATPase.

SnM Synaptic Nano-Machine.

SR Sarcoplasmic Reticula.

TDMA Time Division Multiple Access.

VGCC Voltage-Gated Calcium Channel.

ZAP Impedance Amplitude Profile.

Chapter 1

Introduction

1.1 Nano Communication Networks: What? How? Why?

The concept of nanotechnology was indicated in December 29, 1959 at California Institute of Technology by American theoretical physicist Richard Phillips Feynman. In the unnoticed talk, Feynman considered the possibility of atomic manipulation to create powerful synthetic devices. The term "nanotechnology", however, was explicitly defined later in 1974 by Tokyo Science University Professor Norio Taniguchi as "consisting of processing, separation, consolidation, and deformation of materials by one atom or by one molecule" [122]. These pioneering concepts were further expanded in 1986 by Eric Drexler who proposed the idea of a nano-scale[1] "assembler" which would be able to build a copy of itself and of other items of arbitrary complexity with atomic control [39]. Drexler's idea led to the modern nanotechnology which implies the miniaturization and fabrication of electronic devices. Such devices should be arranged as a set of molecules which are able to perform very simple computation, sensing and actuation tasks at nano-scale. When inter-connected, nano-scale devices should be able to collaboratively execute complex tasks in a distributed manner leading to the concept of **nano-networks** [8].

A nano communication network, hereinafter referred to as a nano-network, is a human-designed system for communicating at the nano-scale, using physical principles that are suited to nano-scale systems [4]. Nano-networks are envisioned to have all features analogous to wired and wireless communication networks. They must be able to collect, encode, transport, receive, decode, and deliver information to the appropriate application, which entails the traditional concepts of communication and information theory. From the communication and information engineering perspec-

[1] Nano-scale refers to dimensions of 1 nm to 100 nm as defined in ISO/TS 27687:2008 definition 2.1 [4].

tive, a challenging issue in nanotechnology involves interfacing between nano-scale components, and between nano-scale and macro-scale networks. To resolve this issue, humans presumably would not need to "create" anything new, but rather to leverage and fine-tune what nature provides [24]. This strategy has been successfully applied to wireless communication systems by fine-tuning the natural wireless transmission which have existed before humans in a form of magnetic storms and lighting. The philosophical question is whether these phenomena transport "information" and from whose perspective information is defined. The fact is, however, that humans have understood these phenomena well enough without changing the laws of nature, and transformed them to what is known today as digital wireless systems used for information transmission from a human perspective.

The analogous strategy can be framed for communications in nano-networks, i.e., nano communications, by fine-tuning the natural nano-scale transmission systems. Natural systems like muscular, cardiovascular, endocrine and nervous systems have been engineered by evolution to transform information from a cellular perspective and keep humans alive. If humans, however, begin to understand these intra-body systems well enough and engineer information to be sent, transported, and received at the cellular level with full control at the human level, the existing natural phenomena will be harnessed again and transformed to what is defined as nano communication systems. Understanding a very specific, powerful, effective, and promising natural paradigm of nano-scale intra-body communications and networking to engineer solutions for useful problems at the human scale is what this thesis is primarily about.

1.2 Nano Communication Paradigms

Albeit favourable in the thesis (see Section 1.3), biological transmission systems are not the only ones to inspire man-made nano-networks; alternatively, nano-networks can be realized by down-sizing conventional communication networks. Hence, interfacing between nano-scale components can be categorized into two main paradigms: **molecular communication**, and **electromagnetic nano communications**. The IEEE 1906.1-2015 [4] has recently become a recommended practice for the electromagnetic nano communications and molecular communication framework standard. This recommended practice contains a conceptual model and a standard terminology for *ad hoc* network communications at the nano-scale aiming to enable researchers from diverse fields to reach a common understanding of the topic.

1.2.1 Molecular Communication

In the simplest general form of communication, the transmitter makes a physical change to an environment, whereas the receiver detects that change. In molecular

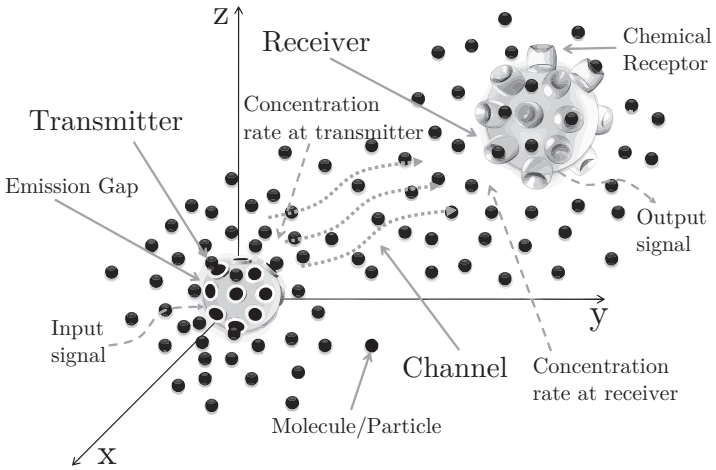

Figure 1.1: Schematic diagram of a molecular communication with two nodes. The figure is adopted from [70] by the author.

communication, the physical change is molecular (or, more precisely, in molecular concentration) as the transmitter emits molecules which should be detected by the receiver, as shown in Fig. 1.1. In communications engineering, molecular communication is a new area of research and basically a cutting edge research field [11,90,105] that is emerging to be very promising networking paradigm in nano-networks due to the dimensional similarities of miniature human-designed entities with biological structures. Molecular communication can be engineered in two ways [90]: first, an entirely artificial device could be designed to communicate using signaling molecules, and second, the molecular communication capabilities which occur ubiquitously at all levels of biological systems including molecule, cell, tissue, and organ levels could be engineered to transport artificial information.

Molecular communication comes in various biological forms ranging from macro- (e.g., pheromonal communication[2] [9]) to nano-scale (e.g., intra-body communications). Specific nano-scale examples of molecular communication are listed:

- **Calcium signaling.** Calcium ions[3] (Ca^{2+}) are second messengers (intracellular signaling molecules) released by cells to regulate physiological changes. Ca^{2+} are stored in endoplasmic reticula (ER) and are released upon stimulation through calcium-release channels which act as *transmitters*. An increase in cytosolic calcium concentration, $[Ca^{2+}]$, encodes a chemical information and propagates as a reaction-diffusion wave. Calcium sensitive proteins act as *receivers* to decode the temporal and spatial nature of $[Ca^{2+}]$ [31].

[2]Pheromones are a type of molecules released by plants, insects, and other animals that trigger specific behaviors among the receptors of the same species.

[3]Ions are electrically charged particles.

- **Quorum sensing.** This is a system of stimuli and response which allows bacteria to monitor the cell population density and coordinate their behavior and gene expression based on the cellular density. Each bacterium synthesizes and propagates molecules called auto-inducers and acts both as a *transmitter* and a *receiver* of molecular communication. The concentration of auto-inducers in the environment encodes the population density of bacteria.
- **Morphogen signaling.** A morphogen is a molecule governing the pattern of tissue development in the process of morphogenesis. In developing a tissue structure, *transmitting cells* produce morphogens and encapsulate them in vesicles that are sent in the environment to propagate toward *receiving cells*. The morphogen can also propagate cell-to-cell through internal pathways, or in a reaction-diffusion manner.
- **Vesicular trafficking.** This is a form of communication where a *transmitting organelle*[4] encodes the information onto the proteins which are encapsulated into vesicles. Vesicles are transported by motor proteins that move along micro-tubules to the *receiving organelle*.
- **Hormonal signaling.** A hormone is a regulatory molecule produced in an organism by *transmitting cells* and transported in tissue fluids to stimulate specific *receiving cells* or tissues into action. Hormonal signaling covers a relatively longer distance. Upon reception of hormones, receiving cells release another type of hormone that acts as a feedback to the transmitting cells. The feedback-based control is essential to control various bodily functions [90].
- **Neuronal signaling.** Separate organs in a body use neuronal signaling to communicate. For example, the brain and the heart signal each other through nerve cells. Moreover, all voluntary and involuntary actions in a body are coordinated by neuronal signaling. In neuronal signaling, or neuronal communication, a *transmitting neuron* sends a message to propagate as reaction-diffusion waves up to distances of over a few meters. The emitted message propagates through the neural[5] "infrastructure" and is ultimately received by *receiving neurons*.

1.2.2 Electromagnetic Nano Communications

Electromagnetic nano communications is an alternative to molecular communication at the nano-scale and also a new area of research which utilizes electromagnetic waves to carry messages following the similar philosophy as in current wireless communication systems. Nonetheless, electromagnetic nano communications requires

[4] An organelle is a small, specialized subunit within a cell which operates like organ by carrying out specific tasks.

[5] Neural means dealing either with neurons or glial cells (see Section 2.2). Neuronal means dealing specifically with neurons.

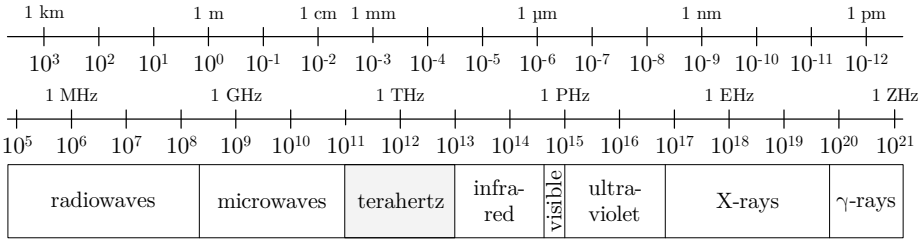

Figure 1.2: Relationship between electromagnetic wavelengths and frequencies of the terahertz band in the electromagnetic spectrum.

addressing a number of new challenges not covered by current wireless communication paradigms [48]. This primarily suggests unexplored frequency bands to be used due to the size of nano-components and their antennas[6]. Moreover, nano-networking requires a large set of functions to be performed including propagation modeling, capacity analysis, modulation schemes, access control, and addressing, where traditional solutions may not be applicable due to the limitations in terms of communication capabilities assigned to nano-components.

In the context of communications at the nano-scale, the terahertz band is envisioned as a wireless technology to satisfy this demand [10]. The terahertz band spans the frequencies between 0.1 THz and 10 THz, and additionally addresses an increasing demands in classical networking domains by alleviating the spectrum scarcity and capacity limitations of current wireless systems. This region is one of the least explored frequency bands for communications, unlike the frequency regions immediately below and above this band, i.e., the microwaves and the far infra-red, respectively, as shown in Fig. 1.2.

The very small size and unique properties of nano-antennas and nano-transceivers, however, are not purposely aimed to be developed to communicate in the terahertz band; instead, the size and properties of nano-antennas and nano-transceivers rather enable nano-scale devices to communicate in the terahertz band. A promising strategy to develop terahertz band compact antennas and transceivers is based on the utilization of graphene.

Graphene is a form of carbon consisting of one-atom thick planar sheets with the atoms arranged in a honeycomb-shaped lattice [94]. The unique properties observed in graphene and its derivatives (graphene nano-ribbons and carbon nano-tubes) have enabled the development of nano-batteries, nano-processors, nano-memories and

[6]Note that the increase in frequency causes size of antenna to decrease; this stems from the relation $c = \lambda \times f$, where c is the speed of light, λ is the wavelength, and f is the frequency, and the fact that efficient radiation of electromagnetic energy requires the radiating antenna to be of the order of one-tenth or more the wavelength of signal radiated.

nano-sensors. Graphene-based communications is an emerging research topic [60, 62, 63, 74, 99] which enables high channel capacity, new information encoding and modulation techniques, and novel networking protocols more suited for resource-limited nano-devices [61].

1.3 Molecular Communication vs. Electromagnetic Nano Communications

Albeit molecular communication has many fundamental issues that are unresolved or at least not agreed upon in the research community, it has the following obvious distinctions with electromagnetic nano communications (THz communications):

- In molecular communication, communication processes use molecules and different coding techniques to encode the message, e.g., temporal sequences, such as the temporal concentration of specific molecules in the medium, or alternatively internal parameters of the molecules, such as the chemical structure [8]. In THz communications, communication processes use electromagnetic waves and temporal sequences to transport and encode the information, respectively.
- In molecular communication, the random walk propagation speed of molecules is much lower relative to the wave propagation speed in communications at THz frequencies (the speed of light) as molecules have to be physically transported from the transmitter to the receiver. More specifically, the time of arrival of molecules is dependent on the diffusivity and increases quadratically with distance; the time of arrival of electromagnetic waves is not dependent on the carrier frequency, and increases linearly with distance [51].
- For free-space propagation, the gain of the molecular energy is inversely proportional to the diffusivity and distance; the gain of THz wave power is inverse-square proportional to the frequency and distance [51]. This result has shown that in free-space, molecular communication energy attenuates at a lower rate than electromagnetic wave signals. For lossy propagation, e.g., intra-body propagation, the explicit boundaries that divide molecular communication from THz communications remain unclear, although the obvious disadvantage of communications at THz frequencies arises from the strong absorption through the medium caused by water molecules.
- In molecular communication, two different types of noise can affect the molecular signal depending on the coding techniques [8]: i) noise can be understood either as an undesired concentration level of molecules that overlaps with information molecules that are transmitted, or ii) noise can be understood as an undesired reaction occurring between information molecules and other molecules present in the communication channel. In THz communications, noise is understood as an undesired electromagnetic signal overlapped

Communication	Molecular	THz
Signal type	Chemical	Electromagnetic
Information carrier	Molecules	Electromagnetic waves
Propagation speed	Extremely low	Extremely high (3×10^8 m/s)
Medium conditions	Affect communication	Greatly affect communication
Noise	Molecules in medium or molecular reactions	Electromagnetic signals
Power consumption	Ultra-low	High

Table 1.1: Main features and differences between molecular communication and THz communications.

with the information signal.

- In molecular communication, processes are chemically driven resulting in ultra-low power consumption; conversely, in THz communications, power consumption is a severe issue which limits the practical duration of an operation.

Main features of molecular communication and THz communications are summarized in Table 1.1. The major advantage that molecular communication has over THz communications is that i) molecular energy attenuates at a lower rate than THz wave signals, and ii) molecular processes consumes significantly less energy than THz waves. The former feature is especially evident in lossy medium and indicates molecular communication for Intra-Body Communications (IBC) which uses the human body as the signal propagation medium. The latter feature is peculiarly welcome in nano-networks as the size and current complexity of the transceivers cannot be easily integrated into nano-scale devices. Even if the integration were possible, the output power of the nano-transceiver would not be enough to establish a bidirectional communication channel [8].

The major drawbacks of molecular communication are the propagation speed and delay of molecules. These features prevent molecular communication in nano-networks used for delay-sensitive applications, which require effective signal propagation and negligible delays. But, is there a specific type of biological molecular communication that keeps the features of typical molecular communication where the particle propagation speed and delay are not demeritorious? Fortunately, there is.

1.4 Neuron-Based Molecular Communication

As implied in Section 1.2.1, neurons are communication entities within the neuronal network and special among the cells of the body in their abundance and ability

to propagate information **rapidly** within the network, which is found as the most fascinating, complex, and advanced biological nano-network. The neuronal nano-network uses neuronal signaling to communicate and rule all other nano-networks within the body, gather information about the internal state of the organism and its external environment, process and evaluate this information to eventually coordinate activities of "end devices", e.g., muscle cells. In neural communication[7], neurons communicate messages using:

1. the *electrochemical transmission* of temporal sequences of electrical pulses called Action Potentials (APs) or spikes from the neuronal body along the axon to the pre-synaptic terminal, i.e., the axonal terminal of the pre-synaptic transmitting neuron (see Section 2.2.1), and
2. *molecular transmission* of particles (neurotransmitters) from the pre-synaptic terminal over the synaptic cleft to the post-synaptic terminal, i.e., the receiving neuron.

The neural communication has the following distinctions with typical molecular communication:

- In the neural communication, communication processes use both APs, which are "constructed" from positively and negatively charged ions, and molecules to encode the message (see Section 2.2.2 for details). In typical molecular communication, communication processes use only molecules to encode the message, as indicated in the previous subsection.
- In the neural communication, APs travel (see Section 2.2.2) through neuronal fibers and reach a synapse. The synapse is the site of functional apposition between two cells, where a transmitting neuron converts the electrical signal into chemical/molecular signal that is released into the synaptic cleft to propagate and eventually bind to the receptors located on the membrane of the receiving neuron (see Section 2.2.3 and Section 2.2.4). In principle, the synaptic transmission is molecular transmission where molecules diffuse slowly. Nonetheless, the synaptic width is approximately 20 nm [111] which is notably less relative to widths of channels in other types of molecular communication. Hence, the propagation speed and delay are rather tolerable than demeritorious in synaptic channel within the neural communication.
- In the neural communication, different types of noise can affect the signaling: i) noise can be understood either as an undesired induced current from the electromagnetic fields that affects the neural firing; ii) noise can be understood as an undesired concentration level of molecules that overlaps with information molecules that are transmitted within a synapse; iii) noise can be understood

[7]Neural network or neural communication means dealing with networks composed of neurons and glial cells, or signaling affected by neurons and/or glial cells, respectively. Neuronal network or neuronal communication means dealing with networks composed only of neurons, or signaling affected only by neurons, respectively.

Communication	Neural	Molecular
Signal type	Ionic and chemical	Chemical
Information carrier	Ions and molecules	Molecules
Propagation speed	High	Extremely low
Noise	Molecules in the synaptic cleft and/or induced electromagnetic fields and/or APs shape deviation	Molecules in medium

Table 1.2: Main features and differences between neural communication and typical molecular communication.

as an undesired reaction occurring between information molecules and other molecules present in the synaptic channel; iv) noise can be understood as changes in axonal functionality reflected through increased delay and duration of evoked APs and decreased amplitude. In molecular communication, two different types of noise can affect the molecular signal, as indicated in the previous subsection.

Main features of neural communication and typical molecular communication are summarized in Table 1.2. The major advantage that neural communication has over molecular communication is the high propagation speed and negligible delays. In addition, in terms of reliability, capacity, data storage, and energy consumption, the neuronal network seems superior over other intra-body networks. Owing to these promoting and promising features, neurons and neural communication are put in the focus of emerging novel studies including this thesis.

1.5 Hypothesis and Research Questions of the Thesis

The focus of the thesis is in developing and analysing a theoretical framework for the neural communication in man-made nano-networks, and is formalized through the following hypothesis:

"The neural information transfer network can be harnessed by understanding the neural communication well enough to transmit data and/or artificial information in neural-like networks; in addition, neural compartments can be interfaced with subjects that affect the neural communication to propose novel treatment strategies for neurodegenerative disorders[8]."

[8]Brain disorders usually remove neurons and synapses from the neural network and lead to anatomically and functionally disconnected clusters which affect the communication performance.

Based on the previous analysis and the state-of-the-art (see Chapter 2 for details), five Research Questions (RQs) are defined for the development and analysis of a theoretical framework for the neural communication, and are listed as follows:

1. **RQ1** – *What are the neural compartments relevant to the signaling aspects of neurons?*
2. **RQ2** –*What types of communication system models can be developed for neural communication?*
3. **RQ3** –*Can neural communication be controlled? If so, how?*
4. **RQ4** –*How the adjacent glial cells, e.g., astrocytes, affect the neural communication? Can the astrocytes be used to control the neural communication? If so, how?*
5. **RQ5** –*What is the information capacity of neurons?*

1.6 Structure and Contributions of the Thesis

Chapter 2 provides necessary neuroscientific background on the neural network, and overview the available work from computational neuroscience and engineering. From the review, deficiencies and shortcomings of the existing works are identified to motivate and justify novel research efforts in the field. This chapter also brings differences of the thesis relative to other works. The major contributions of this chapter address research question RQ1, and are listed as follows.

- The chapter identifies crucial processes and neural compartments from the neural communication perspective; the identified subjects are placed in the focus of research reported in the thesis.
- The chapter identifies, classifies and overviews the available interdisciplinary work related to the biological neural network and potential applications that rely on the neural communication paradigm.

The material in Chapter 2 is based on the following publication ([[124]]):

(I) Mladen Veletić and Ilangko Balasingham. **The neural communication network: A brief review on neuromodeling and neuroengineering**. In *Proceedings of the 24th IEEE Telecommunications Forum (TELFOR 2016)*, pages 1-4, November 2016.

The following chapters present novel scientific results in the field; Chapters 3–5 and Chapter 6 are on *communication* and *information theory* of neurons, respectively.

Chapter 3 investigates the electrochemical neuronal communication related to the intra-cellular pathway within the overall neural communication channel. In this

chapter, the electrochemical neuronal communication is referred to as the intra-neuronal communication. The major contributions of this chapter address research questions RQ2 and RQ3, and are listed as follows.

- The chapter offers an alternative engineering description of the intra-neuronal communication aiming to facilitate its understanding for communications engineers.
- The chapter offers a stochastic description of the intra-neuronal communication owing to randomness due to the intrinsic neuronal dynamics.
- The chapter provides the guidelines for processing design and implementation of bio-mimetic devices[9].
- The chapter alternatively provides the strategy on neuronal stimulation aiming to drive neuronal responses.

The material in Chapter 3 is based on the following publications ([125–127]):

(II) Mladen Veletić, Ilangko Balasingham, and Zdenka Babić. **On spectrum analysis for nanomachine-to-neuron communications**. In *Proceedings of the IEEE International Black Sea Conference on Communications and Networking (BlackSeaCom)*, pages 64-68, July 2013.

(III) Mladen Veletić, Pål Anders Floor, and Ilangko Balasingham. **From nanoscale neural excitability to long term synaptic modification**. In *Proceedings of ACM The First Annual International Conference on Nanoscale Computing and Communication*, NANOCOM' 14, pages 22:1-22:9. ACM, 2014.

(IV) Mladen Veletić, Pål Anders Floor, Zdenka Babić, and Ilangko Balasingham. **Peer-to-peer communication in neuronal nano-network**. *IEEE Transactions on Communications*, 64(3): pages 1153-1166, March 2016.

Chapter 4 investigates propagation modeling in the molecular neuronal communication related to the intra- and extra-cellular pathways within the overall neural communication channel. In this chapter, the molecular neuronal communication is referred to as the inter-neuronal communication. The major contributions of this chapter also address research questions RQ2 and RQ3, and are listed as follows.

- The chapter offers an engineering description of the inter-neuronal communication within bipartite synapses aiming to facilitate its understanding for communications engineers.
- The chapter offers a deterministic description of the inter-neuronal communication; an analytical framework is developed where the chemical and ionic

[9]Bio-mimetics refers to the imitation of the elements of nature for the purpose of solving human problems.

processes in neurons are observed as signals to model biological mechanisms as input-output systems characterized by a frequency response.

- Following the previous chapter, this chapter provides the guidelines for interface design and implementation of bio-mimetic devices.
- The chapter alternatively provides the strategy on synaptic stimulation aiming to initiate synaptic responses.

The material in Chapter 4 is based on the following publications ([126, 129]):

(V) Mladen Veletić, Fabio Mesiti, Pål Anders Floor, and Ilangko Balasingham. **Communication theory aspects of synaptic transmission**. In *Proceedings of the IEEE International Conference on Communications (IEEE ICC 2015)*, pages 2719-2724, June 2015.

(IV) Mladen Veletić, Pål Anders Floor, Zdenka Babić, and Ilangko Balasingham. **Peer-to-peer communication in neuronal nano-network**. *IEEE Transactions on Communications*, 64(3): pages 1153-1166, March 2016.

Chapter 5 extends the analysis from Chapter 4 to the tripartite synapse. Following Chapter 4, the major contribution of this chapter addresses research questions RQ2 and RQ4, and explicitly follows.

- The chapter extends a deterministic description of the inter-neuronal communication to the tripartite synapse; an analytical framework is developed where the chemical and ionic processes in neurons and glial cells (astrocytes) are observed as signals to model biological mechanisms as input-output systems characterized by a frequency response.

The material in Chapter 5 is based on the following publication ([83]):

(VI) Fabio Mesiti, Mladen Veletić, Pål Anders Floor, and Ilangko Balasingham. **Astrocyte-neuron communication as cascade of equivalent circuits**. *Nano Communication Networks*, 6(4): pages 183-197, 2015. Special Issue on Bio-Nano Communication Networks and Systems.

Finally, Chapter 6 investigates information theoretical aspects of neurons, specifically the capacity of bipartite and tripartite synapses. The major contributions of this chapter address research question RQ5, and are listed as follows.

- The chapter presents the analytical framework which enables one to quantify how much information a receiving (post-synaptic) neuron carries about the transmitting (pre-synaptic) neuron in the intra-neuronal communication channel.
- The chapter offers the results which are of primary importance in understanding the performance of the neural communication.

The material in Chapter 6 is based on the following publication ([128]):

(VII) Mladen Veletić, Pål Anders Floor, Youssef Chahibi, and Ilangko Balasingham. **On the upper bound of the information capacity in neuronal synapses**. *IEEE Transactions on Communications*, 64(12): pages 5025-5036, December 2016.

... “It’s an electrifying time to be in neuroscience” [37].

Chapter 2

Neuroscientific Background and State-of-the-Art

2.1 Introduction

Various branches of neuroscience study different aspects of neurons, ranging from molecular to cellular aspects of individual cells to sensory, motor and cognitive tasks in the clusters/networks of cells. Neuroanatomy, molecular neuroscience and computational neuroscience, however, cover signaling aspects in neural networks:

- *Neuroanatomy* examines the neural "hardware" and organization of the neural system which are pivotal for a profound study of neural signaling.
- *Molecular neuroscience* examines the molecular biology of the nervous system including the intra- and extra-cellular processes of individual cells, as well as mechanisms of molecular signaling that affect the performance of the neural communication.
- *Computational neuroscience* examines the neural coding and decoding, and numerous neural information processing functions through different **computational models**. Models that produce a functional relation between stimulation at the input stage and neural spiking, defined as membrane output voltage, are dominant.

Beside neuroscience, neurons are involved in the Information and Communication Technology (ICT) to inspire Artificial Neural Networks (ANNs), i.e., mathematical models widely used in machine learning and data mining to infer a function from observations. The ANN can learn its responses on the basis of observations that it gets from its environment just as biological neural networks.

The biological neural network, as the most powerful and advanced intra-body network, has also become appealing to the ICT-community to produce futuristic neural-

like nano-networks. Such networks are intended to operate upon the **communication models** of neural signaling where a bio-hybrid approach is used for the development, design and fabrication of individual communication entities. Novel neural-like networks are expected to enable various **nano-networking applications** including the IBC which leads to the concepts of Body Area Nano-Networks (BANNs) and In-Body Sensor Actuator Networks (IBSANs). In these concepts, individual network entities are intended to be interfaced with the neural tissue to achieve more advanced and precise interaction at cellular level aiming to offer novel and promising diagnosis and therapies. Moreover, engineering applications of nanotechnology have been investigated in neural prosthetics. A prosthesis must replace damaged sensory, motor or cognitive cells with bio-mimetic neurons having specific functional properties. Bio-mimetic neurons must both receive as inputs and send as outputs spiking activity from/to regions of the brain with which the damaged neurons normally communicated. Apart from medical applications, nano-networks can be designed and applied in environmental and industrial applications to expand the capabilities of conventional communication networks [8].

This chapter aims to:

- provide necessary and sufficient background on biological neural system with a focus on a single neuron and its compartments, functional properties and intrinsic processes;
- identify, classify and overview the available interdisciplinary work related to the biological neural network and potential applications that rely on the neural communication paradigm; albeit the review on computational models used in the field of neuroscience and methods for evaluating the accuracy of computational models exists in the literature [30], a more comprehensive review on neuromodeling including the communications engineering approaches, as well as the review of neuroengineering efforts, is missing;
- motivate the further research.

Section 2.2 of this chapter provides a brief background on relevant anatomical and molecular aspects of neurons and astrocytes studied in neuroanatomy and molecular neuroscience. Section 2.3 provides a detailed overview of neuromodeling approaches applied to a single cell or specific cellular compartments, and their primal applications. Engineered neural-like networks and biological neural networks are reviewed in Section 2.4. Concluding discussion including motivation for further research is brought in Section 2.5.

2.2 Neuroscientific Background

The processes of the human nervous system depend on the inter-connected specialized cells, i.e., **nerve cells** (or **neurons**) and **glial cells** (or **glia**). Neurons are

the fundamental functional units of the nervous system that generate information signals which allow them to transmit information over long distances. Photomicrographs of realistic human neurons are given in Fig. 2.1. Glia are also essential to nervous system function as they support both neurons and neural functions. Photomicrograph of realistic human glial star-shaped cell known as an astrocyte is given in Fig. 2.2.

The human nervous system and inter-connected neurons that make up the system can both be classified.

– The nervous system can be divided in two sections: **Central Nervous System (CNS)** (further divided into two parts: the brain, which contains billions of neurons and trillions of glial cells, and the spinal cord), and **Peripheral**

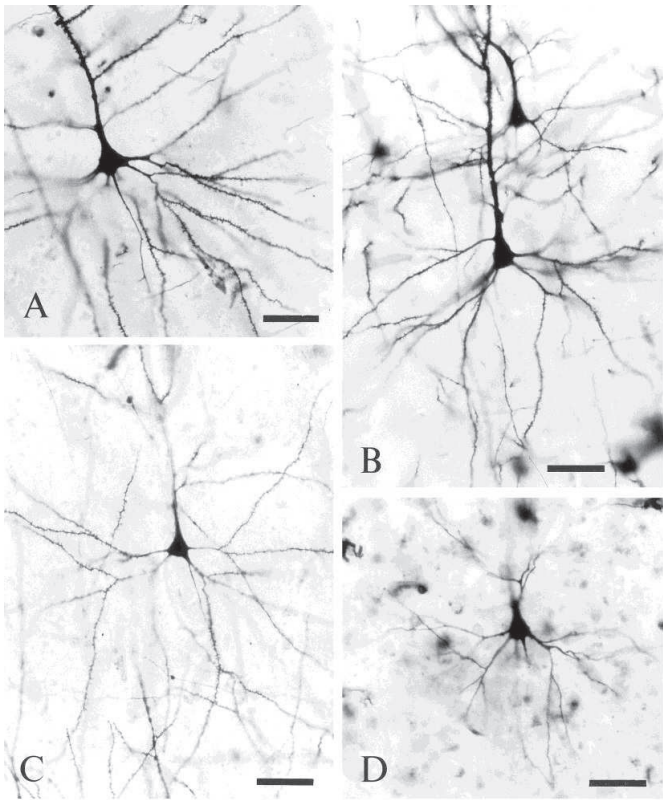

Figure 2.1: Photomicrographs of pyramidal cells stained via Golgi silver staining technique. Neurons from four cases are presented: a 14-year-old male (A), 23-year-old male (B), a 32-year-old female (C), and 106-year-old female (D). Scale bars = 50 μm. Photomicrographs are taken from [59].

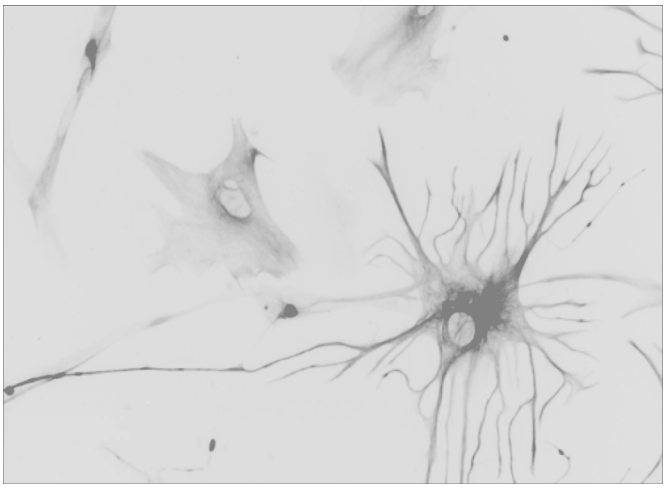

Figure 2.2: Photomicrograph of a 23-week-old fetal brain culture human astrocyte by Bruno Pascal (own work) shared with the CC-BY-SA-3.0 license via Wikimedia Commons. The figure is modified by the author.

Nervous System (PNS) (further divided into two major parts: the somatic nervous system, and the autonomic nervous system). The somatic nervous system is associated with skeletal muscle and voluntary control of body movements. The autonomic nervous system regulates the functions of internal organs (the heart, stomach and intestines) and glands.

– The PNS consists of the *sensory neurons* that bring signals from outer parts of the body into the CNS, and the *motor neurons* that bring signals out of the CNS to the outer parts of the body (muscles, skin, glands). The CNS consists only of the *inter-neurons*, which receive information from other neurons (either sensory neurons or inter-neurons) and transmit information to other neurons (either motor neurons or inter-neurons).

Apart from functional roles, neurons can be anatomically classified, e.g., *unipolar* (that have one axon and one dendrite branching off in opposite directions from the cell body), *bipolar* (that have one axon and one dendrite branch), *pyramidal* (that have one axon and two main dendrite branches), *multipolar* (that have one axon and many dendritic branches), and *Purkinje* cells (that have one axon and a very dense and complicated dendrite arrangement). The multipolar neuronal anatomy[1] is shown in Fig. 2.3 which additionally illustrates the neuron-to-neuron communication channel. The essential compartments are labelled in the figure and defined in the following subsections with the biological and molecular level relevant to the content.

[1]The content of the thesis is generalized to CNS neurons and does not favour any particular anatomy.

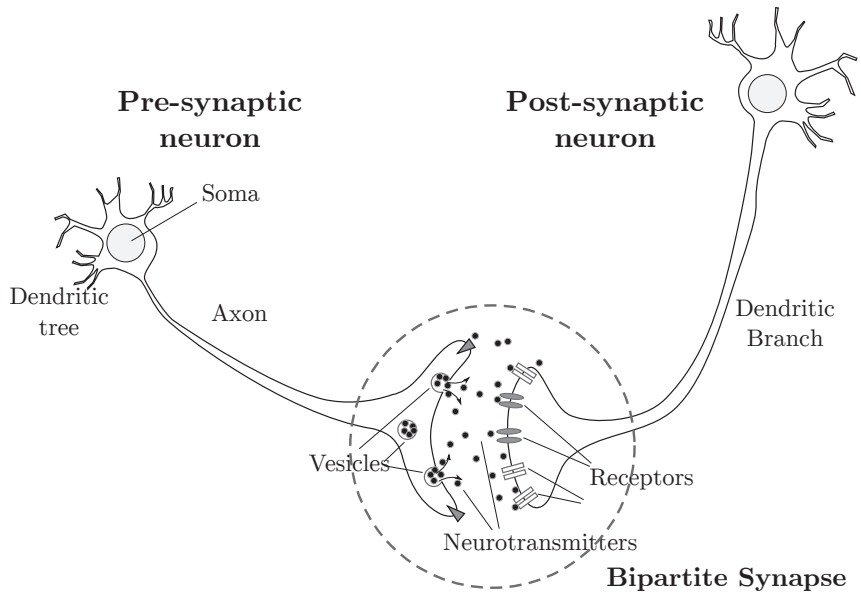

Figure 2.3: Schematic diagram of the transmitting (pre-synaptic) cell and the receiving (post-synaptic) cell in the neuron-to-neuron communication channel with the bipartite synapse.

2.2.1 Neuronal Anatomy

Neurons have a cell body called the *soma* which contains the nucleus and synthesizes neuronal proteins. The soma gives rise to *dendrites* known as short branches that form dendritic trees, collect chemical inputs (incoming information) from adjacent neurons or extra-cellular environment, and help neurons generate a short-lasting electrical response called AP or spike. The spiking sequence encodes the incoming information. It is sent from the soma down through the *axon*. Axons are known as transmission lines extending from the soma and are longer than the dendrites (some axons from spinal neurons can extend up to one meter or more). There are two types of axons occurring in the PNS and the CNS: unmyelinated and myelinated axons (see the next subsection). Myelin is a sheath formed by glial cells that provides a layer of insulation that prevents the loss of the electrical signal from an AP.

After propagating through the axon, the spiking sequence reaches the *pre-synaptic terminal*. It is a synaptic bouton within the axon of the pre-synaptic neuron that contains chemical messengers that transmit signals across the synapse, i.e., *neurotransmitters*. Main neurotransmitters are glutamate, aspartate, D-serine, γ-aminobutyric acid (GABA), dopamine and adenosine. Neurotransmitters are enclosed in small membrane-bound spheres called *synaptic vesicles* which release them into the synaptic cleft to propagate following a law of diffusion, and eventually bind

to chemical receptors located on the membrane of the *post-synaptic terminal* at the dendrites of the receiving neuron. Neurotransmitters act in one of two ways: excitatory, that helps the receiving neuron generate a response, or inhibitory, that prevents the receiving neuron from generating a response. Note that particle transmission takes place only in chemical synapses, which are, however, more common than electrical synapses where the pre- and post-synaptic neurons are connected by gap junctions capable of passing electrochemical signals directly.

The functional integration and physical proximity of the pre-synaptic terminal and post-synaptic terminal refers to the **bipartite synapse** (see Fig. 2.3). When the glial cell is in the vicinity of the pre- and post-synaptic terminal, then the combined contributions of these three synaptic components affect the activity of the chemical synapse. The functional integration and physical proximity of the pre-synaptic terminal, the post-synaptic terminal, and the glial cell refers to the **tripartite synapse** (see Fig. 2.6). Before moving to synaptic components, the processes of initiation and transmission of electrochemical signals that are converted into molecular signals within synapses are explained.

2.2.2 Spike Initiation and Transmission

Spiking sequences serve as physical information carriers. What forms the spike is the difference in electrical potential between the interior of a neuron and the surrounding extra-cellular medium. Three processes are relevant:

1. the *depolarization*, which makes the neuron's membrane potential less negative, either because of the positively charged ions (sodium – Na^+, calcium – Ca^{2+}, and potassium – K^+) flowing in, or the negatively charged ions (chloride – Cl^-) flowing out (see Fig. 2.4);
2. the *repolarization*, which follows after depolarization of neuron's membrane potential to define the drop in membrane potential triggered by the closing of specific ion channels and opening of different ion channels in the membrane (see Fig. 2.4);
3. the *hyperpolarization*, which makes the neuron's membrane potential more negative, either because of the positively charged ions flowing out, or the negatively charged ions flowing in (see Fig. 2.4).

A fluctuation of hyper- and de-polarized electrochemical potentials defines the spiking sequence (see Fig. 2.5) and encodes the message transmitted from a sample network node, i.e., a single cell.

The neuron will typically fire, i.e., generate a spike, only when its membrane potential reaches a variable threshold value of about -55 to -50 mV. However, this is not the only constraint – spiking is controlled by a Refractory Period (RP) defined as the time period during which a cell is incapable of or inhibited from repeating a

spike due to the inactivation property of voltage-gated sodium channels and the lag of potassium channels in closing. Two RPs are defined:

- the Absolute Refractory Period (ARP), as the interval during which a new spike cannot be initiated over the active one regardless the intensity of stimulation, and
- the Relative Refractory Period (RRP), as the interval during which a new spike generation is inhibited but not impossible. The RRP follows immediately after the ARP (see Fig. 2.4).

After initiation, in neurons with unmyelinated axons the AP provokes another one in the membrane immediately adjacent, and moves continuously down the axon like a wave. This is achieved by the mechanism where APs generate local currents that depolarize the axonal membrane adjacent to the AP. When depolarization reaches the threshold, a new AP is produced adjacent to the original one. This propagation is possible only in one direction as the recently depolarized area of the membrane cannot be depolarized again to generate a spike due to the ARP.

Conversely, the spikes cannot propagate through the membrane in myelinated axonal segments. Instead, the ionic current is carried by the cytoplasm to depolarize periodical gaps in the myelin sheath where the axon is reduced in diameter. The gaps are known as nodes of Ranvier which have proteins, called channel proteins, which further allow ions to enter and exit the cell. The current from an AP at one node of Ranvier provokes another AP at the next node. This process is largely con-

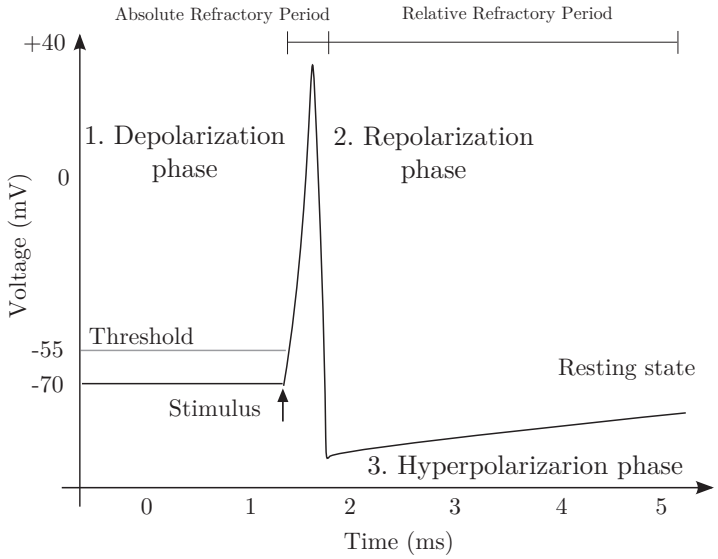

Figure 2.4: The phases in action potential.

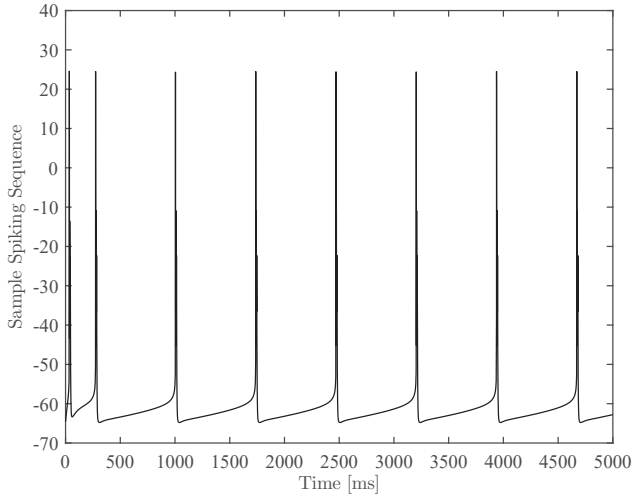

Figure 2.5: A sample sequence of spikes.

trolled by sodium – Na^+ and potassium – K^+ ions which enable a rapid and reliable propagation of electrical impulses. This propagation of the spike from node to node is known as saltatory conduction. In neurons with myelinated axons, spikes travel much faster than spikes in equivalent neurons that lack myelin sheaths. However, unmyelinated axons are short so that the speed of the signal is not that important.

An axon conducts the spiking sequence typically in a direction outward from the soma to different neurons, muscles and glands. The propagation is called orthodromic propagation [35]. Antidromic propagation in the reverse direction is not impossible but is used in a laboratory setting to depolarize the neuron at the pre-synaptic terminal and manipulate the spike to propagate in the opposite direction.

2.2.3 Internal Dynamics of Pre-Synaptic Neurons

When the AP reaches the pre-synaptic terminal, it leads to the opening of Voltage-Gated Calcium Channels (VGCCs) and a resulting influx of calcium ions, Ca^{2+}, into the cellular cytosol[2]. This increases the internal calcium ion concentration, $[Ca^{2+}]_{pre}$ (refer to Table. 2.1 for a list of the symbols used in the text). The excess calcium is absorbed by internal buffers, such as the ER, with a certain time constant. An increase in $[Ca^{2+}]_{pre}$ initiates the chemical mechanisms leading to the release of synaptic vesicles in the pre-synaptic terminal. The vesicles are first transported to the synaptic terminal and then attached to the pre-synaptic membrane. When this

[2]The cytosol is the inner part of the cell, within the cellular membrane.

process is done, the APs are transduced into molecular form which carries messages in the remaining communication pathway between neurons. Molecular messengers are neurotransmitter molecules that are stored in the synaptic vesicles from where they are released into the synaptic cleft to propagate following a law of diffusion.

The probability for neurotransmitter release increases when a high frequency spike train or a burst of spikes reaches the pre-synaptic terminal, since $[Ca^{2+}]_{\text{pre}}$ builds up when many APs are fired over a short time interval. The exact relation between the vesicle release probability and $[Ca^{2+}]_{\text{pre}}$ is complicated. One effect that complicates this matter is that the effective concentration around vesicle release sites depends on the distance to the VGCCs [93]. $[Ca^{2+}]_{\text{pre}}$ needs to reach levels of about 100 μM in the vicinity of a vesicle release site for neurotransmitters to be released. If Ca^{2+} enters at about 10 nm from the vesicle release site, a release of neurotransmitters usually follows, since then $[Ca^{2+}]_{\text{pre}} > 100$ μM. However, if the distance is larger than about $100 - 200$ nm, intra-cellular buffers will bind most of the calcium before $[Ca^{2+}]_{\text{pre}}$ gets close to 100 μM.

2.2.4 Internal Dynamics of Post-Synaptic Neurons

The neurotransmitters that reach the post-synaptic terminal after diffusion through the cleft lock onto receptors embedded in the membrane. The receptor proteins that are activated by neurotransmitters can be classified to ligand-activated ion channels or *ionotropic receptors* – the receptors that open directly in response to neurotransmitter binding, and *metabotropic receptors* – the receptors where neurotransmitter binding triggers a signaling pathway to indirectly open or close channels.

If the neurotransmitters are excitatory, a mixture of Na^+, K^+, and Ca^{2+} flows through the membrane. This influx defines the amplitude of the Excitatory Post-Synaptic Potential (EPSP) in the receiving neuron. EPSPs can also result from a decrease in outgoing positive ions. The flow of ions that causes an EPSP is an Excitatory Post-Synaptic Current (EPSC). There is also the opposite of Inhibitory Post-Synaptic Potential (IPSP), which results from the flow of negative ions into the cell or positive ions out of the cell. EPSPs (and IPSPs) have an additive effect: when multiple EPSPs occur on a single patch of post-synaptic membrane, their combined

Symbol	Description
$[Ca^{2+}]_{\text{pre}}$	Ca^{2+} concentration in the pre-synaptic terminal
$[Ca^{2+}]_{\text{as}}$	Ca^{2+} concentration in the astrocyte
$[IP_3]$	IP_3 concentration in the astrocyte
$[Ca^{2+}]_{mGluR}$	Pre-synaptic Ca^{2+} concentration contribution from mGluR
$[Ca^{2+}]_{AP}$	Pre-synaptic Ca^{2+} concentration contribution from AP spiking

Table 2.1: Symbols defined in Chapter 2 and used throughout the thesis.

effect is the sum of the individual EPSPs; larger EPSPs result in greater membrane depolarization which increases the likelihood that the post-synaptic cell reaches the threshold and fire an AP.

There exists a myriad of neurotransmitter molecules and post-synaptic receptors activated by neurotransmitters, making synaptic communication difficult to fully comprehend. Nonetheless, it is common in neuroscience to analyze only glutamate molecules and AMPA (α-amino-3-hydroxy-5-methyl-4-isoxazole propionic acid) and NMDA (N-methyl-D-aspartate) ionotropic receptors since they mediate most of the synaptic excitation in the CNS [16, p.139], and are therefore the most important for post-synaptic spiking.

AMPA is a fast ion conducting receptor mainly permeable to Na^+ and K^+, and is substantial for providing fast post-synaptic responses due to the pre-synaptic spiking. The current through the AMPA's is typically given by [35]

$$I_{\text{AMPA}}(t) = G_{\text{AMPA}}(t)P_{\text{AMPA}}(t)(V_{EPSP} - E_x), \tag{2.1}$$

where $G_{\text{AMPA}}(t)$ is a modifiable conductance factor, $P_{\text{AMPA}}(t)$ describes the open receptor probability dynamics, V_{EPSP} is the post-synaptic potential, and E_x is the reversal potential of the relevant ion. The reversal potential, or the Nernst potential, of an ion is the membrane potential at which there is no flow of that particular ion from one side of the membrane to the other.

NMDA is mainly permeable to Na^+, K^+ and Ca^{2+}, and is significantly slower than AMPA. The main difference between AMPA and NMDA is that NMDA requires that both pre- and post-synaptic neurons fire subsequently in order to become fully conductive. NMDA activity determines how the conductance of AMPA gates (G_{AMPA}) is modified/changed. They are therefore essential for long term changes in the synaptic strength, which is crucial for memory and learning.

2.2.5 Internal Dynamics of Astrocytes

Astrocytes (see Fig. 2.2) are a particular star-shaped type of glial non-excitable cells which fill the spaces between neurons and support brain functions and inter-cellular coordination. Previously, the role of astrocytes has been relegated to passive neural support in regulating the extra-cellular potassium level [96] and in maintaining the ionic balance, and for the absorption of exceeding neurotransmitter molecules in the synaptic environment [16]. Through the last decades, glial cells are proved to also have an impact in actively promoting and modulating the neural signaling [36, 43, 98, 134].

Astrocytes are inter-connected through gap junctions, forming an astrocytic network where the intra-cellular communication is mainly performed with calcium signaling [31]. In this communication process, the propagation of cytosolic calcium concentration, $[Ca^{2+}]_{\text{as}}$, from one cell to another distant cell including intermediaries is

also called calcium wave. The consequence of the increased $[Ca^{2+}]_{as}$ is the release of neurotransmitters from the astrocyte; the term *gliotransmitters* is more precise when

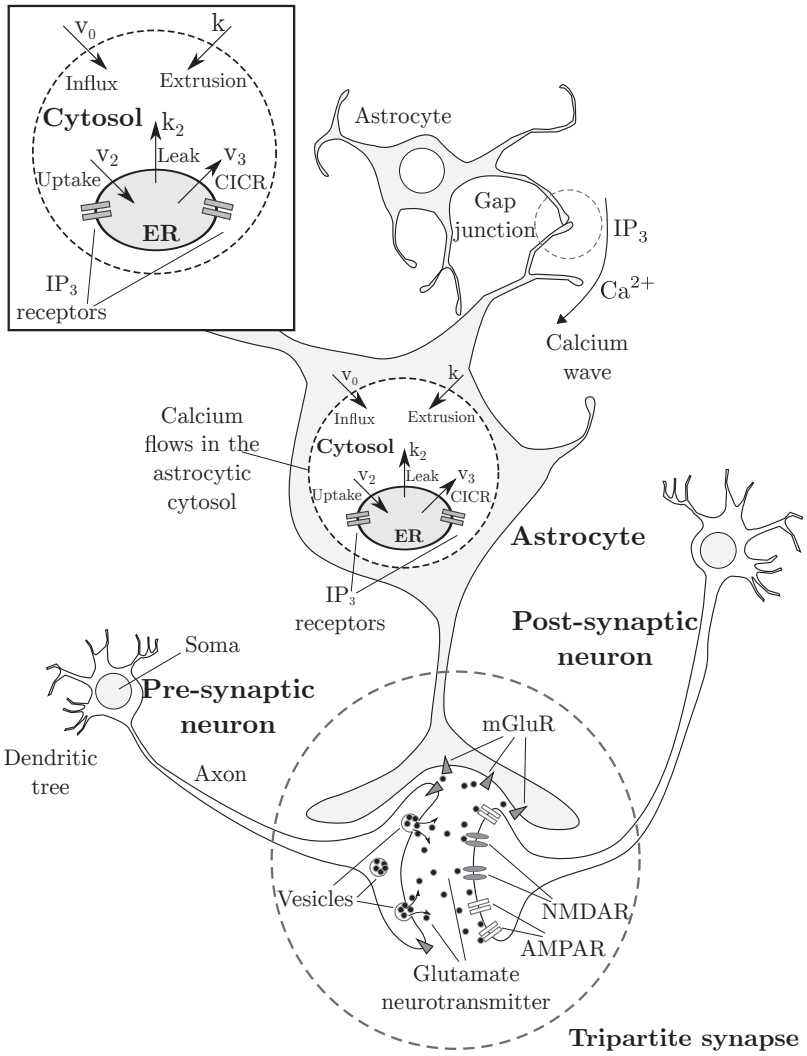

Figure 2.6: Schematic diagram of the transmitting (pre-synaptic) cell, the astrocytic cell, and the receiving (post-synaptic) cell in the neuron-to-astrocyte-to-neurons communication channel with the tripartite synapse. Astrocyte: Ca^{2+} flow into the cytosol from internal IP_3/Ca sensitive store (activated by the presence of IP_3 and Ca^{2+}). Synapse: glutamate is released through membrane fusion by vesicles located in pre-synaptic and astrocytic terminals and binds to mGluR and AMPA/NMDA [83].

dealing with glial cells. Main gliotransmitters are glutamate, D-serine, adenosine, and adenosine triphosphate (ATP) [98], which have direct impact on adjacent neurons equipped with compatible receptors located on the cell membrane. Particularly, glutamate is one of the most important and abundant neuro- and gliotransmitters in the brain, which bind to several types of glutamate-sensitive receptors (AMPA, NMDA, and metabotropic glutamate receptors (mGluRs)).

When the astrocyte cell is in the vicinity of the synapse, the concept of tripartite synapse is introduced to underline the presence of the astrocytic terminal in the vicinity of two neurons. Schematic diagram of the tripartite synapse and their components is depicted in Fig. 2.6.

The mechanisms behind calcium signaling and release of gliotransmitters are complex and take into account several physiological processes. These processes are listed in the following.

- Astrocytic membrane has the mGluRs that once activated by nearby glutamate, trigger intra-cellular release of Ca^{2+} from internal stores. This process is carried out through produced inositol 1,4,5-triphosphate (IP_3) – a secondary messenger molecule which mobilizes Ca^{2+} into the cytosol. The production of IP_3 can alternatively be evoked by external mechanical stimulation of the astrocytic membrane [116] or directly from other astrocytes through permeable gap junctions where IP_3 moves from cell to cell.
- The initial elevation of $[Ca^{2+}]_{as}$ evokes further release of calcium ions from internal stores through the Ca^{2+}-Induced Ca^{2+}-Release (CICR) process which enriches the calcium dynamics.
- The elevation of $[Ca^{2+}]_{as}$, which follows the IP_3 production, triggers the release of gliotransmitter molecules that further diffuse in the synaptic cleft and eventually bind to neuronal receptors. This process provides a kind of astrocytic feedback.

The astrocytic feedback influences/modulates both the pre- and post-synaptic terminal. The primal consequences on the pre-synaptic terminal are further explained in Chapter 5. In addition, a potential impact of astrocytic feedback is reflected to the regulation of brain processes such as *plasticity*, *learning* and *memory*, where glutamate dependent NMDA receptors located on the post-synaptic terminal have a leading role. Although the mechanisms concerning Ca^{2+} dynamics have been described with high accuracy in the literature, the impact of calcium signaling on these processes still remains unveiled and uncertain. Plasticity, learning and memory are, however, not within the scope of this thesis.

The remainder of this chapter reviews accumulated inter-disciplinary knowledge on the neural communication and investigates their potential and limitations. The review is conceptualized around the neuromodeling efforts from computational neuroscience and communication and information technology, and neuroengineering efforts

from communications technology [124].

2.3 State-of-the-Art in Neuromodeling

Spiking neurons are fundamental computational and signaling units of the nervous system. Thus, computational and communication modeling of the neural "hardware" and its activities are of great importance.

- Computational modeling is relevant for characterizing what extremely complex nervous system actually does, how it functions, and why it operates in particular ways. Most computational models are intended to analytically describe and reproduce real-world behavior of particular cellular compartments and/or entire cells, or predict the response to specific input signals.
- Communication modeling of neural signaling, however, is relevant to obtain theoretic quantities on fundamental ionic and chemical signals transmission, noise and interference. Models are mainly created in a way to resemble models of conventional wireless communication systems owing to pragmatic comparison of intriguing neural communication with existing technologies.

Computational and communication models of neural spiking are reviewed in the following subsections.

2.3.1 Computational Models

Computational models attempt to clarify the core principles that underlie neural information processing. These models come from the computational neuroscience and can be classified by the complexity as:

- phenomenological spiking models representing the dynamics of neurons, and
- conductance-based models representing detailed electrophysiology of neurons.

The most famous **phenomenological spiking models** are *Integrate-and-Fire*-based models [6, 30], e.g., Leaky-, Non-Linear-, Quadratic-, Exponential Integrate-and-Fire models, and Spike Response Model, which describe temporal changes in the membrane potential with differential equations augmented by the rule that neuron fires an AP whenever the membrane potential reaches the specified threshold value (≈ -55 mV), i.e.,

$$\text{if} \quad v_m(t) \geq V_{threshold} \quad \text{and} \quad \frac{\mathrm{d}v_m(t)}{\mathrm{d}t} > 0 \quad \Longrightarrow \quad \hat{t} = t. \tag{2.2}$$

The firing time of a neuron is denoted as $\hat{t}$. After firing, the potential $v_m(t)$ is reset to V_{reset}. Integrate-and-Fire models are computationally simple and thus favorable

in computer simulations. Nonetheless, they do not reproduce the neural spiking to a high degree of accuracy.

The most famous **conductance-based models** are *Hodgkin-Huxley*-based models. The Hodgkin-Huxley model is described with a set of non-linear differential equations (see [53]) that can accurately reproduce electrophysiological data. Nonetheless, due to its computational complexity, the model is usually difficult to analyze and implement. This led researchers to propose computationally simpler models, e.g., FitzHugh-Nagumo model [44, 89], Morris-Lecar model [84], Wang-Buzsaki [132] and Hindmarsh-Rose model [52].

A compromise between computationally efficient Integrate-and-Fire models and biologically plausible Hodgkin-Huxley model is a simple spiking model proposed by Izikevich [58]. The Izikevich model is a type of Hodgkin-Huxley model reduced to a two-dimensional system of ordinary differential equations. The Izikevich model is both accurate and favorable in computer implementations.

In addition, computational models can be classified by the level of compartmentalization as single-compartment- and multi-compartment models, that are given for the quantities representing compartments with uniform and non-uniform geometrical and electrical properties, respectively. Integrate-and-Fire- and Hodgkin-Huxley-based models are known as **single-compartment models** which do not explicitly involve the dendrites and/or the axon of a neuron that are at most locally uniform and require a discretization of the spatial variable to treat the differential equations. Conversely, **compartmental models** are the result of a discretization. Among others, the Pinsky-Rinzel model [87, 107] is a known 2-compartment reduction of the complex 19-compartment cable model by Traub [123]. The model is able to accurately characterize the somatic and dendritic membrane potentials. Another model is the Li-Rinzel model [72, 87, 88] used to describe experimental observations on synaptic behavior in case glia cells (astrocytes) are connected to the synapse.

The Pinsky-Rinzel and Li-Rinzel models are of special relevance for the studies provided later in Chapter 5 and Chapter 6. Tabular summary of the neural compu-

Single-Compartment		Multi-Compartment
Physiological Spiking	Conductance-Based	
Integrate-and-Fire	Hodgkin-Huxley	Traub
Leaky Integrate-and-Fire	FitzHugh-Nagumo	Pinsky-Rinzel
Non-Linear Integrate-and-Fire	Moris-Lecar	Li-Rinzel
Spike-Response Model	Wang-Buzsaki	
Izikevich model		

Table 2.2: Tabular summary of the neural computational models reviewed in Chapter 2, Section 2.3.1.

tational models is given in Table 2.2.

2.3.2 Communication Models

Neural communication models are developed as counterparts to the conventional communication models. When focusing on the neural communication, an adequate apprehension is crucial. Recall that temporal spiking sequences described with neural membrane potentials reach a synapse after propagating through the neural fibers. At the synapse, a transmitting neuron converts the electrical signal into chemical signal that is further released into the synaptic cleft to diffuse and bind to receptors of the receiving neuron. Therefore, to properly model the neural signaling, one must clearly differentiate between two phenomenologically different concepts: the *electrochemical transmission* within a neuron, and *molecular transmission* between neurons.

A preliminary step in neural communication modeling using **conventional communication theory** is motivated by the characterization of the signal propagation within neurons aiming to integrate and enable nano-scale implantable devices to support and/or restore the neural communication [49, 50, 77]. The physical neural channel is first analyzed through the blocks of neural processing, where each identified phase is featured a moderate level of biological plausibility. An input/output relationship is defined as transfer functions that depend on operating frequency; a range up to a few kilohertz is exposed where a potential nano-scale device structured according to the identified model could communicate with a cell [50]. Other neural communication performance evaluations, e.g., the probability of error and delay in spike detection at the post-synaptic terminal [13], prefers lower incoming spiking rate and higher number of receptors at the membrane of the receiving neuron. Additional models have been developed to investigate the geometrical and electrical properties and the functionality of unmyelinated and myelinated axons using the cable equation. Many references can be found in [40, 47]. Unlike most axonal models which consider the amplitude of the spike during axonal transmission as all or none, the recent model from [110] considers axon as a system with memory and incorporates the variations in the amplitude of spikes during transmission [42, 113]. A consequent result of the spike shape variations is change in the release of neurotransmitters to the synapse, which affects the amount of stimulation to the dendrite of the post-synaptic cell. Dendrites carry signals between synapses and the soma and also play a central role in neural computation modeling. Although dendrites contain many nonlinear ion channels, they can be modeled as linear-resonant filters [114] that carry signals between nonlinear computational units.

As a specific instance of the molecular communication, the neural synaptic transmission can be analyzed by the adoption of derived molecular communication models [7, 105], where the pre-synaptic terminal can be related to the molecular transmitter, the synaptic cleft to the molecular channel, and the post-synaptic terminal

Model	Theory	Goal	Compartments
[5, 49, 50]	Communication Theory	Design of an interface for nano-machine-to-neuron communications	Dendrites, Soma and Axon
[7, 13, 67, 109, 110, 114]	Communication Theory	Characterize the neural communication for IBC	Dendrites, Soma, Axon and Synapse
[25]	Communication Theory	Characterize the neural communication for IBC	Pre-synaptic Terminal
[26]	Communication Theory	Characterize the neural communication for IBC	Post-synaptic Terminal
[97]	Information Theory	Quantify how much information a neural response carries about the stimulus	Soma
[79]	Communication and Information Theory	Quantify how much information the post-synaptic neuron carries about the pre-synaptic neuron	Synapse
[75, 78]	Information Theory	Quantify how much information the post-synaptic neuron carries about the pre-synaptic neuron	Synapse

Table 2.3: Tabular summary of the neural communication models reviewed in Chapter 2, Section 2.3.2.

to the molecular receiver. Owing to a high compartmentalization at level of individual pre-synaptic terminals, the pre-synaptic terminals are also modeled as an array of transmitters with a high level of biological consistency [25]; owing to a high level of compartmentalization at level of individual dendritic branches and spatially dependent preference for different frequencies, the dendritic tree of the post-synaptic terminal is modeled as a spatio-temporal filter bank, where each filter models the behavior of a dendritic branch [26]. The mathematical formulation that further models diffusion of neurotransmitters in the synaptic cleft and their binding with post-synaptic terminal is recently proposed in [67], incorporating the effects of synaptic geometry in three-dimensional space, the effects of variation in vesicle release site, receptor density, number of neurotransmitters per vesicle, diffusion coefficient of glutamate and re-uptake probability, on EPSP. All referred models do not consider the variations in spike shaping, but can be improved by mechanisms that account the realistic effect of changes in the width of the spikes during axonal transmission [109], to cover the complex process of the release of neurotransmitters to the synapse. In addition to communication theoretical understanding of synaptic transmission, a queueing theory based delay analysis model for synaptic communication is introduced in [5]. Using standard queueing model blocks such as servers, queues and fork-join networks, impulse reception and processing through the neural

system is alternatively modeled as arrival and service processes in queues.

Understanding the strategies that brains use to represent and process information received through the senses and to make behavioral decisions is crucial goal in neuroscience [79]. Hence, the neural communication is investigated in the literature using **conventional information theory** approaches. A few studies on electrochemical neural channel applies Poissonian spiking statistics and channel results aiming to quantify how much information a neural response carries about the time-varying stimulus [97, Chapter 3], [17,119]. These studies are complemented by the Manwani-Koch's theoretical study [79], who quantify how much information the post-synaptic neuron carries about the pre-synaptic neuron, and the Malak-Akan's study, who extend the single-input single-output synaptic channel set-up to the multiple-input single-output and multiple-input multiple-output set-ups [75, 78]. These studies, however, lack an impact of the multi-terminal synaptic interference on the information capacity between neurons, albeit the interference neural models [73, 76] rate neurons as good interference canceling elements. Tabular summary of the neural communication models is given in Table 2.3.

2.4 State-of-the-Art in Neuroengineering

This section keeps the review on communication modeling of the neural network separated from the review of a few other engineering approaches mainly motivated by the interaction of the nano-scale devices with biological neurons. These hybrid systems are intended for designing BANNs, IBSANs, Biological-Integrated Systems (BISs) and neuroprosthesis.

A key application domain of neural-like nano-networks is BANNs, where nano-scale devices are connected to perform physiological sensing, anomaly detection, and neuro-muscular implant control. A first neuron-based BANN [120, 121] is supposed to consist of a set of nano-scale devices and a network of neurons artificially formed into a particular topology. In this concept, nano-scale devices function either as sensors or sinks that interact with neurons in a non-invasive manner utilizing the neural communication principles, whereas neural network serves as an enabling infrastructure for data transmission. A communication protocol is Time Division Multiple Access (TDMA), i.e., neuronal TDMA, that performs scheduling and allows sensors to multiplex neural transmissions and avoid interference and processing limitations due to refractoriness.

The design of an interface between nano-scale sensors and neurons that can initiate signaling in BANN is challenging and requires devoted studies and experiments. So far, individual neurons have been interfaced with hybrid structures consisting of arrays of nano-wire field-effect transistors [101]. Each junction is intended either for detection, excitation, and/or inhibition of neural signal propagation. Nano-wire field-effect-transistors are supposed to provide both local electrical and chemical

stimuli to create detectable spikes in targeted cell. An alternative is to use sensors [12] able to emit an agent invoking trans-membrane calcium chemical signaling which will leverage the vesicle release and induce signaling between neurons. Another option is to use conceptual Synaptic Nano-Machines (SnMs) [80, 81] supposed to be able to interact with the targeted neuron establishing additional connexone channels which allow the flow of ions and currents, and eventually evoke a post-synaptic potentials.

2.5 Motivation for Further Research

As can be inferred from the reviewed literature, still a limited number of efforts have been dedicated to propose a realistic communications engineering description of the neural communication developed for the purpose of understanding, designing and developing neural-like networking paradigm and devices for nano-networking applications. The existing communication models of neurons (reviewed in Section 2.3.2) are considered either as simplified or incomplete in terms of biological blocks involved in signaling processes. Such models are, however, inspirational and methodologically perceptive for developing more accurate and advanced models, where the bottom-up approach of analyzing neural system should be used. Besides, as no other existing investigations in the engineering of neural communication systems have considered the presence of the adjacent neural cells, e.g., glial cells, that are believed to impact the neuronal performance, novel and advanced models should involve their active role and impact on signaling performance. Hence, the creation of realistic and revised frameworks, theories, and inferences upon different system models is primarily what motivates and differentiates the study of the thesis from other neural studies within the ICT domain.

In terms of treatment of neurodegenerative disorders, it can be inferred from Section 2.4 that the reviewed interface solutions help developing two out of three classes of neural prosthesis. The first class of prosthesis aims to compensate for loss of sensory input by replacing the transduction by sensory cells of stimulation from the environment into electrical stimulation; the second class aims to compensate for loss of motor control by delivering functional electrical stimulation at targeted cells. Both stimulation types can be performed through any of the proposed neural interfaces. Nonetheless, novel modalities of stimulation and control of the neural system further motivate novel neural communication models targeted in this study. Biologically meaningful and plausible theoretical frameworks and analysis of the neural communication should alternatively leverage the realization of neural-like devices/networks and the third class of neural prosthetics. The key issue in the third class of neural prosthesis, i.e., a cognitive prosthesis, is not confined only to the communications between man-made devices and neurons. It actually replaces communications between neural clusters, i.e., brain regions, by replacing the damaged neurons with bio-mimetic neurons having adequate functional properties.

Chapter 3

Stochastic Model of Intra-Neuronal Communication

3.1 Introduction

To start understanding the biological neural network, the *electrochemical neuronal channel* introduced in Chapter 1, Section 1.2.2 and imposed as an inevitable part of the overall neural communication, must be considered first. The *molecular neuronal channel* as the succeeding channel in the overall pathway of neural communication is considered in the following chapters.

As clarified in Chapter 2, Section 2.2, which brought the relevant biological neural aspects, a neuron generates APs in response either to chemical inputs normally collected by dendrites, or to the current induced in the soma. The neuronal response is then emitted from the soma, which serves as a *transmitter*, to propagate down through the axon, which serves as a *communication channel* connecting the soma and the pre-synaptic terminal of the same cell. The pre-synaptic terminal serves as a *receiver* of the electrochemical neural response.

Hereinafter, the electrochemical neuronal transmission within the cell is referred in the thesis as the **intra-neuronal communication**. The communication equivalent representation of the intra-neuronal communication system within the overall neuron-to-neuron communication system is highlighted in Fig. 3.1.

The aim of the chapter is to offer an alternative and progressive description of the intrinsic neuronal signaling which would facilitate for communications engineers the understanding of this segment of the neural system. The following study adopts an approach where the chemical and ionic processes are represented with signals. Albeit this chapter devotes to describe and reproduce real-world neuronal behavior, its goal is not directed towards definition of a novel neuroscientific computational model that would outperform the existing computational models in their accuracy

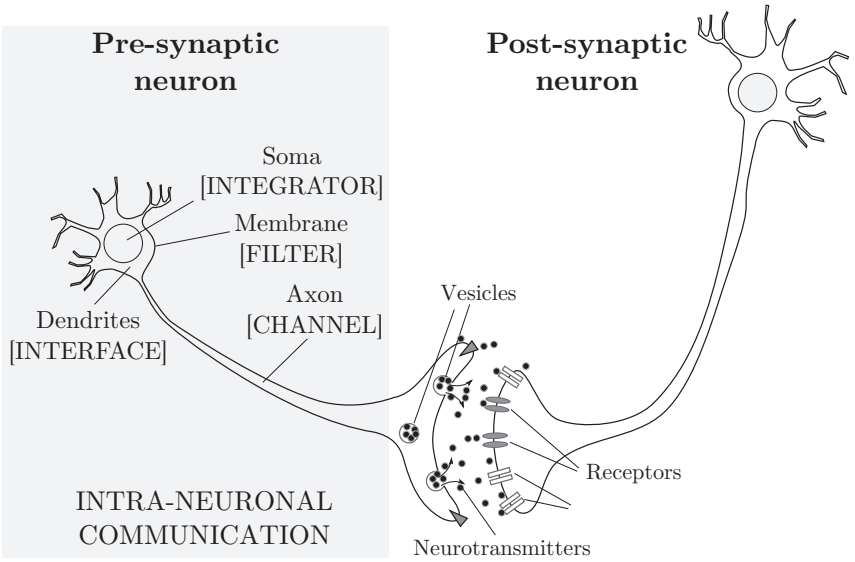

Figure 3.1: The intra-neuronal communication equivalent representation considered in Chapter 3.

and/or efficacy.

The remainder of this chapter is organized as follows. Section 3.2 elaborates on filtering neuronal mechanisms, a nonlinear spike generation machinery (including the effects of spike response variability, randomness associated with physical processes, noise, and trial-to-trial variability), and axonal filtering mechanism. Section 3.3 provides graphical results aiming to further corroborate the understanding of neuronal responses to various stimulation signals. Concluding remarks are given in Section 3.4.

3.2 Communications Engineering Model

Referring to the previous knowledge accumulated in neuroscience, biology and chemistry, potential *deterministic analytical description* of the neuron's response to chemical inputs which would facilitate the understanding of the intra-neuronal communication process would not be valid. The reason is confined to the large trial variability directed to the biological systems even when the same stimulus is applied repeatedly. The statement also stands for neurons which produce random spiking sequences that reflect both the intrinsic dynamics of the cell and the temporal characteristics of the stimulus [35].

The stochastic relationship between a stimulus and a response thus imposes *stochas-*

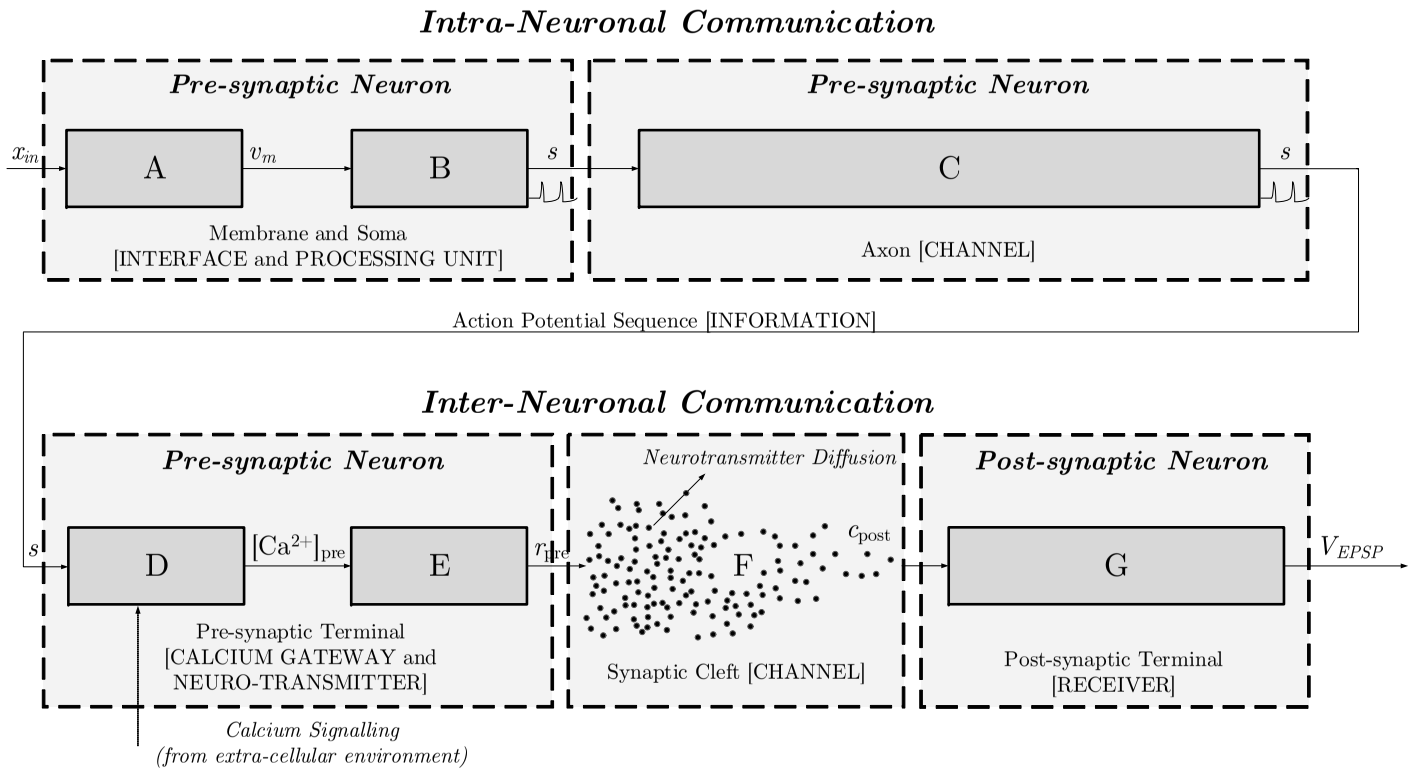

Figure 3.2: Modules composing the overall physical communication model between neurons. The intra-neuronal communication is investigated in Chapter 3. The inter-neuronal communication is investigated in Chapter 4.

tic description of the intra-neuronal transmission as a specific stage in neural signaling.

The intra-neuronal communication is primarily driven by three processes: the *membrane filtering*, *spike initiation*, and *axonal propagation/transmission*. The modules composing the intra-neuronal communication channel are depicted in the upper stage of Fig. 3.2 and modeled in the following sections. Fig. 3.2 shows modules composing the overall communication channel between neurons. The inter-neuronal communication is defined later in Chapter 4.

3.2.1 Cellular Membrane Mechanism

When the overall instantaneous stimulus denoted as x_{in} in Fig. 3.2 is collected, the cellular membrane starts acting as a processing unit which characterizes x_{in} to define the subthreshold membrane potential v_m [112]. From the signal processing perspective, the membrane operates as a frequency-dependent impedance [55, 112] represented by the module **A** in Fig. 3.2.

This can be proved referring to Fig. 3.3 which collects the responses, i.e., the spiking sequences of the Hodgkin-Huxley neuron when stimulated with an Impedance Amplitude Profile (ZAP) current that sweeps linearly over time from 0 Hz to 200 Hz while injecting the soma. From five responses obtained given five maximum values of the ZAP input, it is evident that the membrane reacts as a device that passes frequency components within the certain bandwidth that is amplitude-dependent – larger the amplitude, wider the passing range.

The frequency-and-amplitude-dependent behavior of the membrane is additionally demonstrated in Fig. 3.4 and Fig. 3.5. These figures illustrate two scenarios. In the first scenario shown in Fig. 3.4, the neuron is stimulated by an induced sine wave and a rectangular pulse wave, respectively, both exhibiting amplitudes of ± 80 pA and frequencies of 4 Hz. From the outputs, the neuron responds to the pulse wave while suppressing the sinusoidal input. Conversely, in the second scenario shown in Fig. 3.5, the neuron is stimulated by an induced sine wave and a rectangular pulse wave, respectively, both exhibiting amplitudes of ± 130 pA and frequencies of 4 Hz. It is evident that the neuron responds to both input signals. The neural preference to the pulses, however, comes from the spectral differences of the stimulating waves, where the rectangular sequence contains frequency components at kf_0, where $f_0 = 4$ Hz and $k = 1, 2, 3, \ldots$, unlike the sine wave which contains only the component at $f_0 = 4$ Hz. The neural preference to the higher stimulation amplitudes also comes from the spectral representations where (even attenuated) higher spectral components lead to the augmented subthreshold dynamics which facilitates the production of spikes.

Hence, the analytical definition of the membrane in terms of the magnitude and

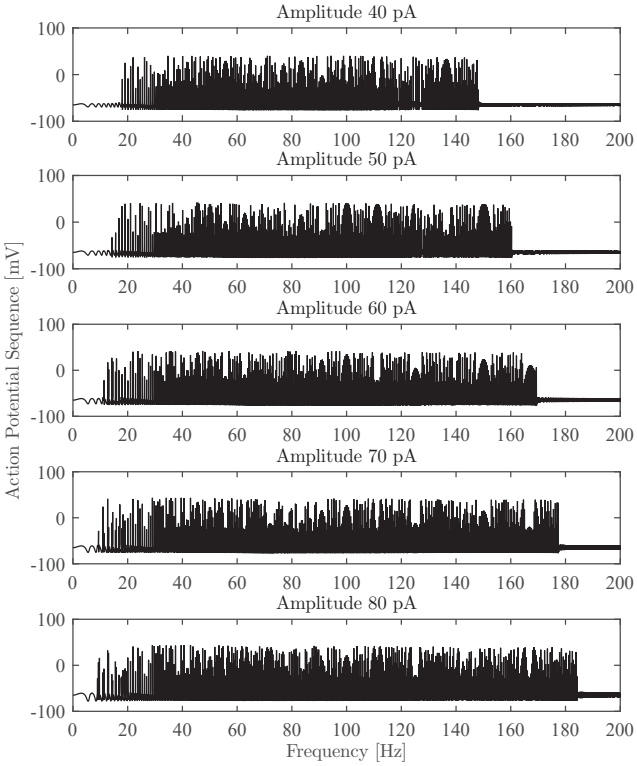

Figure 3.3: Illustration of frequency-dependent neuronal property with spiking trains generated by induced ZAP current. Selection of particular stimulation amplitude values (40-80 pA) is motivated from [106]. The responses are obtained with an open-source simulator NEURON [27].

phase uses a type-specific parameter values, and is expressed as [112]

$$|\mathbf{A}(f)| = \frac{\tau_c}{C}\left[\frac{1+(2\pi f\tau_c)^2}{\left(\alpha+\beta-(2\pi f\tau_c)^2\right)^2+\left((2\pi f\tau_c)(1+\alpha)\right)^2}\right]^{1/2} \tag{3.1}$$

and

$$\phi_{\mathbf{A}}(f) = \operatorname{atan}\left[(2\pi f\tau_c)\frac{\beta-\left(1+(2\pi f\tau_c)^2\right)}{\beta+\alpha\left(1+(2\pi f\tau_c)^2\right)}\right], \tag{3.2}$$

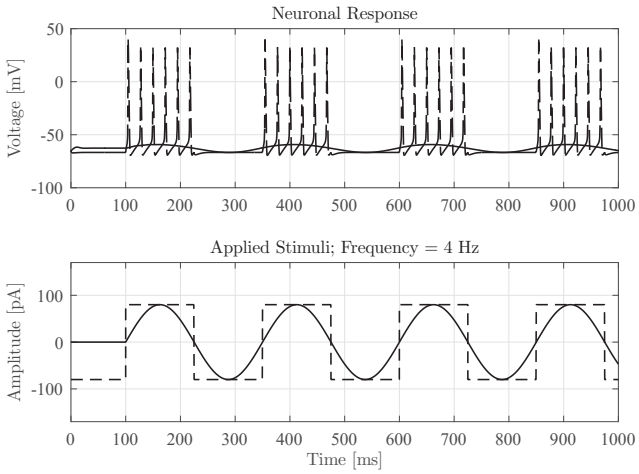

Figure 3.4: Upper graph: the neuronal response affected by rectangular pulse current and sine wave. Lower graph: applied stimuli with amplitude of 80 pA and period 250 ms. The responses are obtained with an open-source simulator NEURON.

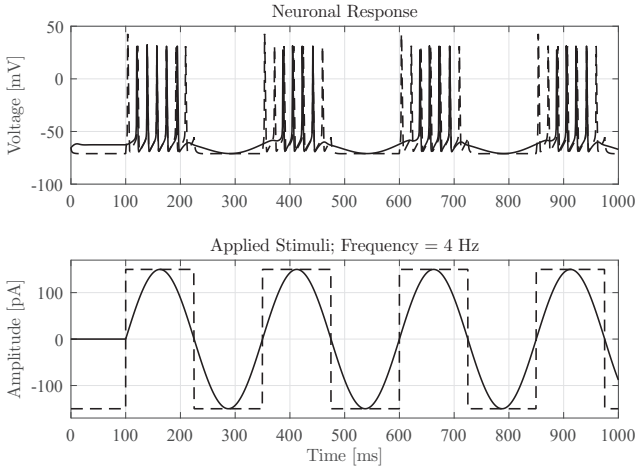

Figure 3.5: Upper graph: the neuronal response affected by rectangular pulse current and sine wave. Lower graph: applied stimuli with amplitude of 130 pA and period 250 ms. The responses are obtained with an open-source simulator NEURON.

respectively. The parameter τ_c stands for the time scale of a variable characterizing the membrane's dynamics, C represents a membrane capacitance, parameter α is proportional to effective leak conductance, and β is proportional to the conductance

measuring a membrane potential variation. Both α and β can be experimentally measured for type-specific cells, and remain unaltered during a stimulation process [32].

3.2.2 Spiking Mechanism

As spoken of earlier, a randomness in the intra-neuronal communication pathway must be accounted due to the intrinsic dynamics of neurons. Some of the processes that lead to random neural behavior are variable levels of arousal and attention, various biophysical processes that affect neuronal firing, cognitive processes that take place during a stimulation, and the stimulation itself.

The straightforward way of introducing the randomness to the intra-neuronal communication analysis is through the mechanism labeled with module **B** in Fig. 3.2, which is further detailed in Fig. 3.6. Its input is the subthreshold membrane potential v_m. Depending on the probability of spiking, the suprathreshold membrane voltage ($v_m > V_{threshold}$) may lead to the spike generation. Conversely, spontaneous generation of spikes at the time of subthreshold voltages at the input ($v_m < V_{threshold}$) is omitted from the analysis in order to keep the reasoning simple. The spike generation mechanism from Fig. 3.6 resembles a binary Z-channel.

The probabilities P_s and P_{ns} that come from Fig. 3.6 depend on complex physiological processes to compensate the simple randomness mechanism. Namely, the spiking probability, denoted as P_s, can be set to 1 when both the ARP and RRP have elapsed, and v_m is above the threshold. During the ARP and v_m below the threshold, the probability P_s can be set to 0. During the RRP, the threshold is higher immediately after a spike and then decays back (usually exponentially [35]) to its resting value. Here, the threshold can be held constant within the RRP, while its 'jitter' is caught by the spiking probability. Since the spiking probability within the RRP increases with time and suprathreshold amplitude of v_m, the probability

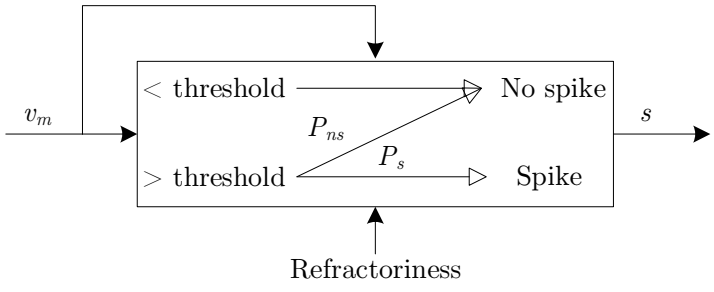

Figure 3.6: Spike release mechanism within the intra-neuronal communication model corresponding to module **B** from Fig. 3.2.

P_s within the corresponding period can be defined as

$$P_s(t, v_m, T^{RRP}) = \frac{\exp\left(\frac{t}{|v_m - V_{threshold}|}\right) - 1}{\exp\left(\frac{T^{RRP}}{|v_m - V_{threshold}|}\right) - 1}. \tag{3.3}$$

Duration of RRP is denoted with T^{RRP}. Transient probability P_{ns}, in contrast, exhibits the opposite behavior relative to that of the probability P_s, i.e., $P_{ns} = 1 - P_s$. $V_{threshold}$ is the threshold for an AP initiation.

Note that not only does the suprathreshold voltage directly drive the probabilities P_s and P_{ns} within the RRP, but also indirectly, through the impact on duration of the ARP: the larger the suprathreshold amplitude, the smaller the ARP (or equivalently, the higher the spiking rate) [82]. The ARP is, however, lower bounded, i.e., $T^{ARP} \geq T^{ARP}_{\min}$, because the neuron cannot fire with the rate higher than that physiologically determined[1]. Limited spike duration is also confined to habituation of (almost) all biological micro- and macro-systems. Hence, a duration of the ARP can be modeled with the following equation:

$$T^{ARP} = T^{ARP}_{\min} + (T^{ARP}_{\max} - T^{ARP}_{\min}) \exp\left(-|v_m - V_{threshold}|\right), \tag{3.4}$$

where $T^{ARP}_{\min}$ and $T^{ARP}_{\max}$ denote the minimum and maximum ARP duration, respectively. An output of the module **B** is a randomly generated spiking sequence denoted as $s(t)$.

3.2.3 Axonal Mechanism

The spiking sequence $s(t)$ propagates through the (myelinated or unmyelinated) axon which is represented by the module **C** in Fig. 3.2.

The experiment on the axonal transmission in the CA[2] region of rat's brain reported in [108], reveals that for low frequency firing rate, spikes propagate through the axon without distortion, and nearly no failure occurs. For high frequency firing rate, the amplitude of the consecutive spikes might decrease in some branches. From the result of this experiment, the axon can potentially be modeled as a modified version of a second order Butterworth filter [13]. According to other physiological reports in the literature (see [110] and references therein), axons act more complex than low-pass filters as their dynamics leads to the variations in the shape and delay of spikes during axonal transmission. This stems from axonal dependency on the previously fired spikes and recovering phases from suppression of axonal functionality which is observed after prolonged high frequency stimulations. This suggests modeling the

[1] For instance, when the sine wave current with frequencies ranging from 40 to 120 Hz is given at the input, the same number of spikes is measured after a certain amplitude value of stimuli [69].

[2] CA refers to *Cornu Ammonis*.

Parameter Value	Description
$T = 10$ [s]	Stimulus period
$I = 100$ [pA]	Injecting current amplitude [106]
$f_{low} = 0$ [Hz]	ZAP current low frequency
$f_{high} = 250$ [Hz]	ZAP current high frequency
$C = 10$ [nF]	Membrane's capacitance [35]
$\tau_c = 1$ [ms]	Cell's dynamics time constant [35]
$V_{rest} = -65$ [mV]	Resting potential
$V_{threshold} = -55$ [mV]	Threshold firing voltage
$SNR = 3$ [dB]	Signal-to-noise ratio per sample
$T_{\min}^{ARP} = 1$ [ms]	Minimum ARP duration
$M = 25$	Number of bins within T period

Table 3.1: List of simulation parameters used in Chapter 3, Section 3.3.

axon as a system with memory. The reader is referred to [110] for detailed study on this issue.

Although axons are important in neural signaling, modeling of complex axonal transmission is not targeted here due to the lack of a firm clarification on the filtering nature of axons, and more detailed information about efficient mechanism the cell uses to filter the axonal disturbances and regenerate the signal. Hence, the author presumes the highly reliable property of the axonal channel (see [50], and discussion about the nodes of Ranvier from [35], Chapter 6) adjusted to its frequency band-limited input. Under this assumption, the axon can be approximated as an ideal all-pass filter and the frequency response (in a frequency range of interest) of the module $\mathbf{C}$ as $\mathbf{C}(f) = 1$. This simplification does not limit the validity of the results presented in the following section.

3.3 Numerical Results

This section is intended to graphically corroborate the understanding of the neuronal behavior. A set of parameters is adopted to define a virtual sample neuron used under simulation scenarios and the simulation framework[3] (see Table 3.1). Intuitively, the neuronal response to the specified stimuli should depend on the intensity of the stimuli: the stronger the excitation is, the more likely neuron is to fire and produce the higher output spiking rates.

As in Section 3.2.1, the performance of the proposed stochastic representation of

[3]Note that the cell simulated in this section follow the foregoing guidelines and differentiates from the Hodgkin-Huxley cell used in Section 3.2.1. The simulation framework is implemented in MATLAB.

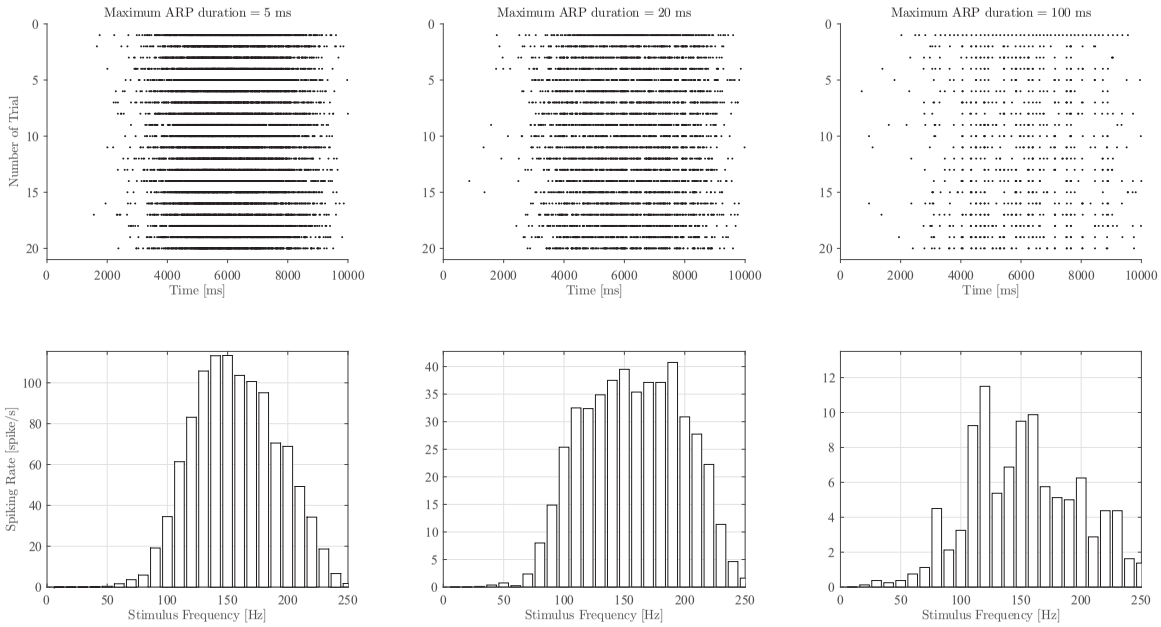

Figure 3.7: Spiking raster-plots (upper panels) and corresponding Peri-Stimulus Time Histograms (lower panels) as functions of different durations of maximum absolute refractory period ($T_{\max}^{ARP}$). Impedance parameter values are $\alpha = 0.2$ and $\beta = 1.1$. Realizations are shown for $N = 20$ trials.

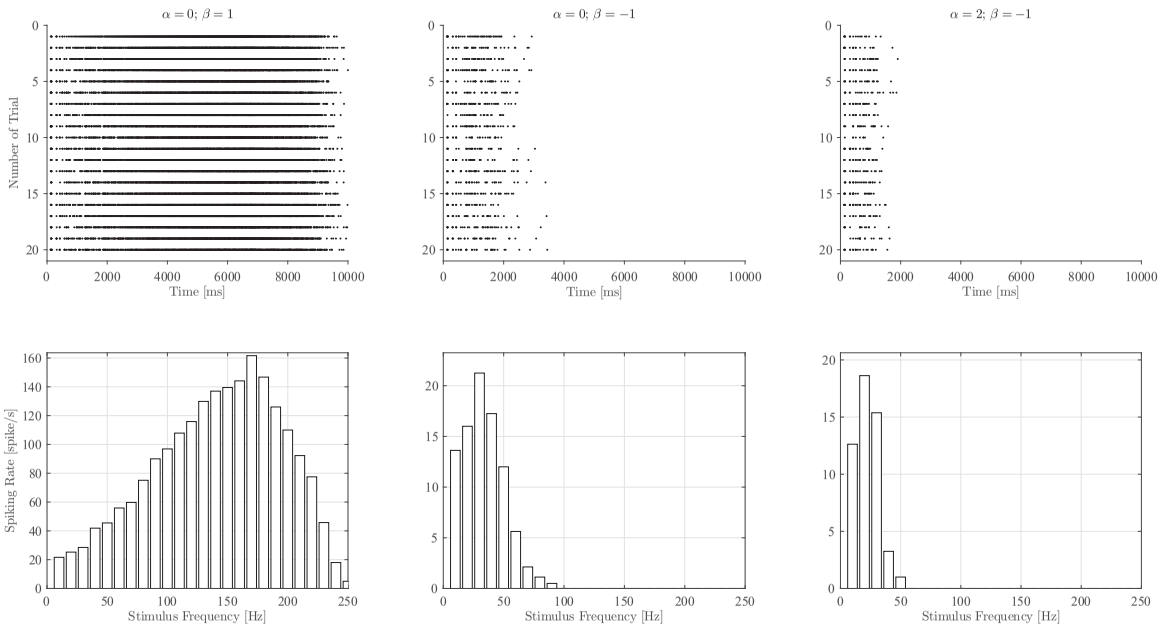

Figure 3.8: Spiking raster-plots (upper panels) and corresponding Peri-Stimulus Time Histograms (lower panels) as functions of different membrane impedance parameters (α and β). Maximum absolute refractory period $T_{\max}^{ARP} = 5$ ms. Realizations are shown for $N = 20$ trials.

end-to-end intra-neuronal communication is tested by probing a sample cell with an input ZAP current that linearly sweeps through frequencies $(0 - 250$ Hz) over time. To this end, two sets of raster-plots displayed in Fig. 3.7 and Fig. 3.8, upper panels, are generated representing the output spiking sequences (with spike timings) for 20 trials. The stochastic representation of the intra-neuronal communication that provides raster-plots of neuronal spiking, helps to evaluate the output spiking rate as a function of the (stimuli) frequency by drawing a bar-graph histogram of the times at which the cell fire.

The so-called Peri-Stimulus Time Histogram (PSTH) is often used in neuroscience to visualize the rate and timing of neuronal spike discharges in relation to an external stimulus. To draw a PSTH, spike trains recorded from a sample neuron are aligned with the onset of an identical stimulus repeatedly presented and then superimposed in time. The PSTHs corresponding to spike timings shown in Fig. 3.7 and Fig. 3.8, upper panels, are plotted as functions of the (stimuli) frequency in Fig. 3.7 and Fig. 3.8, lower panels, respectively.

Raster-plots and PSTHs displayed in Fig. 3.7 are evaluated given $\alpha = 0.2$ and $\beta = 1.1$ [112] that define the module **A**, i.e., the frequency-selective membrane. The normalized frequency-dependent magnitude of the module **A** shown in Fig. 3.9 (solid line) follows a trajectory that resembles one representing a band-pass filter, as discussed in Section 3.2.1. Moreover, three scenarios with different $T^{ARP}_{\max}$ are simulated. Note that $T^{ARP}_{\max}$ and $T^{ARP}_{\min}$ (set to 1 ms) affect the T^{ARP} and T^{RRP}, which again affect the probability of spiking P_s (see Eq. (3.3)) - smaller the T^{ARP}, larger the spiking probability. This effect is clearly observed in Fig. 3.7. The histogram-peaks observed when $T^{ARP}_{\max} = 100$ ms come from the spike counting process performed within each fixed-width bin. In case the bin-width used to create PSTHs are smaller, the peaks would be less. Note that the same applies when $T^{ARP}_{\max} = 5$ ms and $T^{ARP}_{\max} = 20$ ms, where the peaks are, however, not observed for the given bin-width due to higher spiking rate values.

Raster-plots and PSTHs displayed in Fig. 3.8 are evaluated given the $T^{ARP}_{\max} = 5$ ms and $T^{ARP}_{\min} = 1$ ms. Three scenarios with different parameters (α and β) of module **A** are simulated. The intra-neuronal representation in presented scenarios also shows the response to the DC stimulus, which is in line with the normalized frequency-dependent magnitudes of the module **A** shown in Fig. 3.9 (for detailed elucidation, refer to [125]).

To the best of the author knowledge, there exists no real data that may be used to verify the accuracy of the proposed model[4]. The computer validation is practicable with the Hodgkin-Huxley neuron model with frequency-selective membrane that is used to prove a tendency of the virtual cell to first increase and then decrease its spiking rate (see Fig. 3.7), in a scenario where the frequency of the stimulus is in-

[4]The proposed stochastic representation is, however, not intended to outperform other computational models, but rather to offer an alternative engineering based description which would leverage the understanding of the primal neuronal processes.

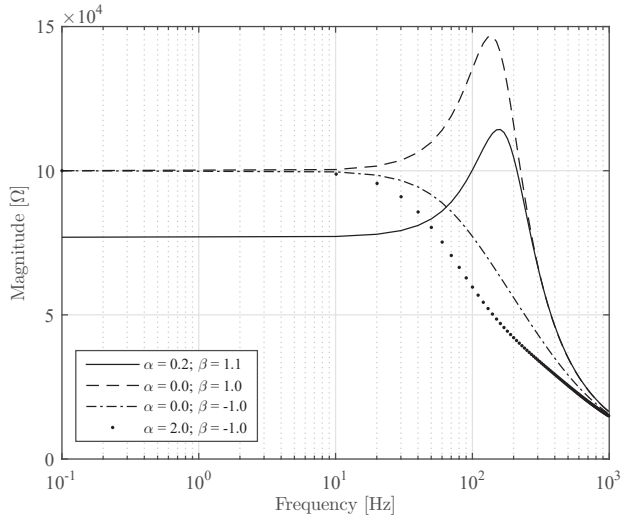

Figure 3.9: The magnitude of membrane's impedance given four sets of parameter values ($\alpha = 0.2, \beta = 1.1$; $\alpha = 0.0, \beta = 1.0$; $\alpha = 0.0, \beta = -1.0$; $\alpha = 2.0, \beta = -1.0$) used under simulation scenarios discussed in Chapter 3.

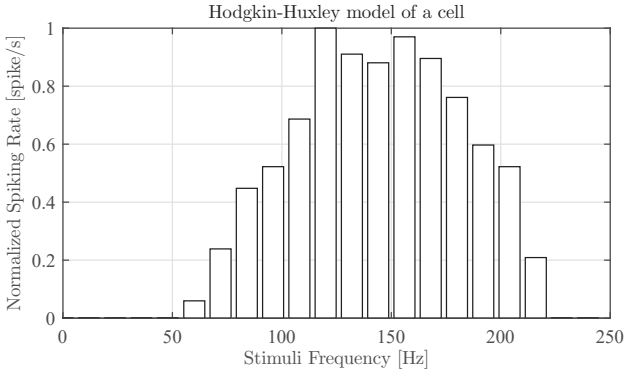

Figure 3.10: The bar-graph diagram representing the amplitude normalized spiking rate generated with an open-source simulator NEURON. A cell with frequency-selective membrane is simulated.

creased and its amplitude is kept constant (100 pA)[5]. With an open-source simulator NEURON [27], the spiking rate is generated as a function of stimuli frequency and displayed in Fig. 3.10. The property of Hodgkin-Huxley cell with frequency-selective membrane to first increase and then decrease its spiking rate with the (stimuli) fre-

[5]Increase in stimuli amplitude in effect leads to an increased firing rate [82].

quency may serve as a proof of validity of the model presented in Section 3.2. The two models, however, cannot be directly compared because of conceptually different parameters used for their definition. In addition, the model presented is by far simpler relative to the Hodgkin-Huxley model.

3.4 Concluding Remarks

Transmission of electrochemical pulses (spikes) takes place from the neuronal front-end interface (dendrites) to the pre-synaptic terminal and in this chapter has been referred to as the intra-neuronal communication. The study has been conceptualized on i) deterministic sub- and supra-threshold oscillations of the cellular membrane's potential, and ii) stochastic spike threshold variability and instability of spiking duration. From the analysis of the spiking raster-plots and corresponding peri-stimulus time histograms created under specified stimulation scenarios, it can be inferred that the power spectral density of the stimuli and stimuli amplitude are both crucial in neuronal behavior and relevant processes that may take place within the neuronal nano-network.

The primal goal of this study has been to leverage the understanding of the complex mechanisms related to the neuronal stimulation, encoding, and intrinsic transmission over neuronal compartments. On the one hand, the description of the intra-neuronal system with an engineering approach is of interest in the design of bio-inspired circuits and techniques attempting to mimic the neuronal behavior. On the other hand, the description of the intra-neuronal system with an engineering approach is of interest for the design of stimulation strategies to obtain a certain effect on neuronal responses. This is pivotal in neuroprosthetics to compensate for loss of sensory input or motor control.

Chapter 4

Deterministic Model of Inter-Neuronal Communication: Bipartite Synapse

4.1 Introduction

This chapter considers the *molecular neuronal channel* introduced in Chapter 1, Section 1.2.2, aiming to propose an alternative description of the neuronal communication system within bipartite synapses. The mechanisms considered here are introduced in Sections 2.2.3 and Sections 2.2.4.

In the bipartite synapse, the electrochemical signals are transduced into molecular signals that are communicated following the law of diffusion. The diffusion-based molecular communication is confined to the transmission of particles/neurotransmitters between two neurons, the pre- and post-synaptic neuron. In the molecular communication pathway, the pre-synaptic terminal within the axon of the pre-synaptic neuron acts as the *molecular transmitter*, the synaptic cleft as the *molecular channel*, and the post-synaptic terminal at the next inter-connected neuron as the *molecular receiver*. Hereinafter, the synaptic neuronal transmission is referred in the thesis as the **inter-neuronal communication**. The communications equivalent representation of the inter-neuronal communication within the overall neuron-to-neuron communication system is highlighted in Fig. 4.1.

In order to obtain analytical expressions for measures of inter-neuronal efficacy, some simplifying assumptions are made. In the model presented, the synapse is assumed to be highly reliable which sets the vesicle release probability to unity and neglects the variability in post-synaptic response. Then, sequential processes along the remaining communication pathway between two neurons can be *deterministically characterized* (under additional limitations provided in the following) with a frequency response as in classic communications systems. Hence, neurons that make highly reliable

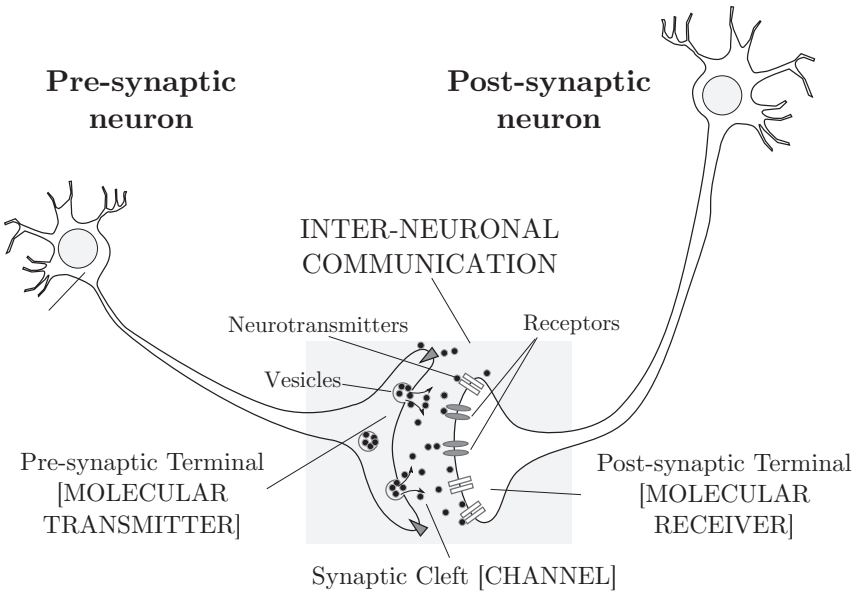

Figure 4.1: The inter-neuronal communication equivalent representation considered in Chapter 4.

synapses (e.g., neurons in the spinal cord) are considered here.

Under this assumption, the aim of this chapter is to develop a firm analytical framework linked with relevant segments in the molecular communication pathway. An engineering approach is adopted, where the chemical and ionic processes are represented with signals, and the biological mechanisms are modeled as input-output systems characterized by a *frequency response*.

Unlike previous models reviewed in Section 2.3.2, the model presented here maps specific neuronal blocks to electrical circuitry. The reasoning and benefit from mapping/mimicking biological systems to ordinary electrical circuitry stand in the knowledge of their dynamics and frequency responses. This distinctive method of equivalence is how dynamics of individual biological blocks are revealed. Another benefit of using a circuital representation resides in the possibility of carrying out a stimulus-response analysis for each process through the corresponding frequency response. In these terms, one can observe to what extent an input impacts on the output of a given process. Moreover, the engineering representation of the relevant processes in this study completely relies on neuroscientific theory and analytical expressions from validated mathematical models that cover often overlooked realistic physiological phenomena, e.g., the effect of *calcium signaling*[1] on vesicle releases.

[1]Calcium signaling refers to the movement of calcium ions from the extra-cellular compartments to the intra-cellular compartments.

The stimulus-response analysis and equivalent transfer functions derived in the following:

- allow one to exploit the relations between different quantities involved in the communication pathway, which should contribute in understanding an impact of the spiking rate to the modules composing a neural synapse, and, ultimately, the receiving peer;
- provide further tools for design and implementation of bio-mimetic devices mimicking the behavior of neurons at micro- and nano-scale;
- help understanding the ability of neurons to dynamically wire over time (neuroplasticity); understanding the neuroplasticity at small-scale is a first step towards understanding the neuroplasticity at large-scale networks of neurons.

The remainder of this chapter is organized as follows. Section 4.2 introduces the schematic representation of the relevant processes along the communication pathway between the pre- and post-synaptic neuron within the bipartite synapse. Sections 4.3, 4.4 and 4.5 propose the representation of the bipartite synapse as a signal processing unit, describing the circuital representation of the biological processes in the pre-synaptic terminal, the synaptic cleft, and the post-synaptic terminal, respectively. In Section 4.5, numerical results are discussed. Section 4.6 brings the conclusions with some observations for future works and prospectives.

4.2 Inter-connected Neuronal Compartments as Signal Processing Units

The neurons that make highly reliable synapses are the subject of the study to derive a deterministic model of synaptic transmission[2]. This section brings a thorough derivation procedures of dynamics/frequency responses of each relevant block by applying a method of equivalence between biological systems and electrical circuitry.

The spiking sequence $s(t)$ at the output of the intra-neuronal communication model is stochastic since its spiking times are variable from trial-to-trial. At this point, however, the analysis treats the *averaged neuronal behavior* represented via its *trial-averaged spiking sequence* $\overline{s(t)}$[3], aiming to define a framework of synaptic transmission in terms of the frequency response, i.e., the normalized magnitude and phase (see Eq. (4.9) and Eq. (4.11) bellow, respectively). To this end, the chemical and ionic processes are represented as signals with a goal to inspect the synaptic transmission of neurotransmitters as diffusion-based particle communication. Considering a deterministic model that describes average system behavior, the complication

[2]Note that some neurons are characterized by their unreliable and random synaptic behavior.

[3]The trial-averaged $\overline{x}$ for any quantity x is the sum of the values of x obtained from many trials involving the same stimulus, divided by the number of trials.

Symbol	Description	Input	Output
(**D**)	Pre-synaptic Neuron	s_t	$[\mathrm{Ca}^{2+}]_{\mathrm{pre}}$
(**E**)	Pre-synaptic Neuron	$[\mathrm{Ca}^{2+}]_{\mathrm{pre}}$	r_{pre}
(**F**)	Synaptic Cleft	r_{pre}	c_{post}
(**G**)	Post-synaptic Neuron	c_{post}	V_{EPSP}

Table 4.1: Input/output signals analyzed in Chapter 4.

between calcium ion concentration and vesicle release probability is evaded.

It is assumed that the information encoded in a spiking sequence modulates the particle (neurotransmitter) concentration at the transmitter side, i.e., the pre-synaptic terminal. Neurotransmitters then propagate through the synaptic cleft, which contains homogeneous fluid medium, following the law of diffusion process. At the receiver side, i.e., the post-synaptic terminal, neurotransmitters from the cleft bind to the AMPA receptors, and evoke the EPSP. Thereby, the analysis of synaptic transmission is distributed into three modules depicted in Fig. 3.2, lower stage:

i) the *transmitter*,

ii) *channel*, and

iii) *receiver*.

The contribution with the transmitter module, which is different from and more complicated than a classic molecular transmitter [103] is highlighted. Owing to neurotransmitter propagation through the channel and neurotransmitter reception both being subject to general particle diffusive-based molecular communication paradigm, pioneering results from [103] are adopted to define an overall physical end-to-end model of synaptic transmission. As stated in Section 4.1, the synaptic transmission is referred to as the *inter-neuronal communication*.

In what follows, a description of the neuron-to-neurons system is proposed by means of circuital representations of the biological processes described so far. Taking Fig. 3.2 as a reference, the input/output circuit for each module (**D**, **E**, **F** and **G**) is defined, identifying and discussing the input and output processes and their equivalent representations as signals (refer to Table 4.1).

4.3 Neurotransmitter Emission

In the model of inter-neuronal communication, emission is performed by the pre-synaptic terminal. The pre-synaptic terminal, however, functions as the transceiver module composed of two sub-modules. They are named here as the *Calcium Gateway* (CaG) and the *Molecular Transmitter* (MTx), respectively, and are labelled as sub-

modules **D** and **E** in Fig. 3.2. The CaG sub-module first receives Ca^{2+} and then enables the succeeding block within the pre-synaptic terminal, the MTx sub-module, to perform its task of emitting neurotransmitters. Calcium signaling is, thereby, substantial in adequate functioning of the neural system.

4.3.1 Calcium Gateway

The spiking sequence is an input to the CaG sub-module, denoted with **D** in Fig. 3.2. Its output is the magnitude of calcium ion concentration at the pre-synaptic terminal, $[Ca^{2+}]_{\text{pre}}$, which is a result of ionic inward Ca^{2+} current through VGCCs during a spike. It is presumed that the sub-module **D** can be considered as a Linear Time-Invariant (LTI) block with its impulse response $h_{\mathbf{D}}(t)$ depending on the calcium influx as well as the internal buffer uptake. Referring to sub-module **D** as LTI system is possible under further assumption that neural activity cannot cause significant decrements in extra-cellular Ca^{2+} levels that might prevent calcium influx and mediate a form of short-term synaptic depression.

The neuronal response generates a contribution to $\overline{[Ca^{2+}]_{\text{pre}}}$ proportional to the number of spikes over a given time interval. Given $\overline{s(t)}$ as input, the average output concentration is given by [35]:

$$\overline{[Ca^{2+}]_{\text{pre}}} = \kappa_1 \int_{-\infty}^{t} h_{\mathbf{D}}(\tau)\overline{s(t-\tau)}\mathrm{d}\tau, \tag{4.1}$$

where factor κ_1 converts the result to moles.

Referring to [35, Chapter 1], the trial-averaged neural response function $\overline{s(t)}$ can be replaced with the time-dependent spiking rate[4], $r_{spike}(t)$, within any well-behaved integral. Then, the following applies (see [35, Eq. (1.6)]):

$$\int h_{\mathbf{D}}(\tau)\overline{s(t-\tau)}\mathrm{d}\tau = \int h_{\mathbf{D}}(\tau) r_{spike}(t-\tau)\mathrm{d}\tau, \tag{4.2}$$

and, equivalently,

$$\mathbf{H}_{\mathrm{D}}(jf)\overline{S(jf)} = \mathbf{H}_{\mathrm{D}}(jf)R(jf), \tag{4.3}$$

where $\mathbf{H}_{\mathrm{D}}(jf)$ is the frequency response, and $\overline{S(jf)}$ and $R(jf)$ are the Fourier transforms of $\overline{s(t)}$ and $r_{spike}(t)$, respectively. In the analysis that follows, $r_{spike}(t)$ is considered instead of $\overline{s(t)}$.

To determine $h_{\mathbf{D}}(t)$ and the corresponding frequency response, the dynamics of concentration resulting from neuronal activity is inspected. In [87], it is described as

$$\frac{\mathrm{d}[Ca^{2+}]_{\text{pre}}}{\mathrm{d}t} = -\frac{1}{\tau_{\mathrm{Ca}}}[Ca^{2+}]_{\text{pre}} + \eta\mathcal{H}(s - 35\ \mathrm{mV}), \tag{4.4}$$

[4] The time-dependent spiking rate at time t is computed by counting all the spikes that occurred at $\overline{s(t)}$ between times t and $t + \Delta t$, and dividing this by interval Δt.

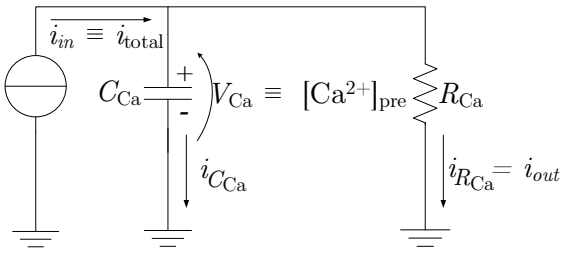

Figure 4.2: Calcium gateway sub-module as equivalent RC circuit model.

where τ_{Ca} is the time constant of Ca-buffer uptake, η is a factor given in [mole/second] determining the rate of Ca^{2+} flow through the membrane, $\mathcal{H}$ is the Heaviside function, and $s(t)$ is the spiking signal (the input of the block **D**). Applying electrical circuit analysis, the CaG sub-module is identified with a parallel RC circuit[5] driven by i_{in} current, as shown in Fig. 4.2. From the Kirchhoff's current law, the input current is equal to the sum of the current flowing through the resistor R_{Ca}, and the current flowing through the capacitor C_{Ca}, i.e., $i_{in} = i_{R_{\text{Ca}}} + i_{C_{\text{Ca}}}$.

The input current i_{in} is related with the ionic current described with $i_{\text{Ca}} = \nu\eta\mathcal{H}(s - 35\text{ mV})$, where ν is a factor that converts from [mole/second] to [coulomb/second]. In active status ($i_{\text{Ca}} \neq 0$), there is an elevation in calcium ion concentration due to the influx of Ca^{2+} from the extra-cellular environment – a process corresponding to the capacitor charging phase. In idle state ($i_{\text{Ca}} = 0$), there is a reduction in calcium ion concentration due to the Ca^{2+} binding performed by intra-cellular buffers – a process corresponding to the capacitor discharging phase. Hence, the capacitor voltage V_{Ca} from Fig. 4.2 is related to $[\text{Ca}^{2+}]_{\text{pre}}$. With this mapping on board and $i_{in} = i_{R_{\text{Ca}}} + i_{C_{\text{Ca}}}$, one gains

$$i_{\text{Ca}} = C_{\text{Ca}}\frac{\xi \text{d}[\text{Ca}^{2+}]_{\text{pre}}}{\text{d}t} + \frac{\xi[\text{Ca}^{2+}]_{\text{pre}}}{R_{\text{Ca}}}, \tag{4.5}$$

where ξ is a factor that converts from [mole] to [volt]. Writing Eq. (4.4) in a rearranged fashion using $i_{\text{Ca}} = \nu\eta\mathcal{H}(s - 35\text{ mV})$, one gains

$$i_{\text{Ca}} = \nu\left(\frac{\text{d}[\text{Ca}^{2+}]_{\text{pre}}}{\text{d}t} + \frac{1}{\tau_{\text{Ca}}}[\text{Ca}^{2+}]_{\text{pre}}\right). \tag{4.6}$$

By comparing Eq. (4.5) with Eq. (4.6), equivalent resistor and capacitor values are computed from analyzed RC circuit as

$$R_{\text{Ca}} = \frac{\xi\tau_{\text{Ca}}}{\nu}, \quad C_{\text{Ca}} = \frac{\nu}{\xi}, \tag{4.7}$$

[5]Note that it is not intended to use electrical circuitry for intra-body information transmission. The reasoning and benefit from mapping biological systems to electrical circuitry stand in the knowledge of their dynamics and frequency responses, as stated previously.

respectively. Hence, the RC network has the equivalent time constant as that of calcium decay, i.e., $R_{\mathrm{Ca}}C_{\mathrm{Ca}} = \tau_{\mathrm{Ca}}$.

As outlined, the aim is to define the normalized magnitude and phase of the inter-neuronal communication system in terms of the system frequency. Given the spiking rate at the input, the system frequency refers to the frequency spectrum of $r_{spike}(t)$. Hence, it is of interest to compute the frequency response of analyzed module, which from the RC circuit shown in Fig. 4.2, is given as

$$\mathbf{H}_{\mathrm{D}}(jf) = (1 + j2\pi f R_{\mathrm{Ca}}C_{\mathrm{Ca}})^{-1} = (1 + j2\pi f \tau_{\mathrm{Ca}})^{-1}. \tag{4.8}$$

The *normalized magnitude* $\Gamma_{\mathbf{H}_{\mathrm{D}}}(f)$ of the CaG sub-module is

$$\Gamma_{\mathbf{H}_{\mathrm{D}}}(f) = \frac{|\mathbf{H}_{\mathrm{D}}(f)|}{\max_f(|\mathbf{H}_{\mathrm{D}}(f)|)}. \tag{4.9}$$

The *group delay* $\tau_{\mathbf{H}_{\mathrm{D}}}(f)$ can be computed as

$$\tau_{\mathbf{H}_{\mathrm{D}}}(f) = -\frac{\mathrm{d}\phi_{\mathbf{H}_{\mathrm{D}}}(f)}{\mathrm{d}f}, \tag{4.10}$$

where $\phi_{\mathbf{H}_{\mathrm{D}}}(f)$ denotes the phase of the sub-module **D** and is defined as

$$\phi_{\mathbf{H}_{\mathrm{D}}}(f) = \mathrm{atan}\left(\frac{\Im(\mathbf{H}_{\mathrm{D}}(f))}{\Re(\mathbf{H}_{\mathrm{D}}(f))}\right). \tag{4.11}$$

4.3.2 Molecular Transmitter

The task of the succeeding MTx block denoted with **E** in Fig. 3.2 is to modulate the neurotransmitter concentration according to the intra-cellular concentration level at the preceding block. Given the $[\mathrm{Ca}^{2+}]_{\mathrm{pre}}$ as an input to the MTx, further modeling, including the neurotransmitter emission, the neurotransmitter propagation through the channel, and the neurotransmitter reception largely resemble the modeling of general molecular communication system [103]. The mathematical framework defined for the particle emission, the particle propagation and the particle reception processes within the molecular communication system are, therefore, adopted in the following to complete a definition of peer-to-peer neural communication system.

Depending on $[\mathrm{Ca}^{2+}]_{\mathrm{pre}}$ as an input to the MTx sub-module, the neurotransmitters are either released or not released from the vesicles. On average, the output of the MTx sub-module is characterized by the neurotransmitter release rate r_{pre}. This rate is defined as the time derivative of the neurotransmitter concentration in the proximity of the pre-synaptic terminal, $\mathrm{d}c_{out}/\mathrm{d}t$, whose level is variable due to the dynamics of neurotransmitters leaving the pre-synaptic terminal. Hence, the sub-module **E** is considered here as an LTI system and identified with a parallel RC

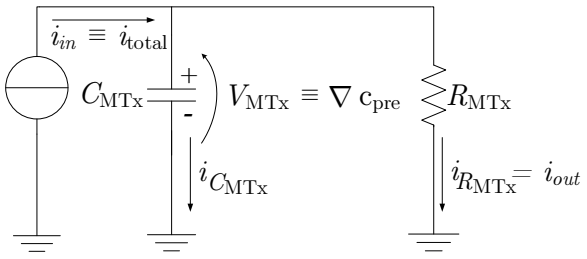

Figure 4.3: Molecular transmitter sub-module as equivalent RC circuit model.

circuit (as shown in Fig. 4.3). Referring to sub-module **E** as LTI system is possible if the vesicle depletion[6] is neglected.

To derive the frequency response of the MTx sub-module, the procedure for the particle emitter module within the general molecular communication channel is adopted [103]. The quantity of neurotransmitter concentration gradient ∇c_{pre} is introduced and equated with the voltage V_{MTx} from Fig. 4.3, i.e., $V_{\text{MTx}} = \varphi \nabla c_{\text{pre}}$, where φ is a factor that converts from [mole/mm^4] to [volt]. The neurotransmitter release rate r_{pre} is proportional to the output current i_{out}, i.e., $i_{out} = \rho r_{\text{pre}}$, where ρ is a factor that converts from [mole/second] to [coulomb]. The effect of the neurotransmitter release rate r_{pre} can be observed as the effect of the neurotransmitter flux J_{pre} given by the net neurotransmitter concentration leaving the pre-synaptic terminal, i.e., $r_{\text{pre}} = \sigma J_{\text{pre}}$, and σ is a coefficient given in [mm^2], as J_{pre} is given in [mole $\cdot$ mm^{-2} $\cdot$ second^{-1}]. The Fick's first law is used to relate the flux J with the concentration gradient ∇c [102]:

$$J = -D \nabla c, \tag{4.12}$$

where D is the diffusion coefficient. In this case, J_{pre} and ∇c_{pre} correspond to J and the negative of the concentration gradient ∇c at the MTx, respectively. Since i_{out} corresponds to J_{pre}, i.e., $i_{out} = \rho \sigma J_{\text{pre}}$, and V_{MTx} to ∇c_{pre}, i.e., $V_{\text{MTx}} = \varphi \nabla c_{\text{pre}}$, then

$$i_{out} = \rho \sigma D V_{\text{MTx}} / \varphi, \tag{4.13}$$

and the resistance $R_{\text{MTx}} = \varphi / (\rho \sigma D)$. D is considered as a constant value for the fluid medium inside the synaptic cleft.

An input signal to MTx is $[\text{Ca}^{2+}]_{\text{pre}}$. Analogous to [103], the input signal is observed through the desired neurotransmitter release rate $\hat{r}_{\text{pre}}$ at the MTx location ($\hat{r}_{\text{pre}} = [\text{Ca}^{2+}]_{\text{pre}} / \tau$, and τ is given in [second]), and then identified with i_{in} from Fig. 4.3, i.e., $i_{in} = \rho \hat{r}_{\text{pre}}$. From the Kirchoff's current law, the current through the capacitor is $i_{C_{\text{MTx}}} = i_{in} - i_{R_{\text{MTx}}}$. Besides, $\nabla c_{\text{pre}} = (c_{in} - c_{out}) / \sigma^2$ [103], where c_{in} denotes the

[6]Note that normal neural activity can though cause vesicle depletion in which case release of neurotransmitters does not follow regardless the level of $[\text{Ca}^{2+}]_{\text{pre}}$.

inside neurotransmitter concentration. Deriving the previous equation, one obtains

$$\frac{\mathrm{d}\nabla c_{\mathrm{pre}}}{\mathrm{d}t} = \frac{1}{\sigma^2}\left(\frac{\mathrm{d}c_{in}}{\mathrm{d}t} - \frac{\mathrm{d}c_{out}}{\mathrm{d}t}\right) = \frac{1}{\sigma^2}\left(\hat{r}_{\mathrm{pre}} - r_{\mathrm{pre}}\right). \tag{4.14}$$

As $\nabla c_{\mathrm{pre}} = V_{\mathrm{MTx}}/\varphi, \hat{r}_{\mathrm{pre}} = i_{in}/\rho$ and $r_{\mathrm{pre}} = i_{out}/\rho$, the following equation yields:

$$\frac{1}{\varphi}\frac{\mathrm{d}V_{\mathrm{MTx}}}{\mathrm{d}t} = \frac{1}{\sigma^2\rho}(i_{in} - i_{out}). \tag{4.15}$$

Note that from Eq. (4.15), the capacitor value becomes $C_{\mathrm{MTx}} = \sigma^2\rho/\varphi$. Hence, the RC network has the equivalent time constant given as $R_{\mathrm{MTx}}C_{\mathrm{MTx}} = \sigma/D$, whose dimension is in [second], as should be. Ultimately, the frequency response of the MTx sub-module is computed from the RC circuit as

$$\mathbf{H}_{\mathrm{E}}(jf) = (1 + j2\pi f R_{\mathrm{MTx}}C_{\mathrm{MTx}})^{-1} = \left(1 + j2\pi f\sigma/D\right)^{-1}. \tag{4.16}$$

4.4 Neurotransmitter Diffusion

When the MTx releases the neurotransmitters, they propagate through the synaptic cleft which serves as the communication channel. Particles follow the rules of the diffusion process to propagate through the channel towards a homogenization, and reach the post-synaptic terminal. Nonetheless, considering a deterministic model that describes average system behavior, the channel can be though considered as an LTI system and denoted with **F** in Fig. 3.2, whose input is the neurotransmitter release rate r_{pre}. The neurotransmitter concentration at the receiver side (post-synaptic terminal), denoted as c_{post}, is considered as the channel output.

Following [50] and [103], the impulse response of the system, $g_d(d,t)$, stems from the particle concentration distribution flux study:

$$g_d(d,t) = \exp\left(-\frac{t}{2\tau_d}\right)\frac{\cosh\left(\sqrt{t^2 - (d/c_d)^2}\right)}{\sqrt{t^2 - (d/c_d)^2}}\mathcal{H}(t - d/c_d), \tag{4.17}$$

where $c_d = \sqrt{D/\tau_d}$ is the wave-front speed, τ_d is the relaxation time, d is the distance from the pre-synaptic terminal, and $\mathcal{H}$ is the Heaviside function. Hence, the frequency response of the channel module is

$$\mathbf{H}_{\mathrm{F}}(jf) = \int_{-\infty}^{\infty} g_d(d_{\mathrm{post}}, t)\mathrm{e}^{-j2\pi ft}\mathrm{d}t, \tag{4.18}$$

where d_{post} is the distance from the pre- to the post-synaptic terminal. Eq. (4.18) is numerically computed.

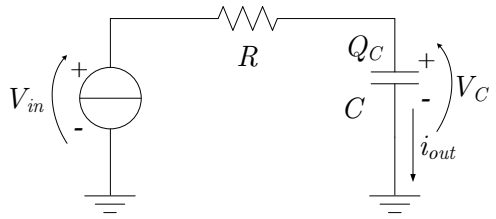

Figure 4.4: Post-synaptic terminal as equivalent RC circuit model.

4.5 Neurotransmitter Reception

The post-synaptic terminal acting as the receiver module (considered as an LTI system), senses the neurotransmitter concentration c_{post} by means of the AMPA receptors, which are assumed to be equally exposed to the c_{post}. As an input to the receiver, denoted with **G** in Fig. 3.2, the neurotransmitter concentration modulates the output referred to as the EPSP, V_{EPSP}.

The output signal is proportional to the ratio $\mathfrak{r}$ of the number of bound chemical receptors (with rate constant k_b) over the total number of the receptors N_R [103]. Since plasticity (dynamic wiring of neurons) is not investigated here, the focus is in AMPA receptors, i.e., $N_R = N_A$. The analysis of the plasticity accounting for different response times and ionic currents addressed to AMPA and NMDA receptors is to be pursued through future research.

If the number of bound AMPA receptors is denoted as n_A, then [103]

$$\frac{\mathrm{d}n_A}{\mathrm{d}t} = N_A \frac{\mathrm{d}\mathfrak{r}}{\mathrm{d}t}. \tag{4.19}$$

Again, the post-synaptic receiver is identified with a serial RC circuit for a proper interpretation of the reception process. In particular, the input neurotransmitter concentration c_{post} is identified with the voltage V_{in} from the Fig. 4.4, i.e., $V_{in} = \xi c_{\text{post}}$, where ξ converts from [mole] to [volt], the number of bound AMPA receptors n_A with the charge Q_C, i.e., $Q_C = \chi n_A$, where χ is given in [coulomb], and the ratio $\mathfrak{r}$ with the voltage V_C, i.e., $V_C = \psi\mathfrak{r}$, where ψ is given in [volt]. The output current is given as $i_{out} = \mathrm{d}Q_C/\mathrm{d}t = C\mathrm{d}V_C/\mathrm{d}t$, or equivalently

$$\chi \frac{\mathrm{d}n_A}{\mathrm{d}t} = C\psi \frac{\mathrm{d}\mathfrak{r}}{\mathrm{d}t}. \tag{4.20}$$

Comparing Eq. (4.19) with Eq. (4.20), one obtains $C = \chi N_A/\psi$.

The rates of increase and decrease in the number of bound AMPA receptors depend on the neurotransmitter concentration c_{post}, the ratio $\mathfrak{r}$, and bound rate constant k_b. When c_{post} increases, the probability of binding a particle increases and vice

versa; when $\mathfrak{r}$ increases, a probability of binding a particle decreases and vice versa. Analogous to [103], a linear relation is assumed

$$\frac{\mathrm{d}n_A}{\mathrm{d}t} = (c_{\mathrm{post}} - \zeta\mathfrak{r})k_b, \tag{4.21}$$

where ζ is a coefficient given in [mole]. From Fig. 4.4, the current through the circuit is given as

$$i_{out} = \frac{V_{in} - V_C}{R}. \tag{4.22}$$

Rewriting Eq. (4.22) as

$$\chi\frac{\mathrm{d}n_A}{\mathrm{d}t} = \frac{\xi c_{\mathrm{post}} - \psi\mathfrak{r}}{R} = \xi\frac{c_{\mathrm{post}} - \zeta\mathfrak{r}}{R}, \tag{4.23}$$

and comparing with Eq. (4.21), one obtains $R = \xi/(\chi k_b)$. Hence, the RC network has the equivalent time constant given as $RC = \xi N_A/(\psi k_b)$, whose dimension is in [second], as should be. Ultimately, the frequency response of the post-synaptic terminal is derived from the serial RC circuit as

$$\mathbf{H}_{\mathrm{G}}(jf) = j2\pi f(\chi N_A/\psi) \times \left(1 + j2\pi f(\xi N_A/(\psi k_b))\right)^{-1}. \tag{4.24}$$

4.6 Numerical Results

In this section, Bode plots confined to the CaG sub-module (sub-module **D**), the neurotransmitter emission performed by the MTx sub-module (sub-module **E**), the neurotransmitter propagation through the channel (module **F**), and the neurotransmitter reception (module **G**) are computed for a diffusion coefficient of neurotransmitters (glutamate) $D = 0.3\ \mu\mathrm{m}^2/\mathrm{ms}$ [136], synaptic cleft width 20 nm [111], the number of receptors $N_R = 100$, and rate constant $k_b = 10^8\ \mathrm{M}^{-1}\mathrm{s}^{-1}$ [103]. Results are displayed in Figs. 4.5, 4.6, 4.7 and 4.8[7] [129].

The normalized magnitude of module **D** (Fig. 4.5) shows non-linear behavior as a function of the frequency and monotonically decreases as the frequency increases. From the plot, it can be observed that module **D** has a normalized attenuation of 0 dB for all frequencies below the corner frequency ($\approx$ 1 kHz). High frequency components in $r_{spike}(t)$ above the corner frequency are attenuated by -20 dB per decade. This means that rapid changes in spiking rate do not propagate well to the other neuron, and are hardly detectable. Conversely, slow changes in spiking rate function are detectable at the output. For input frequencies below the corner, the phase angle is close to zero. At corner, the phase angle is ≈ -45 degrees and then asymptotically approaches -90 as the frequency increases.

[7] Note that the graphs changes for different set of parameters.

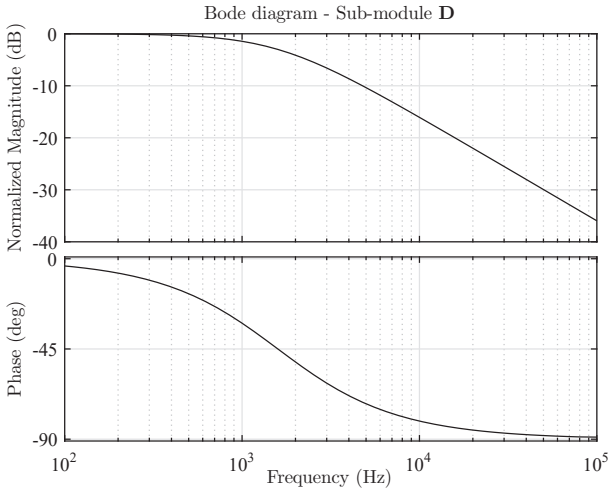

Figure 4.5: The normalized magnitude and phase of calcium gateway. The system frequency refers to the frequency spectrum of the input signal – $r_{spike}(t)$.

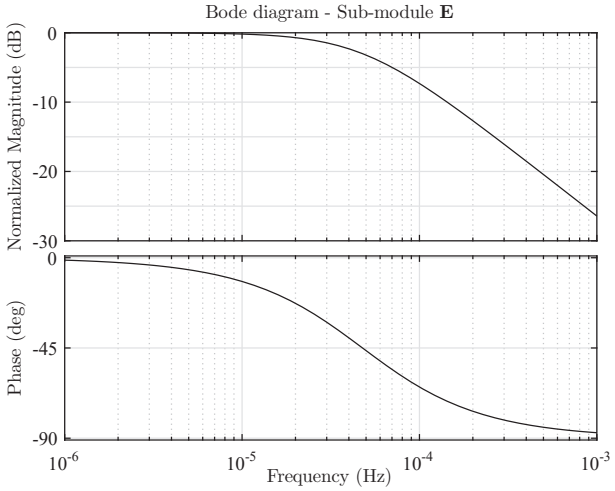

Figure 4.6: The normalized magnitude and phase of molecular transmitter. The system frequency refers to the frequency spectrum of the input signal – $[Ca^{2+}]_{pre}$.

The inference about the normalized magnitude and phase angle of modules **E** and **F** (Figs. 4.6 and 4.7) is analogous since they also act as low-pass filters (with significantly lower corner frequencies). Module **G**, however, acts as a high-pass filter

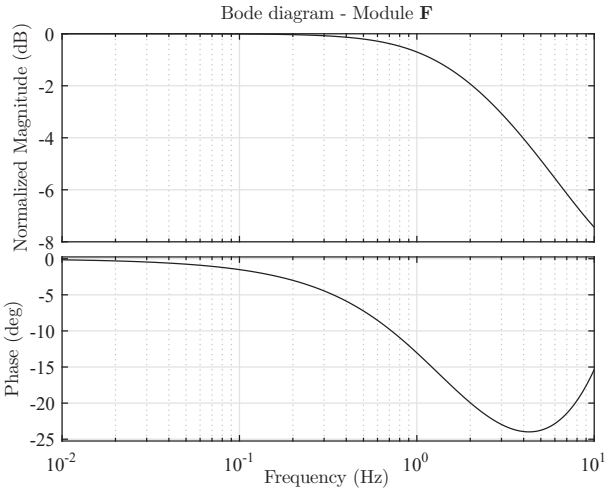

Figure 4.7: The normalized magnitude and phase of synaptic molecular channel. The system frequency refers to the frequency spectrum of the input signal – r_{pre}.

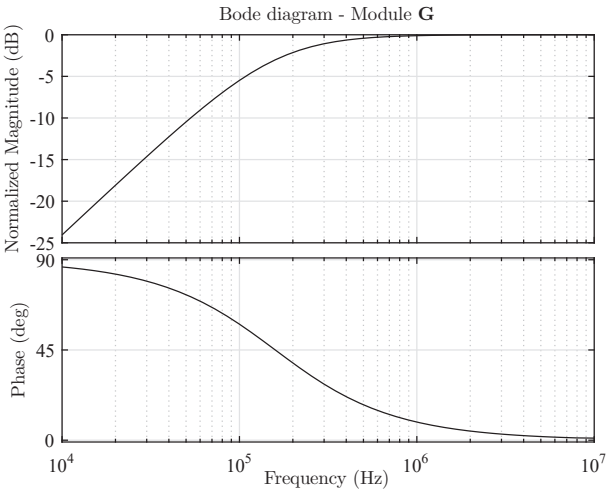

Figure 4.8: The normalized magnitude and phase of molecular receiver. The system frequency refers to the frequency spectrum of the input signal – c_{post}.

(Fig. 4.8). This can be explained considering that if the system frequency of the neurotransmitter concentration c_{post} increases, there are more particles that bind to AMPAs, which leads to an increased magnitude of the output signal V_{EPSP}. Fre-

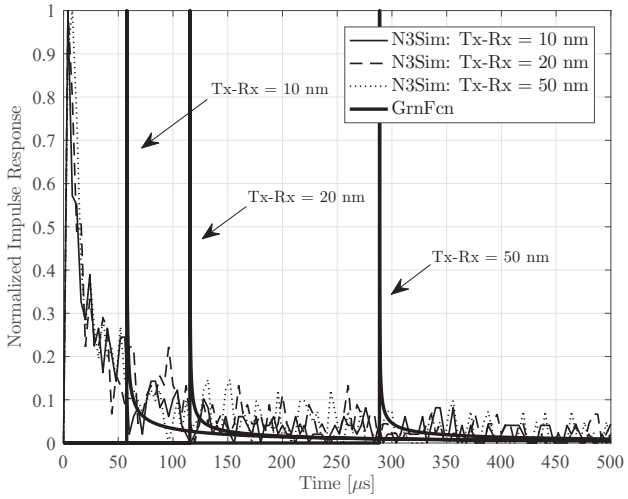

Figure 4.9: Normalized impulse response of synaptic channel obtained theoretically from Eq. (4.17) and from an open-source simulator N3Sim given different distances from the pre- to the post-synaptic terminal.

quency responses evaluated for modules **E**, **F** and **G** are in agreement with frequency responses evaluated for the transmitter, the channel and the receiver that are parts of a general diffusive-based molecular communication system [103].

The Bode diagram of module **F** (synaptic cleft) is evaluated given the channel impulse response (see details in Section 4.4). Synaptic channel is a type of the diffusion-based molecular communication channel, which has been described analytically (see [85], equation (14)) and verified with an open-source simulator N3Sim [57]. On the one hand, the N3Sim is found being unable to differentiate between the impulse responses of different short-range synaptic communication channels, as shown in Fig. 4.9. On the other hand, the normalized amplitudes of the impulse responses shown with tick lines in Fig. 4.9 are found being insignificantly different. This leads to the inference that the distance between the sender and receiver (see Eq. (4.17)) insignificantly affects the frequency response magnitude of the synaptic communication channel, as long the synaptic cleft width takes realistic values. This is, however, not applied to the phase characteristics.

Ultimately, the numerical results presented stem from analytical expressions for measures of inter-neuronal efficacy that are derived under gross simplifications. The results are valid under the following assumptions: i) the synapse is presumed to be highly reliable which sets the vesicle release probability to unity and neglects the variability in post-synaptic response, ii) depletion of extra-cellular Ca^{2+} is neglected, and, iii) depletion of vesicles in pre-synaptic bouton is neglected. This set

of simplifying assumptions has enabled mathematical tractability and LTI system analysis.

4.7 Concluding Remarks

The special molecular synaptic link between neurons where the pre-synaptic cell transfers particles (neurotransmitters) as information carriers to the post-synaptic cell has been investigated in this chapter from the mathematical and communications engineering point of view, providing an alternative representation of the bipartite synaptic system. Electrical circuit representations able to mimic the intra-cellular and extra-cellular processes and to emulate the dynamics of intra-cellular calcium ions in the pre-synaptic cell have been introduced. The behavior of each process has been analyzed in terms of frequency response (magnitude and phase), offering novel contribution to the existing investigations of the neural system.

The potential applications of the proposed approach are manifold. On the one hand, the description of the bipartite synaptic system with an engineering approach is of interest in the design of bio-inspired circuits and techniques attempting to mimic the neuronal processes. Possible neuromorphic devices can be benefited from the modeling of the neuronal processes through elementary input/output circuits. On the other hand, the pre-synaptic neuron can be used to stimulate synapses directly and initiate information propagation in the specified region/cluster of the brain. To this end, understanding the relations between pre-synaptic stimulation and compartmental response is critical. Each electrochemical process involved in the communication operates as a filter, predominately preventing the propagation of rapid variations of the stimulus. In a scenario where the pre-synaptic neuron is externally stimulated, understanding the filtering behavior can give a useful insight in defining the most suitable stimulation pattern to obtain a certain effect on vesicle/neurotransmitter release mechanism.

Chapter 5

Deterministic Model of Inter-Neuronal Communication: Tripartite Synapse

5.1 Introduction

This chapter extends the study from Chapter 4 and proposes an alternative description of the astrocyte-neuron communication systems within tripartite synapses which encompasses the mechanisms introduced in Section 2.2.5. In the literature, a limited number of efforts have been dedicated to propose a communications engineering description of the calcium signaling. Successful attempts in using inter-cellular calcium signaling to establish a communication channel for neural applications have been reported in [91, 92]. By contrast, no other existing investigations in the engineering of neural communication systems have considered the active presence of the astrocyte.

The aim of this chapter is to develop a firm analytical framework linked with relevant segments in the astrocyte-neuron communication pathway. As with Chapter 4, the following study adopts an engineering approach where the chemical and ionic processes are represented with signals, whereas the biological mechanisms are modeled as input-output systems characterized by a *frequency response*. This study maps specific astrocytic and neuronal blocks to electrical circuitry to gain the knowledge of their dynamics and frequency responses. Unlike previous models reviewed in Section 2.3.2, the engineering representation of the relevant processes completely relies on neuroscientific theory and analytical expressions from validated mathematical models that include astrocytes and their active role in neural signaling.

The stimulus-response analysis and equivalent transfer functions derived in the following:

- allow one to exploit the relations between different quantities involved in the coupled astrocyte-neuron entity;
- help in understanding the impact of an artificial stimulation applied to the astrocyte in order to induce a certain response to the neuron;
- provide further tools for design and implementation of bio-mimetic devices mimicking the behavior of neurons and astrocytes at micro- and nano-scale, as well as for the implementation of innovative biomedical tools for the stimulation of neurons at nano-scale, as envisioned in [81] and [80]

The chapter is organized as follows. Section 5.2 recalls the astrocytic impact on adjacent neurons and introduces the schematic representation of the relevant processes along the communication pathway between the astrocyte and the pre-synaptic neuron. Section 5.3 proposes the representation of the tripartite synapse as a signal processing unit, describing the circuital representation of the biological processes in the astrocyte and their effects on the pre-synaptic neuron. In Section 5.4, numerical simulations and results are discussed. Section 5.5 brings the conclusions with some observations for future works and prospectives.

5.2 Astrocytic Impact on the Pre-Synaptic Neuron

After production of IP_3 in astrocytes due to glutamate binding, or external mechanical stimulation, or external astrocytic stimulation, two distinctive effects are observed. First, IP_3 molecules continue moving to adjacent astrocytes through permeable gap junctions, giving rise to analogous calcium release in other cells (recall the biological background from Section 2.2.5). This process is the basis of astrocytic calcium signalling. Second, the increase of internal calcium leads to the release of astrocytic glutamate molecules which bind to receptors on pre- and post-synaptic neurons located in the tripartite synapse.

In the thesis, it is of interest to describe the mechanisms involved in the communication directed from the astrocyte to adjacent neurons, in particular to pre-synaptic neurons, where glial cells act as dynamic regulatory unit mediated by IP_3 and Ca^{2+}. For this reason, the investigation is focused on the impact of the astrocytic activity on the pre-synaptic terminal. The impact of the astrocytic activity on the post-synaptic terminal regulates the neural plasticity, learning and memory, which are, however, not the primal subject of the study.

Since glutamate-sensitive receptors, i.e., mGluRs, are located on the neuronal surface, the pre-synaptic spiking activity is modulated by the astrocyte. To investigate the modulation, the *communication chain* between the astrocyte and the pre-synaptic neuron is introduced in Fig. 5.1, where each module represents a biological

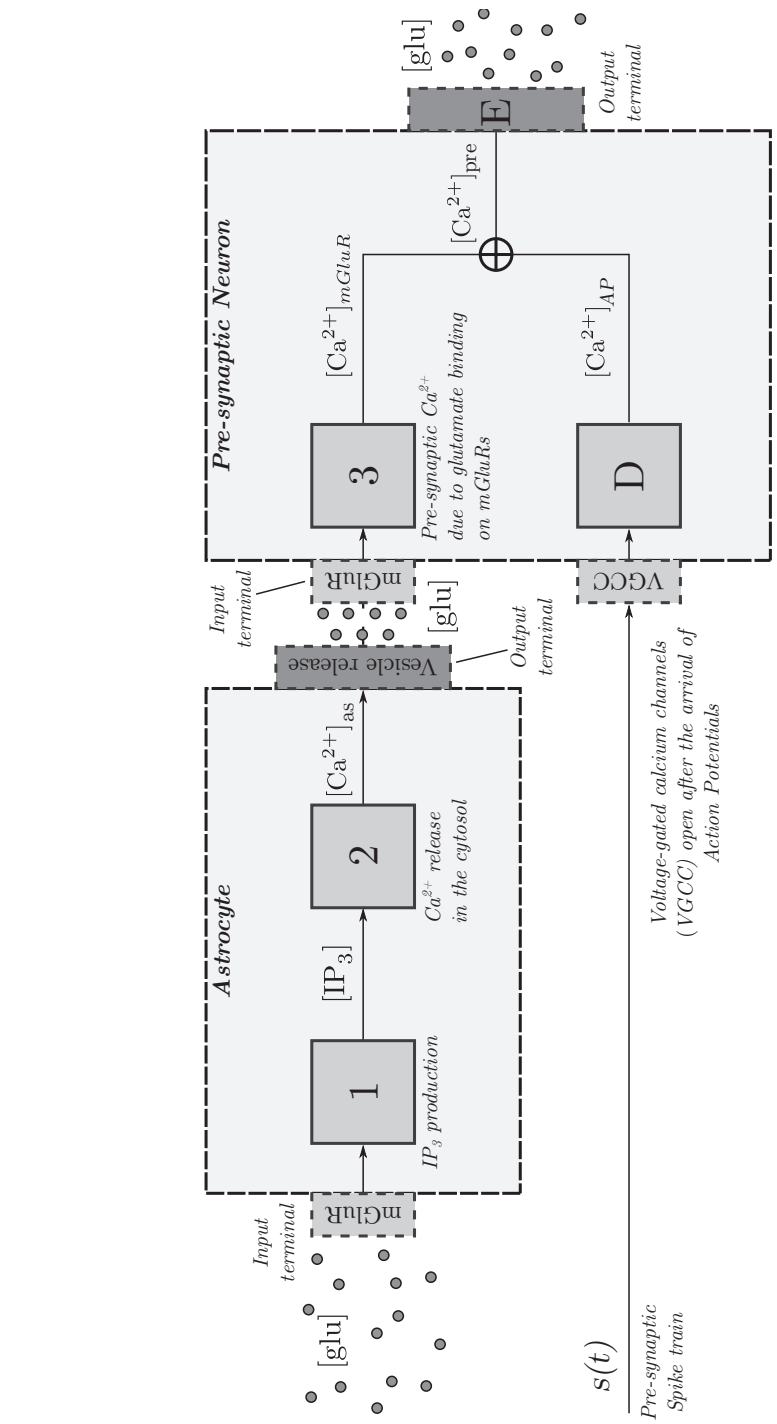

Figure 5.1: Schematic representation of the processes along the communication pathway between the astrocyte and the pre-synaptic neuron. A stimulation applied to the astrocyte evokes IP_3 (module **1**). Internal Ca^{2+} is released from stores (module **2**), enabling the release of astrocytic glutamate in the cleft, which binds to pre-synaptic mGluRs. In the pre-synaptic side, two additive calcium contributions are identified, one is due to the opening of mGluR receptors (module **3**) and one resulting from the spiking activity of the neuron itself through VGCCs (sub-module **D**).

Symbol	Cell	Input	Output
(**1**)	Astrocyte	V_{in}	$[IP_3]$
(**2**)	Astrocyte	$[IP_3]$	$[Ca^{2+}]_{as}$
(**3**)	Astrocyte/Neuron	$[Ca^{2+}]_{as}$	$[Ca^{2+}]_{mGluR}$
(**D**)	Neuron	s	$[Ca^{2+}]_{AP}$

Table 5.1: Input/output signals analyzed in Chapter 5.

process. With this description, the astrocytic processes (modules **1** and **2**) and the neuronal processes (module **3** and sub-module **D**[1]) are easily identified. In the latter, the contribution of calcium due to astrocytic glutamate release, denoted with $[Ca^{2+}]_{mGluR}$, is described with module **3**. Sub-module **D** accounts for the calcium influx into the pre-synaptic terminal when the spiking neuron emits an AP, referred to as $[Ca^{2+}]_{AP}$[2].

5.3 Astrocytic Compartments as Signal Processing Units

In what follows, a description of the neuron-astrocyte system is proposed by means of circuital representations of the biological processes described so far. Taking Fig. 5.1 as a reference, the input/output circuit for each module, i.e., (**1**, **2**) and (**3**, **D**), is defined, identifying and discussing the input and output processes and their equivalent representations as signals (refer to Table 5.1).

The benefit of using a circuital representation resides in the possibility of carrying out a stimulus-response analysis for each process through the corresponding frequency response. In these terms, one can observe to what extent an input (e.g., a molecular/ionic concentration) impacts on the output of a given process. In what follows, the circuital description is defined for each module depicted in Fig. 5.1.

5.3.1 IP_3 Production Process in Astrocytes

The IP_3 synthesis in astrocytes has been described in a simple manner under the hypothesis that a quantized amount of IP_3 molecules is released after the increase of glutamate due to pre-synaptic spiking activity [86, 87]. The lifetime process of IP_3

[1]Sub-module **D** from Fig. 5.1 is the sub-module **D** from Fig. 3.2 where the bipartite synapse is investigated.

[2]Note that $[Ca^{2+}]_{AP}$ corresponds to $[Ca^{2+}]_{pre}$ from Chapter 4 which investigates bipartite synapses.

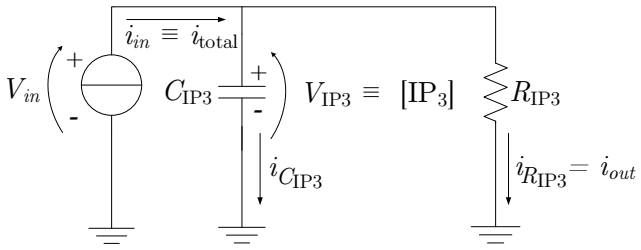

Figure 5.2: IP_3 production process in the astrocyte as equivalent RC circuit model.

concentration in the astrocyte, $[IP_3]$, leads to the following equation:

$$\frac{\mathrm{d}[\text{IP}_3]}{\mathrm{d}t} = \underbrace{\frac{1}{\tau_{\text{IP}_3}}\left([\text{IP}_3]^* - [\text{IP}_3]\right)}_{\text{degradation}} + \underbrace{r_{\text{IP}_3}\,\mathcal{H}(V_{in} - 35\text{ mV})}_{\text{production}} \tag{5.1}$$

The first term on the right side refers to the IP_3 degradation, where $[IP_3]^*$ is the concentration at equilibrium (160 nM from experiments), and τ_{IP_3} is the degradation time constant (1/0.00014 ms). The second term refers to the production of IP_3, where r_{IP_3} is the production rate in nM/s, with typical values in the range 0.1-1.5 μM/s. Coefficients shown in Eq. (5.1) have been measured through experiments reported in [131]. The IP_3 production is enabled when the pre-synaptic potential V_{in} is above a given threshold of 35 mV ($\mathcal{H}$ is the Heaviside function). This is clearly an approximation of what actually happens at molecular level, which allows one to relate the production of IP_3 with the presence of glutamate in the synapse.

The dynamics of the production process of IP_3 described in Eq. (5.1) is similar to the charge/discharge process found in a parallel RC circuit, where the behavior of the capacitor voltage resembles the dynamics of $[IP_3]$. Resorting to the approach reported in Chapter 4, the corresponding equivalent circuit is depicted in Fig. 5.2. However, notice that the flow of neutral IP_3 molecules does not generate an electric current as the flow of polarized ions does. Therefore, the currents flowing in the IP_3 circuit should be considered as equivalent molecular currents which enable the definition of circuit representation of the IP_3 production process. Rearranging Eq. (5.1), one obtains the total equivalent current at the input of the circuit, identified as i_{IP_3}, and representing the stimulation that induce the production of IP_3:

$$i_{\text{IP}_3} = k_i\left(\frac{\mathrm{d}[\text{IP}_3]}{\mathrm{d}t} + \frac{1}{\tau_{\text{IP}_3}}[\text{IP}_3]\right) - k_i\frac{1}{\tau_{\text{IP}_3}}[\text{IP}_3]^* = \text{input}_{stim}, \tag{5.2}$$

where k_i is a coefficient for the conversion from a concentration in [mole] to a charge in [coulomb]. The constant term on the right of Eq. (5.2) depends on the equilibrium concentration of IP_3. Now, compare the expression in Eq. (5.2) with the total current circulating in a parallel RC circuit, given by the sum of currents flowing through

capacitor and resistor

$$i_{in} = C\,\frac{\mathrm{d}V_{\mathrm{IP}_3}}{\mathrm{d}t} + \frac{V_{\mathrm{IP}_3}}{R} = i_{\mathrm{IP}_3}, \tag{5.3}$$

where i_{in} is the input current applied to the RC circuit, as shown in Fig. 5.2. Rearranging Eq. (5.2) to the formula shown in Eq. (5.3), and converting the voltage V_{IP_3} expressed in [volt] to the molecular concentration $[\mathrm{IP}_3]$ expressed in [mole], one obtains the equivalent capacitor and resistor for a RC circuit driven by the astrocytic $[\mathrm{IP}_3]$:

$$C_{\mathrm{IP}_3} = \frac{k_i}{h_i}; \qquad R_{\mathrm{IP}_3} = \frac{\tau_{\mathrm{IP}_3}\,h_i}{k_i}; \qquad R_{\mathrm{IP}_3}C_{\mathrm{IP}_3} = \tau_{\mathrm{IP}_3} \tag{5.4}$$

where h_i and k_i are coefficients for the conversion from [mole] to [volt], and [mole] to [coulomb], respectively. To simplify the reasoning, both coefficients are assumed equal to 1. Therefore, the total IP_3 current is given by the sum of the currents flowing through capacitor, $i_{C_{\mathrm{IP}_3}}$, and resistor, $i_{R_{\mathrm{IP}_3}}$.

The frequency response of astrocytic IP_3 production module stems from the parallel RC circuit shown in Fig. 5.2:

$$\mathbf{H}_1(jf) = (1 + j2\pi f R_{\mathrm{IP}_3}C_{\mathrm{IP}_3})^{-1}. \tag{5.5}$$

The *normalized gain* $\Gamma_{\mathbf{H}_1}(f)$ is

$$\Gamma_{\mathbf{H}_1}(f) = \frac{|\mathbf{H}_1(f)|}{\max_f(|\mathbf{H}_1(f)|)}. \tag{5.6}$$

The *group delay* $\tau_{\mathbf{H}_1}(f)$ is

$$\tau_{\mathbf{H}_1}(f) = -\frac{\mathrm{d}\phi_{\mathbf{H}_1}(f)}{\mathrm{d}f}, \tag{5.7}$$

where $\phi_{\mathbf{H}_1}(f)$ denotes the phase, defined as

$$\phi_{\mathbf{H}_1}(f) = \mathrm{atan}\left(\frac{\Im(\mathbf{H}_1(f))}{\Re(\mathbf{H}_1(f))}\right). \tag{5.8}$$

5.3.2 Cytosolic Ca^{2+} Release Process

Once produced or received from other cells through gap junction, IP_3 molecules bind to receptors located on the surface of intra-cellular calcium stores, i.e., the *sarcoplasmic* and *endoplasmic reticula* (SR, ER), enabling the release of Ca^{2+}. Additional calcium flow occurs spontaneously from ER into the cytosol (leakage flow) while Ca^{2+} dependent ATPase pumps (Sarco/Endoplasmic Reticulum Ca^{2+}-ATPase – SERCA) operate in the opposite direction to uptake Ca^{2+} back into the stores. During rest conditions, $[Ca^{2+}]_{\mathrm{as}}$ is regulated by the balance between passive leakage

from ER and SERCA uptake. When the IP_3 production is sustained for a sufficient time, the CICR combined with the SERCA process can lead to oscillations of $[Ca^{2+}]_{as}$ [18, 36]. The dynamics of $[Ca^{2+}]_{as}$ can be described as follows [86]:

$$\frac{d[Ca^{2+}]_{as}}{dt} = J_{ch}([Ca^{2+}]_{as}, [IP_3]) + J_{leak}([Ca^{2+}]_{as}) - J_{pump}([Ca^{2+}]_{as}), \tag{5.9}$$

where the three fundamental mechanisms, CICR, SERCA and leaking, correspond to J_{ch}, J_{pump} and J_{leak} respectively. For each term, the dependency on either Ca^{2+} or IP_3 is emphasized.

From Eq. (5.2), an equivalent circuit representation is not straightforward because of the presence of two different calcium behavior, constant and oscillatory (the reader is referred to [83], Section 2.3 for a thorough investigation on oscillatory behavior of $[Ca^{2+}]_{as}$). For the sake of simplifying the system, the two phases of the Ca^{2+} release process in the astrocyte are analyzed separately.

In the non-oscillatory phase, $[Ca^{2+}]_{as}$ at steady state can be approximated by a linear or exponential function of $[IP_3]$. In this case, the Ca^{2+} release process can be described through a proportionality constant which relates the input $[IP_3]$ to the output $[Ca^{2+}]_{as}$:

$$[Ca^{2+}]_{as} = K_{Ca-IP_3}[IP_3] + [Ca^{2+}]_{eq}, \tag{5.10}$$

where K_{Ca-IP_3} is the proportionality constant retrieved from the non-oscillatory phase. The term $[Ca^{2+}]_{eq}$ takes into account the initial condition of $[Ca^{2+}]_{as}$ at equilibrium (typically in the range $[0.1 \div 0.3]\,\mu$M.

In the oscillatory phase, $[Ca^{2+}]_{as}$ shows oscillations when $[IP_3]$ is in a range of values (typically in the range $[400 \div 600]$ nM [83]), which depend on the physiological parameters of the cell. Then, the release process in the oscillatory phase can be represented as an oscillator which resonates at the oscillation frequency, followed by a gain circuit that shapes the amplitude as needed. Notice that the resonating frequency assumes very low values, below 1 Hz, since calcium release is a much slower process (in the range of seconds) compared to the neuronal spiking (in the range of milliseconds).

To describe the oscillatory scenario with electronic representation, a simple Wien bridge oscillator which provides an oscillating output signal (a sine-wave) is considered. The equivalent circuit of Fig. 5.1 – module **2** is then depicted in Fig. 5.3. Note that $[IP_3]$ ranging from 400 nM to 600 nM is identified as a power supply voltage driven by the output signal from module **1**. In terms of technical details concerning the electronic configuration of the circuit depicted in Fig. 5.3, note that $R_b = R_f/2$, while R_{swo} and C_{swo} are selected in accordance to the oscillating frequency, i.e.,

$$f_o = \frac{1}{2\pi R_{swo} C_{swo}} \tag{5.11}$$

An equivalent circuit representation of cytosolic $[Ca^{2+}]_{as}$ production depends on the operating phase, constant or oscillatory. When modeling the non-oscillatory phase,

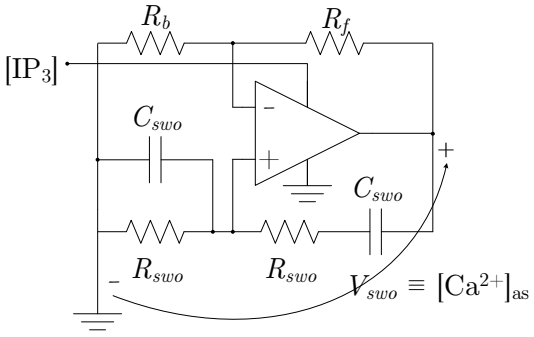

Figure 5.3: Ca^{2+} release in the astrocyte cytosol as equivalent Wien bridge oscillator.

$[Ca^{2+}]_{as}$ can be approximated by a linear function. Thus, the frequency response is also constant, i.e.,

$$\mathbf{H}_2^{(l)}(jf) = \text{constant} = K_{Ca-IP_3}, \tag{5.12}$$

where K_{Ca-IP_3} has been defined in Eq. (5.10). At oscillatory phase, however, the frequency response stems from the Wien bridge oscillator which resonates at a given frequency ($f_o = 1/(2\pi R_{swo} C_{swo})$):

$$\mathbf{H}_2^{(o)}(jf) = \frac{j2\pi f R_{swo} C_{swo}}{1 - (2\pi f R_{swo} C_{swo})^2 + j6\pi f R_{swo} C_{swo}}. \tag{5.13}$$

5.3.3 Glutamate Binding on Pre-Synaptic mGluR

A primary consequence of the augmented concentration of glutamate in the synapse is the impact on the neural activity of nearby neurons. Since NMDA receptors are the primal source of Ca^{2+} in post-synaptic neurons and critical for plasticity processes such as Long Term Depression (LTD) and Long Term Potentiation (LTP), the astrocytic feedback is expected to have a significant impact on post-synaptic neurons. However, the focus in this study is on the pre-synaptic side. In this case, the rise of calcium level in the pre-synaptic terminal due to mGluR activation from astrocytes can be determined mathematically from available data [100]. In particular [87]:

$$\frac{\mathrm{d}[Ca^{2+}]_{mGluR}}{\mathrm{d}t} = -\gamma_1 [Ca^{2+}]_{mGluR} + \alpha_1 [Ca^{2+}]_{as} \mathcal{H}([Ca^{2+}]_{as} - 196.4\,\mathrm{nM}), \tag{5.14}$$

where $[Ca^{2+}]_{mGluR}$ is the calcium increase due to mGluR activation, whereas $[Ca^{2+}]_{as}$ is the cytosolic calcium level in the astrocyte as determined in Eq. (5.9). The constants α_1 and γ_1 refer to the production and decay rate of Ca^{2+}, respectively, where the production rate is assumed linearly dependent on $[Ca^{2+}]_{as}$ and triggered

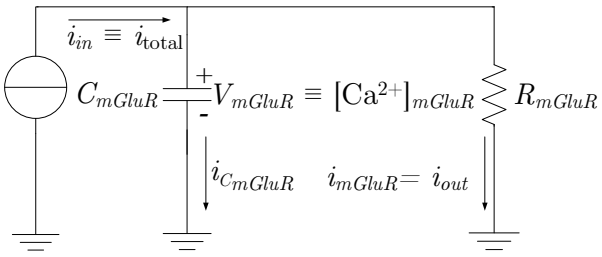

Figure 5.4: Pre-synaptic calcium due to glutamate binding on mGluRs as equivalent RC circuit model.

when the astrocytic $[\text{Ca}^{2+}]_{\text{as}}$ exceeds a given threshold, obtained from the same data [100].

Similarly to the IP_3 production/degradation process, the mGluR-dependent calcium process can be represented with an equivalent RC circuit with charge/discharge determined by the decay/production dynamics of $[\text{Ca}^{2+}]_{mGluR}$. The equivalent circuit is depicted in Fig. 5.4. Resorting to Eq. (5.3) and Eq. (5.14), one obtains the equivalent capacitor and resistor for the mGluR calcium contribution:

$$C_{mGluR} = \frac{k_m}{h_m}; \qquad R_{mGluR} = \frac{h_m}{k_m \, \gamma_1}, \tag{5.15}$$

where coefficients h_m and k_m convert from [mole] to [volt], and from [mole] to [coulomb], respectively, to ensure that the quantities are consistent with voltage and current in the RC circuit.

Analogous to the IP_3 production/degradation process, the frequency response of the module describing the calcium increase in the pre-synaptic neuron due to the activation of mGluRs stems from the parallel RC circuit:

$$\mathbf{H}_3(jf) = (1 + j2\pi f R_{mGluR} C_{mGluR})^{-1}. \tag{5.16}$$

5.3.4 Total Pre-Synaptic Calcium Concentration

In the pre-synaptic terminal, two primal contributions to the concentration of calcium ions can be identified. The first one, identified with $[\text{Ca}^{2+}]_{AP}$, is due to the APs arriving at the pre-synaptic terminal and enabling the release of calcium ions through VGCCs. The other calcium source, denoted as $[\text{Ca}^{2+}]_{mGluR}$, is given by the augmented astrocytic activity in terms of glutamate release activating the pre-synaptic mGluRs (Section 5.3.3). Then, the total pre-synaptic level of calcium ions, $[\text{Ca}^{2+}]_{\text{pre}}$ can be approximated as follows [87]:

$$[\text{Ca}^{2+}]_{\text{pre}} = [\text{Ca}^{2+}]_{AP} + [\text{Ca}^{2+}]_{mGluR}. \tag{5.17}$$

The dynamics of $[Ca^{2+}]_{AP}$ is based on the same concept used for $[IP_3]$ and $[Ca^{2+}]_{mGluR}$, where the increase in concentration is triggered when the pre-synaptic membrane potential exceeds a given threshold:

$$\frac{\mathrm{d}[Ca^{2+}]_{AP}}{\mathrm{d}t} = -\gamma_2[Ca^{2+}]_{AP} + \alpha_2\mathcal{H}(s - 35\,\mathrm{mV}). \tag{5.18}$$

The terms α_2 and γ_2 ($\alpha_2 = 4.27 \times 10^6\,\mathrm{nM\ ms^{-1}}$ and $\gamma_2 = 10\ \mathrm{ms^{-1}}$ [87]) denote the production and decay rate, respectively, similarly to Eq. (5.14), and make the charge-discharge of $[Ca^{2+}]_{AP}$ phase very fast in order to follow the rapid discharge pattern of the AP train ($s(t)$). However, $[Ca^{2+}]_{AP}$ can still be represented with an equivalent RC circuit as in Chapter 4, where the equivalent capacitor and resistance are defined as:

$$C_{AP} = \frac{k_a}{h_a}; \qquad R_{AP} = \frac{h_a}{k_a\,\gamma_2}; \qquad R_{AP}C_{AP} = \gamma_2 \tag{5.19}$$

The coefficients h_a and k_a take into account the unit conversion as discussed previously in Sections 5.3.1 – 5.3.3. The frequency response of sub-module **D** is regulated by the same dynamics of modules **1** and **3**:

$$\mathbf{H}_{\mathrm{D}}(jf) = (1 + j2\pi f R_{AP}C_{AP})^{-1}. \tag{5.20}$$

Note that $\mathbf{H}_{\mathrm{D}}(jf)$ from Eq. (5.20) corresponds to $\mathbf{H}_{\mathrm{D}}(jf)$ from Eq. (4.8), as C_{AP} and R_{AP} correspond to C_{Ca} and R_{Ca} derived previously in Chapter 4, Section 4.3.1.

5.4 Numerical Results

This section shows the behavior of the biological processes described in Section 5.3 through mathematical models and their equivalent circuital representation. First, the time behavior of the processes involved in the astrocyte-neuron system is discussed, from the initial stimulation applied to the astrocyte at the input of module **1**, to the final calcium elevation observed in the pre-synaptic terminal at the output of module **3** and sub-module **D**. Finally, the frequency response of each biological process is presented through the proposed electronic representation. The aim is to compare the time behavior with the frequency response of the circuital representation, discussing the relations between different modules.

5.4.1 Time Behavior of Input/Output Signals

Starting from the leftmost side of the block description in Fig. 5.1, the charge-discharge behavior of astrocytic $[IP_3]$ and $[Ca^{2+}]_{\mathrm{as}}$ are shown observing the input/output quantities driving modules **1** and **2**. To this end, a scenario is proposed

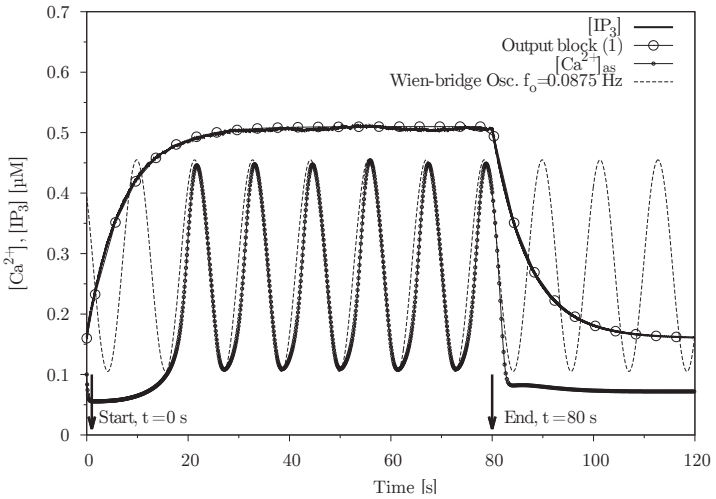

Figure 5.5: The electronic circuit of module **2** mimics the oscillatory behavior of $[Ca^{2+}]_{as}$ observed when a constant stimulation is applied to the astrocyte for 80 s. The measured oscillation frequency is 0.0875 Hz, driven by the level of IP_3 obtained from module **1**. The output of module **1** is also shown for comparison. The close similarity can be noticed between the electronic output and the observed calcium wave [83].

where a constant stimulation (V_{in}) is applied at the input of module **1** for 80 s in order to trigger the production of IP_3 molecules. As discussed before, in a realistic system the production of IP_3 is originated through mechanical stimulation, injection, or after the glutamate release of the adjacent pre-synaptic neuron [87,116]. However, this mechanism is modeled with a constant input to simulate the raising of $[IP_3]$ in the cell. The temporal behavior of $[IP_3]$ and $[Ca^{2+}]_{as}$ is depicted in Fig. 5.5. As can be noticed, when the stimulation is interrupted at $t = 80$ s, the level of IP_3 decreases following the discharge constant τ_{IP_3}. For comparison, the output of the RC circuit in module **1** is also shown with circles, observing that the dynamics of the voltage across the capacitor, Eq. (5.3), is the same observed for $[IP_3]$, Eq. (5.1). In this particular scenario, the elevation of astrocytic $[IP_3]$ induces an oscillatory behavior of $[Ca^{2+}]_{as}$, with measured frequency equal to 0.875 Hz. As shown in Fig. 5.5, the calcium oscillation is characterized by a regular sinusoidal behavior which can be synthesized by the Wien-bridge circuit in Fig. 5.3.

To demonstrate the impact of the astrocytic activity on the total Ca^{2+} level in the pre-synaptic terminal[3], under the hypothesis that the pre-synaptic neuron has a constant spiking activity, two sample scenarios are discussed proposing a comparison

[3]The reader is referred to [83], Section 4.1 for a thorough investigation on time behavior of $[IP_3]$ and $[Ca^{2+}]_{as}$.

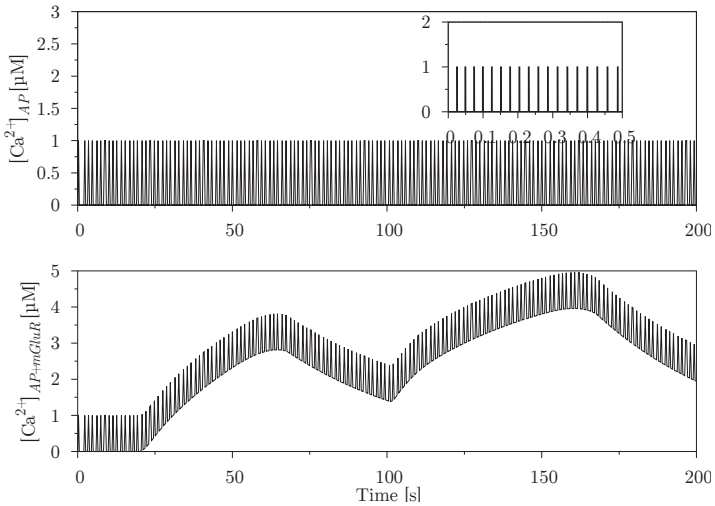

Figure 5.6: Scenario 1: the astrocyte is activated for 60 seconds with a square wave signal. Upper plot: every time an action potential reaches the pre-synaptic terminal, a rapid increase of calcium level is observed in the terminal (values are normalized to the maximum). Lower plot: in correspondence of astrocytic glutamate release, further calcium ions flow into the terminal, increasing the ionic concentration [83].

between the intra-cellular Ca^{2+} level in the pre-synaptic neuron without and with astrocytic activation[4].

In the first scenario, depicted in Fig. 5.6, a constant astrocytic activation is sustained for 60 s and repeated at $t = 120$ s. In the upper plot, the impulsive calcium level is noticed due to voltage gated channels opened after an AP is emitted. In the lower plot, the contribution $[Ca^{2+}]_{mGluR}$ (bottom-right plot of Fig. 5.6) is summed to $[Ca^{2+}]_{AP}$ to obtain the total calcium level in the pre-synaptic terminal. In correspondence of an increase of astrocytic calcium and the consequent glutamate release, the level of $[Ca^{2+}]_{mGluR}$ increases with a much slower dynamics (seconds) when compared to the voltage-gated calcium level $[Ca^{2+}]_{AP}$ (milliseconds).

In the second scenario, the stimulation pattern is active for shorter time, 10 s, whereas the inactive phase is longer, 20 s. Then, the stimulation is represented with a square wave with duty cycle equal to 30%. The same reasoning applies to the second scenario, depicted in Fig. 5.7, where a shorter astrocytic activation is considered (each activation pulse lasts 10 s).

[4] A CA3 neuron characterized by a spiking frequency of 30 Hz (30 action potentials emitted per second) and astrocyte are simulated. The neural dynamics follow the physiological Pinsky-Rinzel model [107].

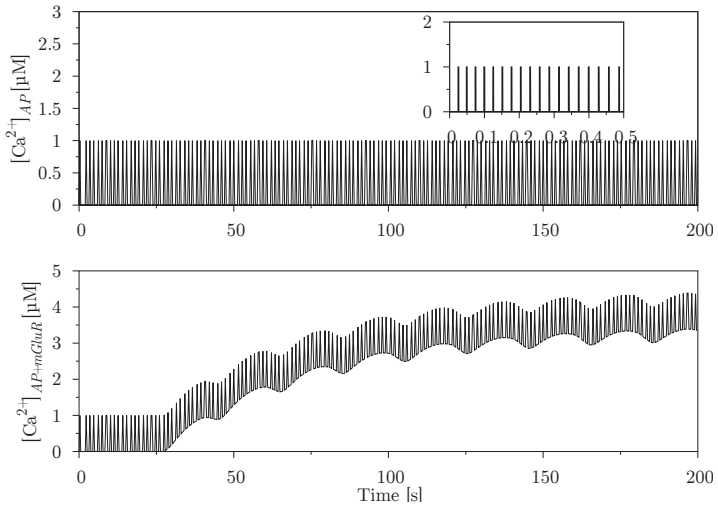

Figure 5.7: Scenario 2: the astrocytic activation is sustained for a shorter period of time, 10 s [83].

5.4.2 Frequency Response of Equivalent Circuits

The alternative representation of the astrocytic feedback processes including the cytosolic IP_3 production, cytosolic calcium release, glutamate release and glutamate binding to pre-synaptic mGluR, has been described in Section 5.3 through adequate electronic circuits. As an effective tool for giving an insight into the performance of astrocyte-neuron communication, the frequency response (in terms of *normalized gain* and *group delay*) of each individual circuit is inspected.

The normalized gain of IP_3 production module **1** is computed from Eq. (5.6) for a frequency[5] range from 0 Hz to 10 Hz and degradation time constant $R_{IP_3}C_{IP_3} = \tau_{IP_3} = 1/0.00014$ ms [87]. The normalized gain is shown in Fig. 5.8 demonstrating the filtering role of the production module. Hence, the production module generates $[IP_3]$ with a slow dynamics.

The gain of the succeeding module **2** operating in the non-oscillatory phase is constant. In the oscillatory phase, however, the gain is computed from Eq. (5.6) inserting $\mathbf{H}_2^{(o)}(jf)$ instead of $\mathbf{H}_1(jf)$. Since the calcium dynamics should be modeled as a slow process, the resonating frequency assumes very low values. For illustrative purposes, the normalized gain of Wien bridge oscillator is plotted for two different scenarios. In the first one depicted in Fig. 5.9, the oscillator has been configured to generate an oscillatory signal with frequency $f_o = 0.1$ Hz to emulate $[Ca^{2+}]_{as}$ oscillations when $[IP_3] = 650$ nM (refer to [83]). The second scenario depicted in Fig. 5.10

[5]The frequency here relates to the temporal changes of the corresponding input signals.

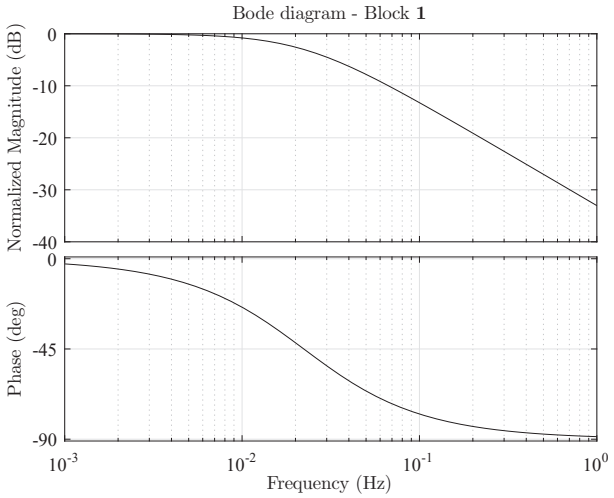

Figure 5.8: The normalized magnitude and phase of the cytosolic IP_3 production. The system frequency refers to the frequency spectrum of the input signal – V_{in}.

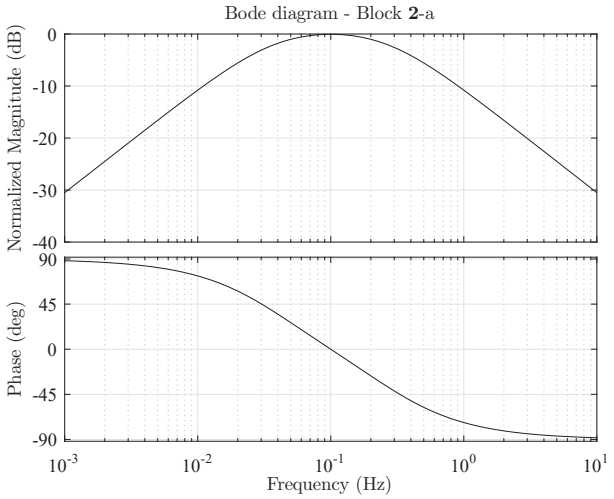

Figure 5.9: The normalized magnitude and phase of the cytosolic calcium release - the oscillatory phase $f_o = 1/10$ s. The system frequency refers to the frequency spectrum of the input signal – $[IP_3]$.

considers an oscillatory signal with $f_o = 0.04$ Hz to represent $[Ca^{2+}]_{as}$ oscillations when $[IP_3] = 650$ nM (refer to [83]).

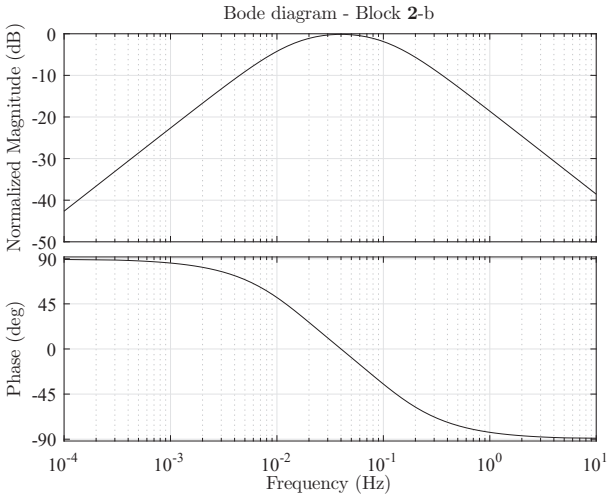

Figure 5.10: The normalized magnitude and phase of the cytosolic calcium release - the oscillatory phase $f_o = 1/25$ s. The system frequency refers to the frequency spectrum of the input signal – $[IP_3]$.

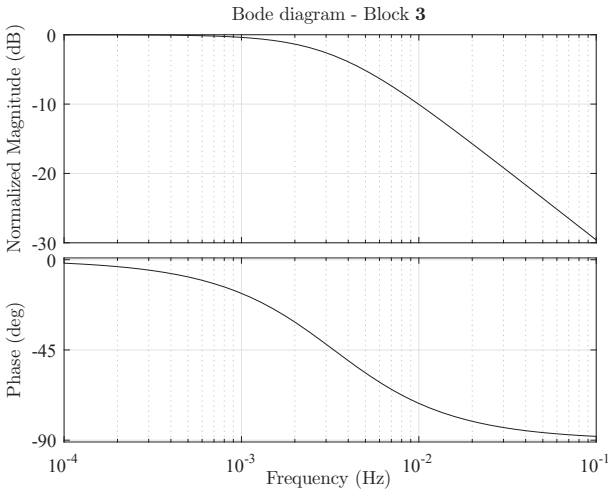

Figure 5.11: The normalized magnitude and phase of the glutamate binding. The system frequency refers to the frequency spectrum of the input signal – $[Ca^{2+}]_{as}$.

The normalized gain of the module representing the rise of $[Ca^{2+}]_{mGluR}$ in the pre-synaptic terminal is computed from Eq. (5.6) inserting $\mathbf{H}_3(jf)$ instead of $\mathbf{H}_1(jf)$

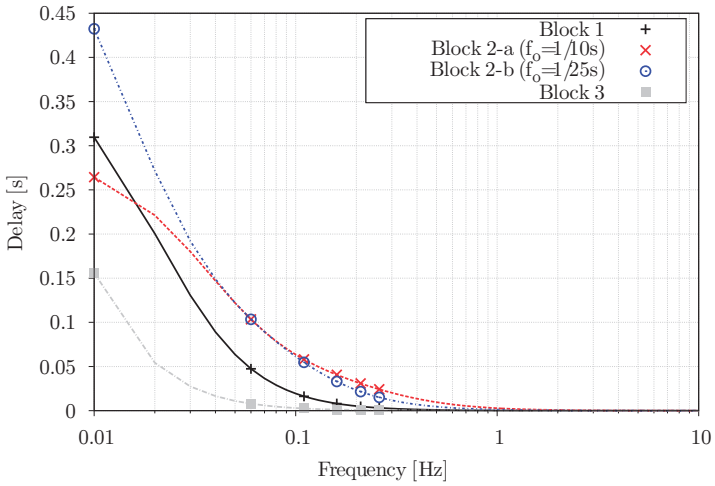

Figure 5.12: The group delay of the three equivalent modules: the cytosolic IP_3 production, cytosolic Ca^{2+} release, and glutamate binding to the pre-synaptic terminal.

for $R_{mGluR}C_{mGluR} = \tau_{mGluR} = 1/\gamma_1 = 48$ s [87]. The normalized gain is shown in Fig. 5.11. The module acts as a low-pass filter. Although $[Ca^{2+}]_{as}$ from the oscillator usually has a low frequency, $[Ca^{2+}]_{mGluR}$ seems to have even slower dynamics.

The phases of individual modules are computed from Eq. (5.8). Individual phase functions are depicted in the lower plots of Figs. 5.8 – 5.11. Individual delay functions are computed from Eq. (5.7) and depicted in Fig. 5.12. At very low frequencies up to 0.1 Hz, the group delay incurred by each individual module is non-linear which produces distorted calcium signaling. For frequencies larger than 0.1 Hz, the astrocyte modulation of the neuronal activity does not incur the distortion and the process of astrocyte modulation can be observed as instantaneous.

The sub-module **D** represents the calcium release process through VGCCs subsequent to the arrival of the APs to the pre-synaptic terminal. This process is discussed in Chapter 4, Section 4.3.1. Thus, detailed discussion in this chapter is omitted. Recall that the sub-module **D** acts as a low-pass filter but with larger cut-off frequency compared to the previously described modules. The system frequency here refers to the temporal changes of the spiking rate function. In a bandwidth of interest, the module incurs a constant delay of 6 μs.

5.5 Concluding Remarks

Upon the considerations discussed in the chapter, it has been shown that the intracellular calcium dynamics of astrocytes is a critical process with significant impact

on the regulation of the neuronal activity. In a tripartite synapse, the astrocyte cell actively interacts with the neuronal response of adjacent pre-synaptic neurons, providing a feedback which is believed to regulate several brain processes. This special link between neuron and glial cells has been investigated from the mathematical and communications engineering point of view, providing an alternative representation of the astrocyte-neuron system. Circuital representations able to mimic the intracellular processes and to emulate the dynamics of intra-cellular calcium ions, such as calcium oscillations and IP_3-dependent Ca^{2+} release, have been introduced. The behavior of each process has been analyzed in terms of frequency response (magnitude and phase), offering results which match the expected behavior of the related chemical processes.

The potential applications of the proposed approach are manifold. On the one hand, the description of the tripartite synaptic system with an engineering approach is of interest in the design of bio-inspired circuits and techniques attempting to mimic the neuronal processes, including the astrocytic network. As inferred in Chapter 4, possible neuromorphic devices can be benefited from the modeling of the neuronal and astrocytic processes through elementary input/output circuits. On the other hand, the astrocyte can be used to stimulate indirectly adjacent neurons. To this end, understanding the relations between astrocytic stimulation and neuronal response is critical. Each electrochemical process involved in the communication operates as a filter, preventing the propagation of rapid variations of the molecular concentrations in the astrocyte. In a scenario where the astrocyte is externally stimulated, understanding the filtering behavior can give a useful insight in defining the most suitable stimulation pattern to obtain a certain effect on adjacent pre-synaptic neurons.

Chapter 6

Information Theory of Neural Communication

6.1 Introduction and Motivation

Unlike the previous chapters which are focused on communication theoretical study of neurons, this chapter turns into information theoretical study of neurons.

The beauty of Shannon's information theory is the generality that encompasses all communications and processing systems regardless of whether the signals communicated are digital or analog. This enables researchers to deploy information theory to numerous fields, including the analysis of biological communication systems such as the brain and neural communication networks, where the signals involved are analog.

Neurons respond with stochastic action potentials that are further communicated over synapses which are often unreliable. Although it is not clear whether this unreliability is a 'bug' or a 'feature' of neurons [68], the question that arises is: How does one examine measurements to determine how close to the limits the neural system is operating [97]? Here comes another beauty of information theory and the ability to transform the previous question to: How effectively does the output represent the input? Henceforth, instead of finding good measurement techniques in assessing effectiveness and establishing performance limits, the key information-theoretic quantities are used [33]. Fig. 6.1(a) shows the well-established model underlying classical information theory [33, 97].

The available information-theoretic analysis are ubiquitously applied to a *single neuron* to obtain theoretic quantities on how much information a neuronal output/response carries about the time-varying input/stimulus (see the next section, and [17, 21, 56, 97, 118, 119], and references therein). Unlike previous analysis, the study presented later in this chapter applies information theory to a *single synapse*

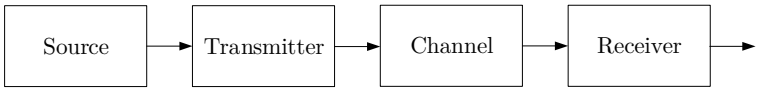

(a) The information-theoretic model for classical communications.

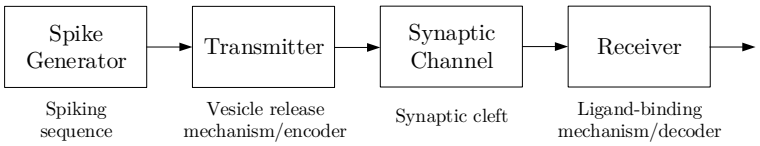

(b) The information-theoretic model for a single synapse.

Figure 6.1: The classical information theory model and its equivalent in the neuroscience. The figure adapted by the author from [97, Chapter 3].

with an objective to quantify how much information a receiving/post-synaptic neuron carries about the transmitting/pre-synaptic neuron. The synaptic channel capacity is investigated with particular emphasis since the communication paradigms within a synapse and within a single neuron are phenomenologically different. Recall the communication within a synapse in a neuron-to-neuron communication channel means the molecular transmission of particles from the pre-synaptic terminal to the post-synaptic terminal. The communication within a neuron, however, means the electrochemical transmission of ions, e.g., Na^+, Ca^{2+}, K^+ and Cl^- [126]. The information-theoretic model for a single synapse is shown in Fig. 6.1(b).

When referring back to the quantification on how much information the spiking sequence carries about the stimulus, two methods are straightforward [21]. The first is the 'direct' method of calculating mutual information from the neuronal response R by estimating its entropy, $H(R)$, and neuronal noise, $H(R|S)$, i.e.,

$$I(R,S) = H(R) - H(R|S). \tag{6.1}$$

In this method, the spike train noise is determined by repeating a dynamic stimulus many times to get the response distribution under the same stimulus conditions. The second method adds the assumption that the neuronal response amplitudes have Gaussian probability distribution in the frequency domain, and computes an upper bound on mutual information – *capacity*. These approaches, however, can be extended to the analysis of noisy and unreliable synapses. As an example, if the capacity is estimated, one should assume i) the post-synaptic response[1] amplitudes have Gaussian probability distribution in the frequency domain [135], ii) the stimulus S is the mean post-synaptic response obtained from many repetitions of identical

[1]The post-synaptic response can be referred to as changes in the membrane potential of the post-synaptic terminal that should not be confused with action potentials, or to the current that causes changes in membrane potential.

stimulus conditions, and iii) the actual response R is the response on individual trials, which equals the mean signal plus a noise term. With this approach, one does not need knowledge on neural physiology and information processing. It is enough to treat a channel as a black box and apply tools from statistical estimation theory in estimating the capacity from empirically recorded input and output signals. This is unambiguously the advantage of this approach. The disadvantage is, however, that one must collect data to estimate theoretical limits. But, can the neural compartments (peculiarly those forming the synapse) be understood as communications devices to bypass the need to record the data?

The remainder of this chapter is organized as follows. Section 6.2 cites the closely related works on information theoretical aspects of neurons. More specifically, Section 6.2.1 states favorable information capacity result derived for a single neuronal channel – in this thesis appointed as the intra-neuronal channel. Similarly, Section 6.2.2 states the information capacity results derived (the theoretical lower bounds) for a single synaptic channel – in this thesis appointed as the inter-neuronal channel. The remainder of the chapter brings novel information theoretical results of synapses. More specifically, Section 6.3.1 defines a system model used for capacity computation. Section 6.3.2 provides a brief introduction to the recognized analogies between neural and optical communication systems vastly used throughout the chapter. The theoretical upper bounds on the capacity of a synapse under the five scenarios defined above are derived in Section 6.3.3, and plotted in Section 6.3.4. An illustrative example of a realistic hippocampal channel is considered in Section 6.3.5. Concluding remarks and notes on future work are given in Section 6.4.

6.2 Related Work

6.2.1 Information Capacity of Intra-Neuronal Link

Capturing the capacity of a single neuron, i.e., the intra-neuronal link, has been delegated by Don H. Johnson in [97, Chapter 3]. It has been found as equivalent to answering the question: How well a neural code can express a stimulus set? To calculate this capacity, Johnson has modeled spike discharge patterns with the point process, wherein the occurrence of a spike depends on the stimulus and on previous spikes. The selected point process has been the simplest Poisson process, wherein the intensity does not depend on previous spikes. This assumption allows expressing the intensity as an instantaneous rate function $\lambda(t)$. Then, capacity has been calculated by maximizing the mutual information, I, between two jointly defined random quantities, X and Y:

$$\mathcal{C}_R = \lim_{T\to\infty} \max_{p_X} \frac{1}{T} I(X;Y), \tag{6.2}$$

where T denotes the length of the observation interval, and p_X denotes the probability distribution of X. Relevant to the intra-neuronal link, X and Y denote the neuronal stimuli and response, respectively.

Following the method given in Eq. (6.2), the capacity of the single-neuron channel attained by a Poisson process and a random discrete-stimulus set $\lambda \in (0, \lambda_{\max})$ has been found according to:

$$\mathcal{C}_R = \frac{\lambda_{\max}}{\mathrm{e} \ln 2}. \tag{6.3}$$

When the maximal rate varies with time, e.g., to describe a neuron's response to a suddenly applied stimulus, capacity result generalizes:

$$\mathcal{C}_R = \frac{1}{\mathrm{e} \ln 2} \lim_{T \to \infty} \frac{1}{T} \int_0^T \lambda_{\max}(t) \mathrm{d}t. \tag{6.4}$$

If, however, more realistic point process models spike discharges to embrace refractoriness and historical dependencies, smaller capacities are calculated. For example, if absolute refractory period is T^{ARP}, the capacity under a maximal rate constraint of $\lambda_{\max}$ is given by:

$$\mathcal{C}_R = \frac{1}{1 + \lambda_{\max} T^{ARP}} \frac{\lambda_{\max}}{\mathrm{e} \ln 2}. \tag{6.5}$$

Note that the capacity achieving input has been found in a form of a square wave that randomly switches between the minimal and maximal rates in a way that the probability of the input equaling $\lambda_{\max}$ is 1/e. This signal is known as a random telegraph signal which has infinite bandwidth. Telegraphic-like inputs are, however, not realistic in neuroscience.

6.2.2 Lower Bound on the Information Capacity of Inter-Neuronal Link

Concerning the synaptic communication channel, the closest related study is the work by Manwani and Koch [79]. They relied on neural hardware to derive *theoretical lower bounds on the information capacity*[2] of a simple model of the bipartite synapse under signal estimation and signal detection paradigms. The signal estimation paradigm assumes the information to be encoded in the mean spiking rate of the pre-synaptic neuron, with the objective to estimate the continuous input signal from the post-synaptic response. The signal detection observes the input as binary,

[2]Lower bounds derived in [79] depend on the signal and synaptic parameters and thus need not hold for synapses whose properties depart strongly from Manwani-Koch's choice of parameter values. Given the parameter set, the true capacity of information transmission over synapse could take any value greater than or equal to the lower bound. In addition, note that in general case capacity lower and upper bounds define the region to which the actual capacity may belong. Nonetheless, the upper bounds derived in following sections of this chapter utilize different signal and synaptic parameters and cannot be used together with lower bounds from [79].

and the presence/absence of a pre-synaptic spike is to be detected from the post-synaptic response. The efficacy of information transfer in synapses is characterized by deriving optimal strategies under these two paradigms [79].

Under signal estimation paradigm, the theoretical lower bound on the information capacity has been derived for an ideal synapse as [79]:

$$\mathcal{C}_{LB}^{(a)} = B_\theta \log_2 \left(1 + \frac{c_{\lambda_1}^2 \lambda_1}{2B_\theta}\right). \tag{6.6}$$

B_θ is the bandwidth of input signal $\theta(t)$, and c_{λ_1} is the contrast of the pre-synaptic neuron's spiking rate defined as the ratio between the standard deviation of the spiking rate fluctuations σ_{λ_1} and the spiking rate λ_1, i.e., $c_{\lambda_1} = \sigma_{\lambda_1}/\lambda_1$.

The theoretical lower bound on the information capacity has been derived for an unreliable and noisy synapse as [79]:

$$\mathcal{C}_{LB}^{(b)} = B_\theta \log_2 \left(1 + \frac{c_{\lambda_1}^2 \lambda_1}{2\kappa B_\theta}\right). \tag{6.7}$$

Relative to the lower bound on information rate for an ideal synapse (Eq. (6.6)), the lower bound in Eq. (6.7) depends on a shot-noise-related factor

$$\kappa = \frac{1 + \rho_q^2}{P_{rel}}, \tag{6.8}$$

where ρ_q is the coefficient of variation of synaptic quantal amplitude ${q_n}^3$, and P_{rel} is the vesicle release probability.

As a reference, the Manwani-Koch's result is reproduced for an ideal synapse (Eq. (6.6)) in Fig. 6.2(a) given different values of the input signal bandwidth B_θ. The information rate monotonically increases with B_θ, but saturates at high B_θ. From Fig. 6.2(a), given $B_\theta = 10$ [kHz], the lower bound on the information capacity is above 6 [bit/s]. The Manwani-Koch's result for an unreliable and noisy synapse (Eq. (6.7)) is reproduced in Fig. 6.2(b). Given $B_\theta = 10$ [kHz], the lower bound on the information capacity is approximately 2.5 [bit/s]. Although not visible from Fig. 6.2, lower bound curves saturate for very high spiking rates.

Under signal detection paradigm, channel performance has been quantified by the mutual information between the binary random variables, X and Y ($X = 1$ if a spike occurred at the pre-synaptic terminal, else $X = 0$, and $Y = 1$ if a spike is detected at the post-synaptic terminal, else $Y = 0$) [33]:

$$I(X;Y) = \mathcal{H}(P_Y) - p_0 \mathcal{H}(P_F) - (1 - p_0)\mathcal{H}(P_M), \tag{6.9}$$

[3] Manwani and Koch model the post-synaptic response to the release of a single vesicle by an alpha function multiplied by a random variable q_n drawn from a gamma distribution; ρ_q is defined as a ratio $\sigma_q/\bar{q_n}$, where σ_q denotes the standard deviation and $\bar{q}$ denotes the mean of the quantal amplitude q_n.

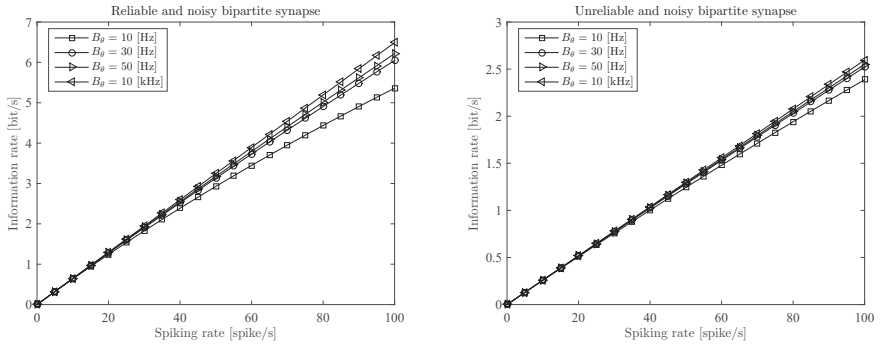

(a) (b)

Figure 6.2: (a) The capacity lower bound as a function of the spiking rate given various stimulus bandwidths B_θ for an ideal synapse. The ratio $c_{\lambda_1} = 0.3$. (b) The capacity lower bound as a function of the spiking rate given various stimulus bandwidths B_θ for an unreliable and noisy synapse. The constant vesicle release probability $p_{rel} = 0.4$, ratio $c_{\lambda_1} = 0.3$, and coefficient $\rho_q = 0$.

where $P_Y = p_0(1 - P_F) + (1 - p_0)P_M$ and $\mathcal{H}(x) = -x \log_2 x - (1 - x) \log_2(1 - x)$ is the binary entropy function. Probabilities p_0 and $(1 - p_0)$ are prior probabilities of $X = 0$ and $X = 1$, respectively, and

$$P_F = \text{Prob}[Y = 1|X = 0], \qquad P_M = \text{Prob}[Y = 0|X = 1]. \tag{6.10}$$

Albeit Manwani and Koch derived theoretical lower bounds on the information capacity of a simple model of the bipartite synapse [79], it is not instructive to compare the study and corresponding results with the following ones as the underlying system models are different.

6.3 Upper Bound on the Information Capacity of Inter-Neuronal Link

Chapter 2 accumulated the knowledge about the neural anatomy, physiology, and the manner in which information is processed and communicated at various stages in single neurons. The main neural compartments with two possible configurations forming the concepts of bipartite and tripartite synapses are simplified in Fig. 6.3. Recall that the bipartite synapse is an important component of the communication channel between neurons. Specifically, it is the site of functional apposition between two cells, where a transmitting pre-synaptic neuron/terminal converts the spiking signal into neurotransmitter molecules, that are released into the synaptic cleft to

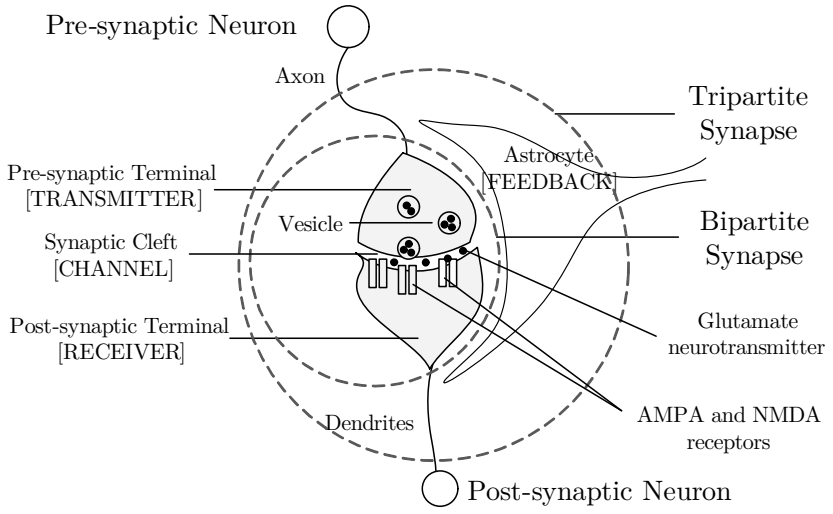

Figure 6.3: Schematic diagram of the neuronal anatomy with bipartite and tripartite synapses. Alike neurons, astrocytes can release glutamate into the cleft in response to an increased activity of adjacent neurons, acting as feedback units to the neuron.

propagate and bind to the AMPA and NMDA receptors[4] located on the membrane of the receiving post-synaptic neuron/terminal. When the astrocyte cell is in the vicinity of the synapse, the concept of tripartite synapse is introduced (Section 2.2.5) to underline the presence of the astrocytic terminal in the vicinity of two neurons. Astrocytes cannot produce spikes and therefore were not initially suspected as playing an important and active role in neural communication. However, they are numerous, accounting for over 70% of all cells in the central nervous system (this number is specific for higher mammals), and are now known to appreciably support neural functions and inter-cellular coordination.

As spoken of in the introductory section, the ultimate goal of this section is to quantify how much information a receiving/post-synaptic neuron carries about the transmitting/pre-synaptic neuron. This quantification should provide a supplementary insight into the efficacy of information transmission between neurons by deriving *theoretical upper bounds on the information capacity* of bipartite and tripartite synapses. To this end, different system models and set-ups with progressive complexity are tackled. More specifically, a noisy bipartite synapse with: i) reliable vesicle release, ii) unreliable vesicle release with constant release probability, iii)

[4]In case the neuroplasticity (dynamic wiring of neurons) is not considered (as in this study), it is common in neuroscience to analyze only AMPA receptors since they mediate most of the synaptic excitation in the central nervous system. Otherwise, NMDA receptors are also important.

unreliable vesicle release with time-varying release probability, and iv) unreliable vesicle release followed by an unreliable neurotransmitter propagation and binding to the receiving neuron is analyzed. Then, the analysis is extended to the concept of a noisy and unreliable tripartite synapse. The findings and results shall be of primary importance in understanding the performance of the neural communication paradigm as a candidate for future nano-networks.

6.3.1 System Model

Given the stimuli $\theta(t)$ at the input of the pre-synaptic neuron (refer to Fig. 6.3), which is typically a dendritic current, I_d, or somatic current, I_s, the spike encoder generates a sequence of action potentials encoding the information contained in the stimulus. The simplest model of the spike train is the non-homogeneous Poisson process [25] with rate depending on the magnitude of the stimulus. However, the neuronal membrane is refractory immediately after a spike, which leads to the firing probability that depends not only on the stimulus but also on the preceding spike train. As a consequence, the refractoriness precludes two consecutive spikes to be independent and causes the spike train to become more regular than a Poisson process with the same firing rate [17]. Thus, a more theoretically grounded way would be to modify the Poisson process to include refractoriness. Albeit Berry and Meister [19] did that way by defining the instantaneous firing rate as the product of a *free firing rate*, which depends only on the stimulus, and a *recovery function*, which depends only on the time since the last spike, they proved the free firing to be a more fundamental response measure if neurons use a "firing rate code" in which the message lies in the instantaneous spiking. A refractory period actually causes the modified rate to saturate and miss out gradations in the stimulus. Motivated by this inference, this study practically neglects the refractoriness in the synaptic capacity analysis – it is believed that a spiking sequence $s(t)$ described as a *non-homogeneous Poisson impulse process* directed by the intensity that is proportional to the stimulus, i.e., $\lambda_1(t) \propto \theta(t)$, is adequate for derivation of upper bounds on information rates in neural synapses. Thus,

$$s(t) = \sum_{n=1}^{N_1(t)} \delta(t - t_n), \tag{6.11}$$

where t_n is the arbitrary spike generation time, and $\{N_1(t) : 0 \leq t \leq T\}$ is a non-homogeneous Poisson process whose rate, $\lambda_1(t)$, is a temporal function, and

$$\mathbb{E}[N_1(t)] = \int_0^t \lambda_1(u)\mathrm{d}u. \tag{6.12}$$

The operator $\mathbb{E}[\cdot]$ denotes expectation. The signal $s(t)$ propagates down the axon, a nerve fiber that conducts impulses away from the neuron's body (see Fig. 6.3), and reaches the pre-synaptic terminal of the transmitting neuron.

Numerous physiological mechanisms [83, 126, 129] convert the spiking sequence $s(t)$ into a chemical form $q(t)$ generated by means of neurotransmitter release machinery.

- The release of neurotransmitters upon arrival of individual action potentials is modulated by the **vesicle release probability**, P_{rel}, driven by the intracellular calcium concentration within the pre-synaptic terminal of the transmitting neuron, $[\mathrm{Ca}^{2+}]_{\mathrm{pre}}$. For the tripartite synapse, $[\mathrm{Ca}^{2+}]_{\mathrm{pre}}$ is found from the Pinsky-Li-Rinzel model [72, 87, 88, 107]. The relation between $[\mathrm{Ca}^{2+}]_{\mathrm{pre}}$ and P_{rel} is found from the Bertram-Sherman-Stanley four-gate model of the vesicle release process. The model contains four independent gates (S_1 – S_4) with different opening and closing rates, and with S_4 closing most rapidly and S_1 closing most slowly, i.e., [20]

$$P_{rel}(t) = O_1(t)O_2(t)O_3(t)O_4(t), \tag{6.13}$$

  where O_js are the open gate probabilities associated with gates S_js, and

$$\frac{\mathrm{d}O_j(t)}{\mathrm{d}t} = k_j^+[\mathrm{Ca}^{2+}]_{\mathrm{pre}}(t) - \frac{O_j(t)}{\tau_j}, \quad j = 1, 2, 3, 4. \tag{6.14}$$

  k_j^+ and k_j^- are opening and closing rates ($\mathrm{ms}^{-1} \times \mu\mathrm{M}^{-1}$), respectively: $k_1^+ = 3.75 \times 10^{-3}$, $k_1^- = 4 \times 10^{-4}$, $k_2^+ = 2.5 \times 10^{-3}$, $k_2^- = 1 \times 10^{-3}$, $k_3^+ = 5 \times 10^{-4}$, $k_3^- = 0.1$, $k_4^+ = 7.5 \times 10^{-3}$, $k_4^- = 10$, and $\tau_j = 1/(k_j^+[\mathrm{Ca}^{2+}]_{\mathrm{pre}} + k_j^-)$.

  Owing to the property of splitting non-homogeneous Poisson processes [28], the neurotransmitter sequence that is injected into the synaptic cleft by the pre-synaptic terminal is defined here as a non-homogeneous Poisson process given as

$$q(t) = \sum_{n=1}^{N_2(t)} q_n \delta(t - t_n), \tag{6.15}$$

  where q_n is the number of injected neurotransmitters at the arbitrary time t_n, $\{N_2(t) : 0 \leq t \leq T\}$ is a non-homogeneous Poisson process, and

$$\mathbb{E}[N_2(t)] = \int_0^t P_{rel}(u)\lambda_1(u)\mathrm{d}u. \tag{6.16}$$

There are two more sources of unreliability in the remaining communication pathway between two neurons:

- The neurotransmitter propagation towards the post-synaptic membrane is random and caused by the stochastic nature of the Brownian motion of neurotransmitters in a fluid medium of synaptic cleft. Based on the analogy between the advection-diffusion equation and the Fokker-Planck equation, Chahibi and Akyildiz [28] found a single drug particle delivery in particulate drug delivery system within the cardiovascular network to follow a Bernoulli distribution.

The advection-diffusion equation is based on the generalized Taylor dispersion equation that governs the cross-sectional concentration of particles. The Fokker-Planck equation is the basis of the random motion of particles. As the mentioned analogy is valid in fluid synaptic cleft, a single neurotransmitter delivery (*not* binding), described with the **neurotransmitter propagation probability**, P_s, should then also follow a Bernoulli distribution.

- The neurotransmitter binding to the membrane of the post-synaptic neuron is characterized by the ligand-binding mechanism. The first time derivative of the probability of having n_b bound receptors among the N_R receptors, $\mathrm{d}P_{n_b}/\mathrm{d}t$, is found to depend on three terms: the probability P_{n_b-1} of having n_b-1 bound chemical receptors and having a binding reaction, the probability P_{n_b+1} of having n_b+1 bound chemical receptors and having a release reaction, and the negative of the probability P_{n_b} of having either a release reaction or a binding reaction [104], i.e.,

$$\begin{aligned}\frac{\mathrm{d}P_{n_b}(t)}{\mathrm{d}t} &= c_R(t)k_+(N_R-n_b+1)P_{n_b-1}(t)\\ &+ k_-(n_b+1)P_{n_b+1}(t)\\ &- \left[k_-n_b + c_R(t)k_+(N_R-n_b)\right]P_{n_b}(t).\end{aligned} \tag{6.17}$$

In Eq. (6.17), $c_R(t)$ is the neurotransmitter concentration, and k_+ and k_- are the neurotransmitter binding and release rates, respectively.

The binding of neurotransmitters to the AMPA and NMDA described with the **neurotransmitter binding probability**, P_b, similarly depends on the number of receptors in an open state. Hence, the first derivative of the probability P_b is defined here as

$$\frac{\mathrm{d}P_b(t)}{\mathrm{d}t} = c_R(t)k_+(N_R-n_b)P_b(t). \tag{6.18}$$

In a simplified scenario, the neurotransmitter binding probability, P_b, can be modeled to follow a Bernoulli distribution.

6.3.2 The Synaptic Poisson Channel

Given the system model in previous section, what follows is motivated with a principal analogy between the **optical communications system** and **synaptic communication system**. This principal analogy turns out to be essential to this study, as it enables the calculation of the capacity of a *Poisson-type synaptic channel*, using results derived for the optical communication channel. The capacity of the optical communication channel was found in [29, 34, 46, 54, 64, 115].

The transmitter in the optical communications system is a *laser* and is related to the *pre-synaptic terminal* in the synaptic communication system. The channel in the

optical communications system is an *optical fiber* and is related to the *synaptic cleft* in the synaptic communication system. The receiver in the optical communications system is a *photo-detector* and is related to the *post-synaptic terminal* in the synaptic communication system. The analogy stems from the following:

- At the transmitter in the optical communications system, a laser emits a stream of photons with a time-varying rate that is proportional to the amplitude of the input current. It has been shown [14] that the emission of photons corresponds to the point process, and the transmitted beam fluctuations generated by a single-mode laser obey Poisson statistics. Hereof, the sequence of photons is typically modeled as a non-homogeneous Poisson point process with a time-varying rate [14, 130].

  The analogy between the emissions of photons and neurotransmitters arises as the neurotransmitter sequence injected into the synaptic cleft by the pre-synaptic terminal can also be modeled as a non-homogeneous Poisson point process (see Eq. (6.15)) [25], as justified in the previous section.

- The relation between channels is of less relevance, but evident: the photon particles propagate through the fiber in the optical communications system; the neurotransmitter particles propagate/diffuse through the cleft in the synaptic communication system.

- A stream of photons is received by a photo-detector which is able to determine and count the arrival times of individual photons. The expectation of the count varies as the input signal that modulates the laser beam, plus the effect of noise [14]. The noise is due to detector "dark current" and background radiation, which is thought to obey Poisson statistics.

  The analogy between the receptions of photons and neurotransmitters arises from the following. A stream of neurotransmitters is received by AMPA and NMDA receptors at the post-synaptic terminal. AMPA and NMDA receptors become conductive for Na^+ and K^+ ions leading to a change (increase) in post-synaptic membrane potential known as an Excitatory Post-Synaptic Potential (EPSP). Multiple EPSPs that are generated by the dendritic compartments of the receiving neuron sum up constructing a membrane potential that may lead to another spiking sequence[5]. As the photon counting process, the neurotransmitter binding and influx of ions into the receiving neuron varies as the input spiking sequence at the pre-synaptic terminal, plus the effect of noise. The noise here is due to spontaneous vesicle release, which is also thought to obey Poisson statistics [88].

Applying Poissonian spiking statistics and channel results in the capacity analysis of neurons has been previously done to quantify how much information a neuronal response carries about the time-varying stimulus [97, Chapter 3], [17,119]. Although

[5]With just one synapse and/or one incoming spiking sequence, the receiving neuron is not capable of generating another spiking sequence.

the Poissonian nature of the synaptic channels has been indicated every time the spiking sequence obeyed Poisson statistics, to the best of the author knowledge this is the first time the analogies between the neural system and optical system are introduced. Apparently, applying the optical Poisson channel results to the capacity analysis of a neural synapse is done for the first time in the literature.

6.3.3 The Synaptic Channel Capacity

The synaptic Poisson channel is an additive noise channel with output $Y = N + X$, where N is the channel noise and X is the transmitted signal into which the message $\theta(t)$ is encoded. Both N and X are Poisson-type point processes. N represents the **noisy effect** of spontaneous vesicle release and is directed by the intensity $\lambda_0'(t) = P_s(t)P_b(t)\lambda_0(t)$, where $\lambda_0(t)$ is the intensity of spontaneous release at the pre-synaptic terminal. X is directed by the spiking-dependent intensity $\lambda_1'\left(t, \lambda_1(t,\theta)\right) = P_{rel}(t)P_s(t)P_b(t)\lambda_1(t)$. Thus, the output Y is also a Poisson-type point process directed by the intensity

$$\begin{aligned}\lambda_2(t) &= \lambda_0'(t) + \lambda_1'(t,\lambda_1) \\ &= P_s(t)P_b(t)\left[\lambda_0(t) + P_{rel}(t)\lambda_1(t)\right]. \end{aligned} \tag{6.19}$$

Note that λ_0' and λ_1' stem from the property of splitting non-homogeneous Poisson processes [28], and are valid only when the neurotransmitter release, propagation and binding processes are independent. This issue is thoroughly considered later in Section 6.3.3.

The rate of the spontaneous vesicle releases, $\lambda_0(t)$, that can occur when the pre-synaptic membrane is not depolarized, depends on the pre-synaptic calcium concentration $[Ca^{2+}]_{pre}$ as [88]

$$\lambda_0(t) = a_3\left(1 + e^{\left(a_1 - [Ca^{2+}]_{pre}(t)\right)/a_2}\right)^{-1}. \tag{6.20}$$

The coefficients a_1, a_2 and a_3 depend on the number of active zones, which are the sites of neurotransmitter release.

Given $\lambda_1(t) = \lambda_1$, the pre-synaptic calcium concentration is nontime-varying at the time instants of action potential arrivals, $[Ca^{2+}]_{pre}(t) = [Ca^{2+}]_{pre}$. In other words, the envelope of the concentration is nontime-varying, as demonstrated later in Section 6.3.5. This assumption implies from Eq. (6.20) that $\lambda_0(t) = \lambda_0$ at the time instants of action potential arrivals. This is applicable to the bipartite synapse where the primal contribution to the calcium concentration is due to the action potentials arriving at the pre-synaptic terminal, i.e., $[Ca^{2+}]_{pre} = [Ca^{2+}]_{AP}$. For the tripartite synapse, the spontaneous vesicle release $\lambda_0(t)$ is time-varying, owing to additional contribution to the calcium concentration due to the astrocytic feedback (refer to [83]), i.e., $[Ca^{2+}]_{pre} = [Ca^{2+}]_{AP} + [Ca^{2+}]_{astro}$ (which produces the time-varying calcium concentration).

As mentioned earlier, the content of this chapter elaborates on the problem considering synapses with increasing complexity. For the sake of clarity, the uncertainties induced by the particle propagation through the synaptic cleft and the ligand-binding mechanism are not considered at first, i.e., $P_s(t)$ and $P_b(t)$ are both unity. Under this simplification, the system models for the bipartite- and tripartite synapses are

$$\lambda_2(t) = \lambda_0 + P_{rel}(t)\lambda_1, \tag{6.21}$$

$$\lambda_2(t) = \lambda_0(t) + \tilde{P}_{rel}(t)\lambda_1, \tag{6.22}$$

respectively. Relative to $P_{rel}(t)$ in Eq. (6.21), $\tilde{P}_{rel}(t)$ in Eq. (6.22) is additionally affected by the astrocyte.

Throughout the paper, the information processing limits are analyzed subject to the **rate amplitude constraint**

$$\lambda_2 \in [\lambda_0, \lambda_0 + \Lambda], \tag{6.23}$$

where Λ is the maximum spiking rate at the input, and an **average energy constraint**

$$\mathbb{E}\left[\int_0^T \lambda_2(t)\mathrm{d}t\right] \leq (\Lambda_0 + \lambda_0)T, \tag{6.24}$$

where Λ_0 is an arbitrary spiking rate, $0 \leq \Lambda_0 \leq \Lambda$. The peak constraint given in Eq. (6.23) is associated with neuron's inability to fire with the rate higher than that physiologically determined as the neuronal membrane has an upper rate at which it can depolarize [35]. The maximum spiking rate varies among neuron types; refer to [3] for electrophysiological values of maximum firing rates across neuron types. The average energy constraint in Eq. (6.24) is directly associated with metabolically expensive neuron's signaling, as analysis of synaptic signaling confirmed that the nervous system use much energy to generate and communicate signals [71]. The resting metabolic energy thus naturally constraints the flow of information between synapses and limits neural performance and neural consumption.

Noisy and Reliable Vesicle Release

At the outset, let the investigation begin with a special and simple case: the bipartite synapse with a vesicle release that is noisy – spontaneous vesicle releases occur without neuronal spiking, but reliable – vesicle releases follow the arrival of individual spikes to the pre-synaptic terminal. Hence, the vesicle release probability $P_{rel} \to 1$, and from Eq. (6.21) the output of the channel is a non-homogeneous Poisson process directed by the intensity $\lambda_2(t) \to \lambda_0 + \lambda_1(t)$. This means the channel output is only a noisy version of the channel input.

The optical counterpart of this problem is known in the literature; see the work by M. Davis [34]. At this point, refer back to fundamental analogies provided in

Section 6.3.2. This analogy associates the upper bound for the synaptic Poisson channel capacity with the upper bound for the optical Poisson channel capacity which allows omission of detailed derivation. When adapted to the synaptic Poisson channel, the upper bound for the synaptic Poisson channel capacity is then given as [29]

$$\mathcal{C}_{UB}^{(a)} = \max_{0\leq\mu\leq\sigma} \left[\mu\phi(\Lambda) - \phi(\mu\Lambda)\right], \tag{6.25}$$

where $\phi(x) = (\lambda_0 + x)\ln(\lambda_0 + x) - \lambda_0 \ln \lambda_0$, μ is the probability of the channel input taking the value Λ, and σ is the ratio of average-to-peak power, $0 \leq \sigma \leq 1$. Eq. (6.25) is maximized for

$$\mu_{\max}^{(a)} = \frac{\lambda_0}{\Lambda}\left[\frac{1}{\mathrm{e}}\left(1 + \frac{\Lambda}{\lambda_0}\right)^{\left(1+\lambda_0/\Lambda\right)} - 1\right], \tag{6.26}$$

whence the *upper bound on the capacity for the bipartite synaptic Poisson channel with reliable vesicle release* is calculated as [34]

$$\mathcal{C}_{UB}^{(a)} = \begin{cases} \mu\phi(\Lambda) - \phi(\mu\Lambda), & \mu < \mu_{\max}^{(a)}, \\ \dfrac{\lambda_0}{\mathrm{e}}\left(1 + \dfrac{\Lambda}{\lambda_0}\right)^{\left(1+\lambda_0/\Lambda\right)} - \lambda_0 \ln\left[\left(1 + \dfrac{\Lambda}{\lambda_0}\right)^{\left(1+\lambda_0/\Lambda\right)}\right], & \mu \geq \mu_{\max}^{(a)}. \end{cases} \tag{6.27}$$

This result resembles the capacity of a single neuron cell described with a Poisson channel [97, Chapter 3], where the noise effects come from spontaneous spike generation. In case randomness in the synapse is involved, the data processing inequality [33] suggests the channel capacity must be less than or equal to Eq. (6.27).

Noisy and Unreliable Vesicle Release with Constant Release Probability

If the synaptic channel output is directed by the intensity

$$\lambda_2(t) = \lambda_0 + P_{rel}(t)\lambda_1(t), \tag{6.28}$$

where $P_{rel}(t) \in [0, 1]$, the approach taken by Chakraborty and Narayan [29] can be adapted in the analysis of the optical Poisson fading channel, where the output rate is

$$\lambda_2(t) = \lambda_0 + S(t)\lambda_1(t), \tag{6.29}$$

with $S(t)$ representing the channel fade, and λ_0 the effect of "dark current" and background radiation in optical communication channel. The probability $P_{rel}(t)$ in Eq. (6.28) corresponds to the channel fade $S(t)$ in Eq. (6.29).

In this subsection, the channel capacity is derived for a noisy and unreliable bipartite synapse where vesicle releases follow the arrival of individual spikes to the presynaptic terminal with constant release probability. This problem can be associated

with the scenario in optical communications system when channel fade in Eq. (6.29) is constant, i.e., $S(t) = s$, and the receiver possess perfect Channel State Information (CSI) while the transmitter has no CSI. The assumption of known CSI is pivotal for the mathematical tractability. Note that the best solution to this problem would be to derive the upper bound on information rate when neither the pre- and post-synaptic terminal would have the CSI. However, the close-form bound without CSI is unknown at present; it is of primary importance in future research efforts since this will help in finding more exact capacity bounds for neural synapses. Furthermore, the case with known CSI at the post-synaptic side and no CSI at the pre-synaptic side is preferred here over the case with perfect CSI at both the pre- and post-synaptic terminals, as the former is likely to be the tightest upper bound. Under these assumptions, the corresponding channel capacity is found as [29]

$$\mathcal{C} = \max_{0 \le \mu \le \sigma} \left[\mu\phi(s\Lambda) - \phi(\mu s\Lambda) \right], \tag{6.30}$$

where μ is the probability of the channel input taking the value Λ, σ is the ratio of average-to-peak power, $0 \le \sigma \le 1$, and s is the channel fade.

Unlike the problem of capacity calculation for Poisson channels [34, 64], capacity calculation for Poisson fading channels has to account for the output rate that is not only a noisy, but also a diluted (scaled) version of the input rate. Nonetheless, the problem of maximization given by Eq. (6.30) for Poisson fading channel is found to be equivalent to the problem of maximization for Poisson channel defined by Kabanov as [64]

$$\mathcal{C} = \max_{0 < \lambda < \Lambda} \left[\frac{\lambda}{\Lambda}\phi(\Lambda) - \phi(\lambda) \right], \tag{6.31}$$

where $\lambda \in [0, \Lambda]$ denotes the input rate. By comparing Eq. (6.30) and Eq. (6.31),

$$\mu \equiv \lambda/\Lambda \quad \text{and} \quad s\Lambda \equiv \Lambda. \tag{6.32}$$

Hence, as long as the receiver has the CSI as advocated in [29], the scaling of the output rate *does not* impose principal changes to the method of maximization described by Kabanov.

Following this important inference and Section 6.3.2, the *upper bound on the capacity for the bipartite synaptic Poisson channel with constant vesicle release probability* is defined here as

$$\mathcal{C}_{UB}^{(b)} = \begin{cases} \mu\phi(P_{rel}\Lambda) - \phi(\mu P_{rel}\Lambda), & \mu < \mu_{\max}^{(b)}, \\ \dfrac{\lambda_0}{\mathrm{e}} \left(1 + \dfrac{P_{rel}\Lambda}{\lambda_0}\right)^{\left(1+(P_{rel}\Lambda)^{-1}\lambda_0\right)} - & \\ \qquad \lambda_0 \ln \left[\left(1 + \frac{P_{rel}\Lambda}{\lambda_0}\right)^{\left(1+(P_{rel}\Lambda)^{-1}\lambda_0\right)} \right], & \mu \ge \mu_{\max}^{(b)}, \end{cases} \tag{6.33}$$

where $\mu_{\max}^{(b)}$ is obtained by maximizing Eq. (6.30) with $s = P_{rel}$, i.e.,

$$\mu_{\max}^{(b)} = \frac{\lambda_0}{P_{rel}\Lambda}\left[\frac{1}{\mathrm{e}}\left(1+\frac{P_{rel}\Lambda}{\lambda_0}\right)^{\left(1+(P_{rel}\Lambda)^{-1}\lambda_0\right)} - 1\right]. \tag{6.34}$$

Noisy and Unreliable Vesicle Release with Time-Varying Release Probability

If the probabilities from the previous scenario are time-varying, i.e., S in Eq. (6.29) is a random variable, and the receiver possesses perfect CSI while the transmitter has no CSI, the corresponding optical channel capacity is found similarly (refer to Eq. (6.30)). The maximum of the averaged conditional mutual information is then given as [29]

$$\mathcal{C} = \max_{0\le\mu\le\sigma} \mathbb{E}\left[\mu\phi(S\Lambda) - \phi(\mu S\Lambda)\right], \tag{6.35}$$

where the expectation is taken over the distribution of random variable S, and μ is the probability of the channel input taking the value Λ, σ is the ratio of average-to-peak power, $0 \le \sigma \le 1$, and S is the channel fade.

Considering the vesicle release probability P_{rel} in synaptic communication system is time-varying, as defined by Eq. (6.13), the *upper bound on the capacity for the bipartite synaptic Poisson channel with time-varying vesicle release probability* is

$$\mathcal{C}_{UB}^{(c)} = \max_{0\le\mu\le\sigma} \mathbb{E}\left[\mu\phi(P_{rel}\Lambda) - \phi(\mu P_{rel}\Lambda)\right], \tag{6.36}$$

where the expectation is taken over the distribution of the random variable P_{rel}.

Noisy and Unreliable Bipartite Synapse

The most complex and realistic scenario has the added effects of unreliability incurred by the neurotransmitter propagation through the synaptic cleft and the ligand-binding mechanism. The output rate of the Poisson channel is then directed by the intensity

$$\lambda_2(t) = P_s(t)P_b(t)\left[\lambda_0 + P_{rel}(t)\lambda_1(t)\right]. \tag{6.37}$$

The effect of spontaneous vesicle release $P_s(t)P_b(t)\lambda_0$ and the probability product $P_{rel}(t)P_s(t)P_b(t)$ in Eq. (6.37) now correspond to the "dark current" λ_0 and the channel fade $S(t)$ in Eq. (6.29), respectively. Nevertheless, the problem of calculating the channel capacity for a noisy and unreliable bipartite synapse is *not* equivalent to the problem of calculating the capacity for the optical Poisson fading channel, where the output rate is given by Eq. (6.29).

Namely, the assumption in Section 6.3.3 is that the noise (λ_0) and signal sources ($\lambda_1' = P_{rel}(t)\lambda_1$) are independent and thus uncorrelated (refer to Eq. (6.28)). If

$X = \lambda_0$ and $Y = \lambda_1'$, then $\mathrm{Cov}[X, Y] = 0$, i.e., $\mathbb{E}[XY] = \mathbb{E}[X]\mathbb{E}[Y]$. In the current scenario where the system model is described with Eq. (6.37), the multiplicative term $P_s(t)P_b(t)$ is associated with the intensity of both the noise and the signal sources. As described in Section 6.3.1, the neurotransmitter propagation probability P_s follows a Bernoulli distribution, i.e., $P_s = p_s$ for a given synapse, and is connected to the diffusion and neurotransmitters being lost in the cleft. This is independent on signal and noise, regardless the quantity of the particles. The neurotransmitter binding probability P_b is though random and time varying, and is connected to the ligand-binding mechanism. Now, if $X = \lambda_0$, $Y = \lambda_0'$ and $Z = p_s P_b$, consider the uncorrelatedness of the variables $U = XZ = p_s P_b \lambda_0$ and $V = YZ = p_s P_b \lambda_1'$ (see Eq. (6.37)). The variables X, Y, Z are assumed as pairwise uncorrelated ($\mathrm{Cov}[X, Y] = 0$, $\mathrm{Cov}[X, Z] = 0$ and $\mathrm{Cov}[Y, Z] = 0$), although not pairwise independent as P_b depends on the neurotransmitter concentration at the post-synaptic side as given by Eq. (6.18), where the neurotransmitter concentration is dependent on the input signal λ_1. Under these assumptions[6]

$$\mathrm{Cov}[U, V] = \mathrm{Cov}[XZ, YZ] = \mathbb{E}[X]\mathbb{E}[Y]\mathrm{Var}[Z] \geq 0. \tag{6.38}$$

Hence, the right hand side is zero when $\mathrm{Var}[Z] = 0$, i.e., the ligand-binding mechanism is either ideal or the neurotransmitter binding probability follows a Bernoulli distribution, i.e., $P_b = p_b$ for a given synapse[7]. Only then the variables $U = XZ$ and $V = YZ$ are uncorrelated and the problem of calculating the channel capacity for a noisy and unreliable bipartite synapse is equivalent to the problem of calculating the capacity for the optical Poisson fading channel, where the output rate is given by Eq. (6.29). Otherwise, the computation of the capacity remains an issue.

With the simplified amendment that both the neurotransmitter propagation and binding follow a Bernoulli distribution, the *upper bound on the capacity for the bipartite synaptic Poisson channel with constant vesicle release probability*, $\mathcal{C}_{UB}^{(d')}$, follows similarly from Eq. (6.33). The *upper bound on the capacity for the bipartite synaptic Poisson channel with time-varying vesicle release probability*, $\mathcal{C}_{UB}^{(d'')}$, follows similarly from Eq. (6.36).

Noisy and Unreliable Tripartite Synapse

In the set-up with the astocytic feedback to the pre-synaptic terminal, the spontaneous vesicle release is time-varying, $\lambda_0(t)$, as mentioned earlier. To compute the capacity for the tripartite synapse, the result provided by Frey [46], who considered the information capacity of the Poisson channel with random noise intensity in optical channels, is adapted.

[6]The result of $\mathrm{Cov}[AB, CD]$, where A, B, C and D are jointly distributed random variables, and the conventional asymptotic approximation procedure from [66, page 232] are used. The result in Eq. (6.38) yields given $A = X$, $B = Z$, $C = Y$ and $D = Z$ that are pairwise uncorrelated.

[7]The scenarios when $\mathbb{E}[X] = \mathbb{E}[\lambda_0] = 0$ and/or $\mathbb{E}[Y] = \mathbb{E}[P_{rel}\lambda_1] = 0$ are of no interest.

Hence, the *upper bound on the capacity for the tripartite synaptic Poisson channel with constant vesicle release probability* is given as

$$\mathcal{C}_{UB}^{(e')} = \frac{1}{T}\int_0^T \mathcal{C}_{UB}^{(d')}(\lambda, \Lambda, \mu)\mathrm{d}t. \tag{6.39}$$

The *upper bound on the capacity for the tripartite synaptic Poisson channel with time-varying vesicle release probability* is given as

$$\mathcal{C}_{UB}^{(e'')} = \frac{1}{T}\int_0^T \mathcal{C}_{UB}^{(d'')}(\lambda, \Lambda, \mu)\mathrm{d}t. \tag{6.40}$$

The capacities $\mathcal{C}_{UB}^{(d')}$ and $\mathcal{C}_{UB}^{(d')}$ are defined in previous subsection for the case when both the neurotransmitter propagation and binding follow a Bernoulli distribution. The results from Eq. (6.39) and Eq. (6.40) are proved by the proof of Theorem 1 given in [46] by making changes analogous to those made by Davis in Kabanov's proof [34].

6.3.4 Analytical Examples

The best way to test the credibility of theoretical models would be to estimate the rates from experimental data and then compare results. To this end, one must collect data to estimate experimental information limits, which is a challenging task as discussed in the introductory paragraphs of this chapter. Instead, a graphical evaluation of the closed-form expressions for the information capacity bounds derived in Sections 6.3.3 is given. The provided numbers depend on selection of parameters (λ_0 and P_{rel}) that are cell-type specific.

The upper bound on information rate from Eq. (6.27) for bipartite synaptic Poisson channel with reliable vesicle release is plotted in Fig. 6.4 given various rates λ_0. As observed, the information capacity is higher for less noisy synapses. Given $\lambda_0 = 0.1$ [s^{-1}], the information rate goes up to 36.5 [bit/s] and saturates for peak spiking rates higher than 37 [spike/s]. For lower peak spiking rates, the information rate rises exponentially. Conversely, for very noisy synapses, the maximum information capacity is lower, e.g., given $\lambda_0 = 20$ [s^{-1}], the capacity reduces to 20 [bit/s], but becomes less sensitive as λ_0 increases.

The upper bound on the information rate for an unreliable (constant P_{rel}) and noisy bipartite synapse is plotted in Fig. 6.5 given various rates λ_0 and vesicle release probability $P_{rel} = 0.4$, and in Fig. 6.6 given various probabilities P_{rel} and rate $\lambda_0 = 10$ [s^{-1}]. Relative to Fig. 6.4, the information rates in Fig. 6.5 are lower. From Fig. 6.5, given $\lambda_0 = 0.1$ [s^{-1}], the information rate goes up to 22 [bit/s] and saturates for peak spiking rates higher than 37 [spike/s]. For lower peak spiking rates, the information rate rises exponentially. As in Fig. 6.4, for very noisy synapses, the maximum information capacity is lower, e.g., given $\lambda_0 = 20$ [s^{-1}], the capacity drops

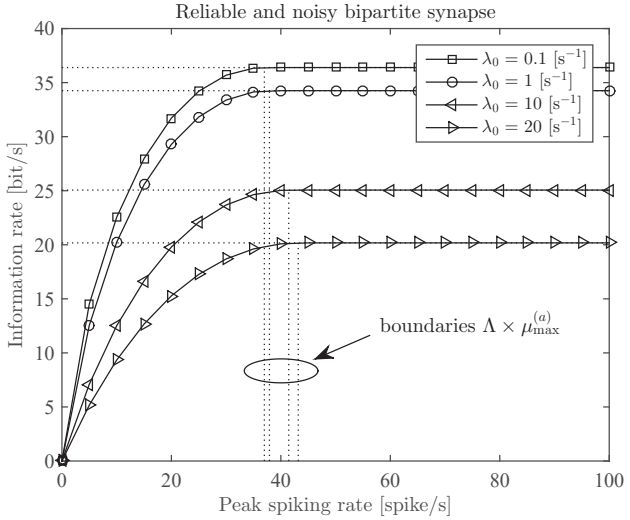

Figure 6.4: The upper bound on information rate as a function of the peak spiking rate Λ given various rates λ_0 for a synapse with reliable vesicle release, $P_{rel} = 1$. Vertical line segments show boundaries $\Lambda \times \mu^{(a)}_{\max}$.

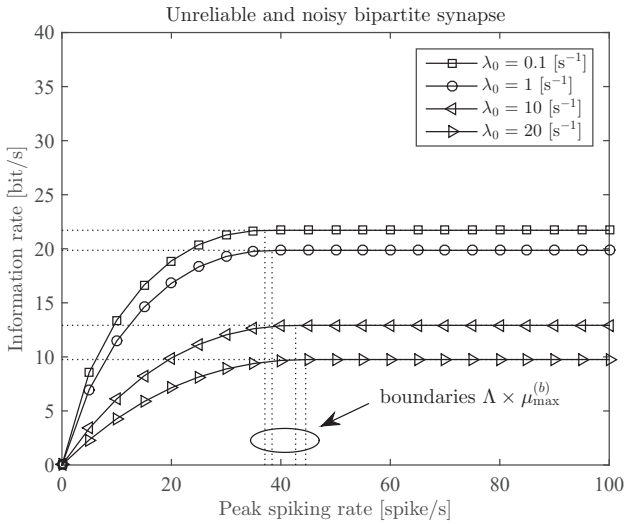

Figure 6.5: The upper bound on information rate for an unreliable synapse, $P_{rel} = 0.4$. Vertical line segments show boundaries $\Lambda \times \mu^{(b)}_{\max}$.

bellow 10 [bit/s], but becomes less sensitive as λ_0 increases. Ultimately, as shown in Fig. 6.6, intuitively higher information rates are observed for higher P_{rel} values.

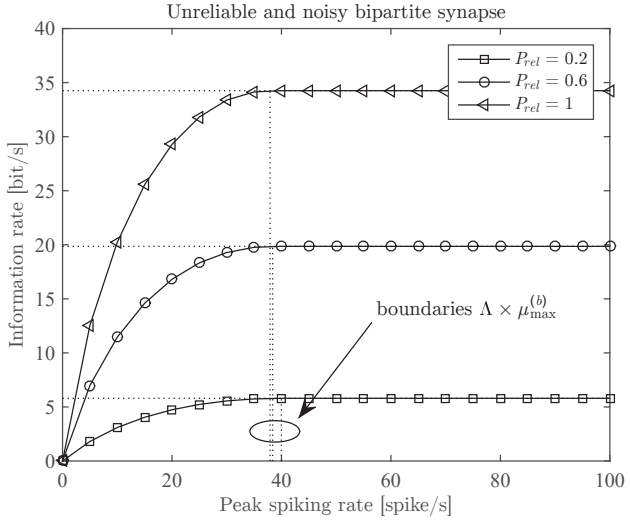

Figure 6.6: The upper bound on information rate as a function of the peak spiking rate Λ given various probabilities P_{rel} and $\lambda_0 = 10$ [s^{-1}] for an unreliable synapse. Vertical line segments show boundaries $\Lambda \times \mu_{\max}^{(b)}$.

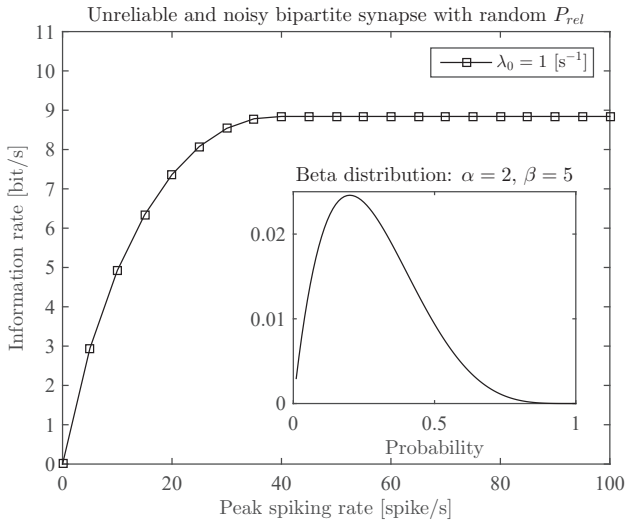

Figure 6.7: The upper bound on information rate as a function of the peak spiking rate Λ given beta distributed P_{rel} and $\lambda_0 = 1$ [s^{-1}] for an unreliable synapse.

With $P_{rel} = 1$, the information capacity coincides with the capacity in Eq. (6.27).

The upper bound on the information rate for an unreliable and noisy bipartite synapse is plotted in Fig. 6.7 by assuming the probability of the vesicle release P_{rel} follows a beta distribution with shaping parameters $\alpha = 2$, $\beta = 5$ (shown in the inset). Beta density function is selected after considering Fig. 2b from [22]. This result is essential for evaluation of the capacity upper bounds for unreliable synapses with time-varying vesicle release. Given $\lambda_0 = 1$ [s^{-1}], the information rate goes up to 9 [bit/s] and saturates for peak spiking rates higher than 40 [spike/s].

6.3.5 Simulation Example

In this example, a hippocampal synapse is simulated to record the signals transmitted, as well as other ionic and numerical quantities, from which one can learn about the synaptic behavior and extract parameters requisite for capacity computation. The primary aim is to identify real set-up with some of the analysis in Section 6.3.3, and then practically gain insight into the theoretical information capacity bounds. To this end, the simulator based on the validated models from computational neuroscience is developed:

1) Pinsky-Rinzel model [87,107] - The model is a 2-compartment reduction of the complex 19-compartment cable model by Traub [123]. The model is shown to be able to describe experimental observations on neural behavior, and is used in this study for current and potential dynamics of the pre-synaptic hippocampal neuron;

2) Li-Rinzel model [72,87,88] - The model is able to describe experimental observations on synaptic behavior when the astrocyte is connected to the synapse, and is used to quantify the feedback from the astrocyte to the pre-synaptic terminal;

3) Bertram-Sherman-Stanley model [20] - The model is used to describe the process of neurotransmitter release that is based on the finding that release can be gated during the opening of individual Ca^{2+} channels. In this four-gate model, all gates must be activated for release to occur;

4) Wang-Buzsaki model [132] - The model is used for current and potential dynamics of the post-synaptic neuron.

The simulation framework is implemented in Julia [95] – an open-source high-level dynamic programming language that provides high performance of utilized computational models of neurons.

Referring back to Section 6.3.3 that provides expressions to calculate the upper bounds on the information capacity under different set-ups, one needs to estimate the effect of spontaneous vesicle release, λ_0, and probabilities P_{rel}, P_s and P_b. With a simulator based on the models provided above, it is not possible to extract the neurotransmitter propagation and neurotransmitter binding probabilities required

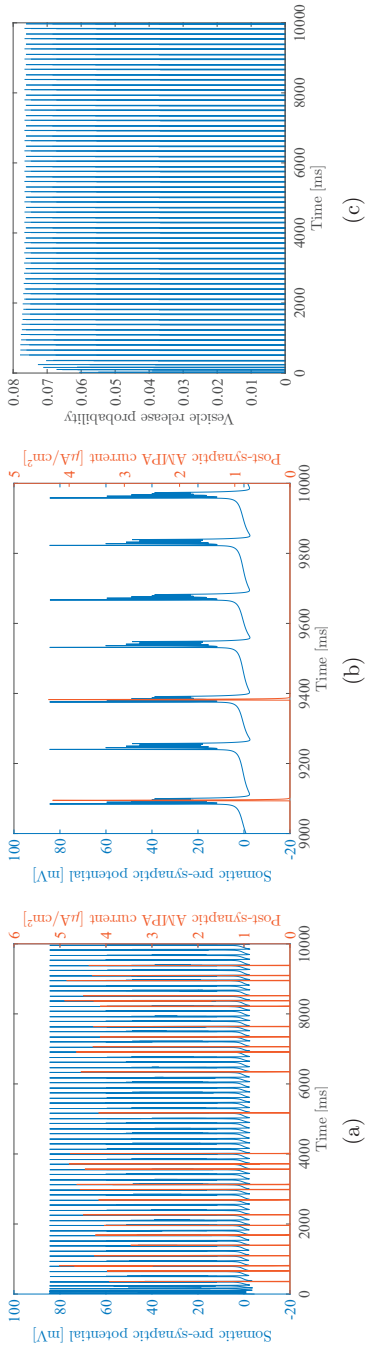

Figure 6.8: Simulation time $T_s = 10$ [s]; (a) A realization of the spiking sequence (blue) with rate $\lambda_1 = 35.2$ [spike/s] (spiking threshold is set to 30 mV) at the pre-synaptic neuron given the amplitude of stimulus somatic current $I_s = 1.5$ [μA/cm^2]; Corresponding current response (orange) at the post-synaptic neuron. (b) A realization of the spiking sequence and post-synaptic current response in $t \in [9000, 10000]$ ms; this plot visualizes the regular patterns of spiking bursts that are not visible in (a). (c) Vesicle release probability at the pre-synaptic neuron.

in Sections 6.3.3 and 6.3.3. This limitation can potentially be overcome with additional computational models that unlike the ones used in the simulation framework treat the diffusive propagation of particles and the ligand-binding mechanism. Instead, simulated scenarios are identified with simplifications where P_s and P_b are not involved.

Realistic Bipartite Synapse

For the bipartite synapse, the intra-cellular calcium concentration can be approximated as constant at the time instants of action potential arrivals (the envelope of the concentration is constant), as demonstrated later in Fig. 6.10(b). Thus, $\lambda_0(t) = \lambda_0$, and is estimated from Eq. (6.20), where $a_1 = 7181$ μM, $a_2 = 606$ μM, and $a_3 = 100$ ms^{-1} [88].

To determine the vesicle release probability, P_{rel}, a detailed inspection is required. In general, the vesicle release probability is calculated from Eq. (6.13) as a time-varying temporal function. Nonetheless, this may not strictly apply to all bipartite set-ups. Namely, Fig. 6.8 illustrates the scenario when the bipartite synapse is stimulated with the somatic current $I_s = 1.5$ [μA/cm^2], leading to approximately constant vesicle release probability observed after arrivals of action potentials (see Fig. 6.8(c)). In realistic scenarios, the vesicle release probability has a small value – in the simulated scenario, $P_{rel} \approx 0.078$.

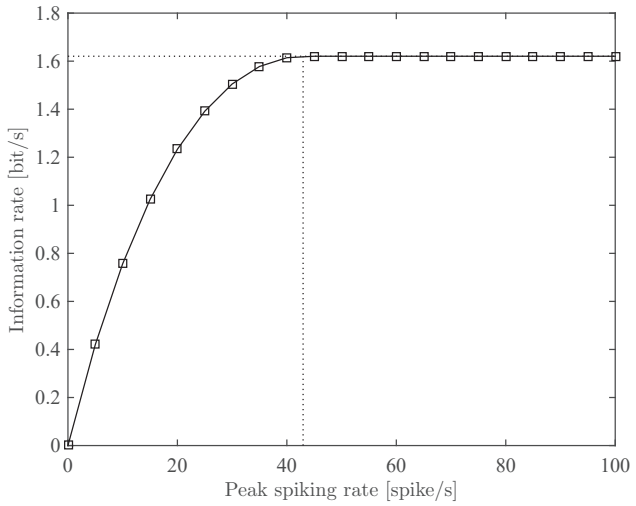

Figure 6.9: The upper bound on the capacity for the realistic bipartite synapse with $P_{rel} \approx 0.078$ and $\lambda_0 = 1.44$ s^{-1}.

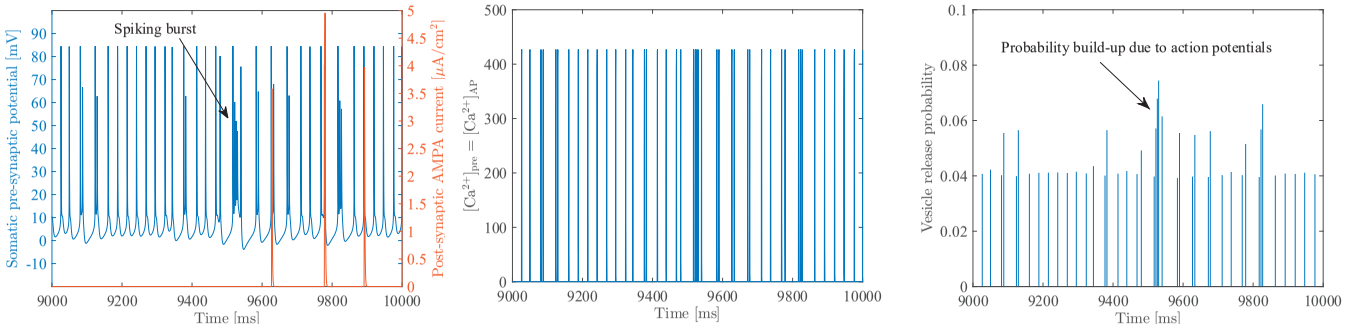

Figure 6.10: Amplitude of stimulus somatic current $I_s = 2$ [μA/cm^2]; simulation time $T_s = 10$ [s]; time window presented $T_w = 1$ [s]. (a) A realization of the spiking sequence (blue) with rate $\lambda_1 = 46.6$ [spike/s] at the pre-synaptic neuron; Corresponding current response (orange) at the post-synaptic neuron. (b) The intra-cellular calcium concentration at the pre-synaptic terminal. (c) Vesicle release probability at the pre-synaptic neuron with notable modulation from the spiking bursts.

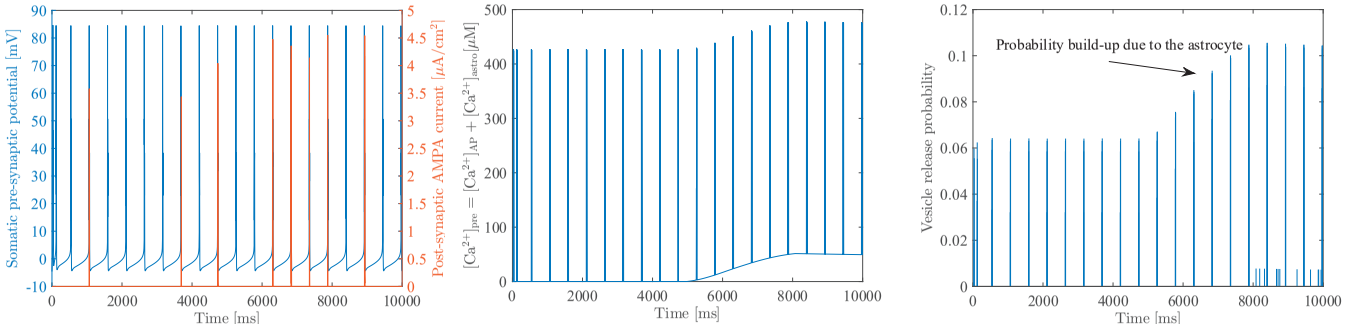

Figure 6.11: Amplitude of stimulus somatic current $I_s = 0.7$ [μA/cm^2]; simulation time $T_s = 10$ [s]. (a) A realization of the spiking sequence (blue) with rate $\lambda_1 = 4$ [spike/s] at the pre-synaptic neuron; Corresponding current response (orange) at the post-synaptic neuron. (b) The intra-cellular calcium concentration at the pre-synaptic terminal with notable modulation from the astrocytic activity. (c) Vesicle release probability at the pre-synaptic neuron with notable modulation from the astrocytic activity.

Albeit not plotted in Fig. 6.8, the intra-cellular calcium concentration is approximately constant after arrivals of action potentials, and $[Ca^{2+}]_{pre} = [Ca^{2+}]_{AP} = 427$ μM, which lead to $\lambda_0 = 1.44$ s^{-1}. With requisite parameters estimated, the upper bound on the capacity for the simulated bipartite synapse is computed with Eq. (6.33), and plotted in Fig. 6.9 as a function of the peak spiking rate. Thereby, the simulated bipartite synapse limits the information rate to 1.6 [bit/s].

In addition, it can be inferred that an arbitrary realistic bipartite set-up can also be approximated with scenario considered in Section 6.3.3 where Eq. (6.33) is used to define the upper bound on the information capacity when the stimulus is within a certain range – for hippocampal neurons the somatic current is empirically determined within the range $[0, 1.5]$ [μA/cm^2].

On the other hand, when the stimulus is strong ($I_s > 1.5$ [μA/cm^2]), as in the scenario presented in Fig. 6.10, the vesicle release probability is not constant after arrivals of spikes due to the spiking bursts that appear. Thereby, an arbitrary realistic bipartite set-up corresponds to the scenario considered in Section 6.3.3 where Eq. (6.36) is used to define the upper bound on the information capacity when the stimulus is strong ($I_s > 1.5$ [μA/cm^2]). Note that Eq. (6.36) requires the probability distribution of P_{rel}.

Realistic Tripartite Synapse

For the tripartite synapse, the envelope of the intra-cellular calcium concentration is time-varying due to the astrocytic contribution. This is shown in Fig. 6.11 where the tripartite synapse is stimulated with the somatic current $I_s = 0.7$ [μA/cm^2], leading also to the time-varying vesicle release probability observed after arrivals of action potentials (see Fig. 6.11(c)). The upper bound on the information capacity for the tripartite synapse is thus computed from simplified versions of Eq. (6.39) and Eq. (6.40) (the effects of P_s and P_b are neglected) regardless the intensity of the stimulus.

Note, however, that the feedback from astrocytic activity to the intra-cellular calcium concentration can be insignificant in some intervals disguising the change in the vesicle release probability P_{rel}. As many things around neurons, the modulation of the probability P_{rel} due to the astrocyte is stochastic in nature.

6.4 Concluding Remarks

The way information theory characterizes the neural channels and their ability to convey neurotransmitters that encode the information, despite the disturbances introduced, is very interesting to neuroscience and ICT community that develops

neural-like nano-networks. Unlike previous contributions, this study has provided the capacity upper bounds of synaptic transmission between two neurons.

Specifically, the synaptic transmission channel has been identified with optical communication channel, indicating all the relevant analogies. Then, different set-ups with progressive complexity, that are found in the brain, have been considered to provide the capacity upper bounds of noisy bipartite and tripartite synapses. The effects of uncertainties confined to the neurotransmitter release, transmission, and binding have been modeled. Numerical evaluations of the closed-form expressions for the information capacity bounds have been derived for the noisy bipartite synapse with reliable vesicle release, and noisy bipartite synapse with unreliable vesicle release with constant and time-varying release probabilities. The results show that a few tenths of bits per second can possibly be achieved, depending on the noise and reliability levels in the synapse. Conversely, if the probabilities associated with unreliability along the remaining communication pathway between neurons undergo distribution other than Bernoulli's, the closed-form formulas for the upper bound on the information channel capacity remain unknown.

Moreover, realistic synapses have been simulated using a developed simulator to record quantities that are indicating synaptic nature and are required for the information capacity evaluation. The simulated hippocampal bipartite synapse has been shown to convey up to 1.6 [bit/s]. Also, the quantities that suggest the way the information capacity should be computed in tripartite synapses have been extracted.

Chapter 7

Conclusions

The network of biological neurons, which continuously operates numerous processes of the body, is considered as the most advanced information transfer network in terms of reliability, capacity, data storage, and energy consumption. Owing to these features considerably enabled by the signaling between neurons, neurons and neural communication are put in the focus of emerging novel studies. The focus of this thesis has been in developing and analysing a theoretical framework for the neural communication in man-made nano-networks. The framework has been formalized through hypotheses that the neural information transfer network could be harnessed by understanding the neural communication well enough to transmit data and/or artificial information, and that neural compartments could be interfaced with subjects that affect the neural communication to propose novel treatment strategies for neurodegenerative disorders.

To this end, Chapters 3–5 of the thesis have considered communication theoretical aspects of neurons by adopting the approach wherein the neural compartments are considered as input/output communicating modules, and relevant ionic and chemical processes as signals. The considered signaling processes have been divided into two concepts: the intra- and inter-neuronal communication. The former is confined to the exchange of ions throughout the neuron that transfers APs from the cell body to the synapse. The latter is confined to the transmission of particles (neurotransmitters) throughout synaptic clefts between neurons. Following the conclusions from Chapters 3–5, the descriptions of the neuronal and astrocytic processes with a communications engineering approach are of interest in the design of bio-inspired circuits and techniques attempting to mimic the neural processes. On the one hand, possible neuromorphic devices, which can be benefited from the modeling of the neuronal and astrocytic processes through elementary input/output circuits, could be either inter-connected to communicate using the neural signaling and form artificial nano-networks, or used to restore communication between detached neural clusters by replacing the damaged neurons. On the other hand, the descriptions of neurons, and bipartite and tripartite synaptic systems as input/output systems are

of interest for the design of stimulation patterns that lead to programmed neural responses (spiking patterns) and/or synaptic responses (learning and memory). In a scenario where the neuron is externally stimulated, understanding the filtering behavior can give a useful insight in defining the most suitable stimulation pattern to obtain a certain effect on neural response and/or the pre-synaptic terminal. In a scenario where the astrocyte is externally stimulated, understanding the filtering behavior can give a useful insight in defining the most suitable stimulation pattern to obtain a certain effect on adjacent pre-synaptic neurons.

Ultimately, Chapter 6 of the thesis has considered information theoretical aspects of neurons aiming to check the capacity limits of the neural system. The major contribution of this study is the identification of the similarity between synaptic channels and optical communication channels. The closed-form formulas for the upper bound on the information capacity in neural synapses then stem from the identified analogies and optical channel capacity results available in the literature. Following the conclusion from Chapter 6, it has been inferred that a few tenths of bits per second can be achieved over synaptic channels, depending on the noise and reliability levels in the synapse. Nonetheless, if the probabilities associated with unreliability confined to the binding of neurotransmitters undergo distribution other than Bernoulli's, the closed-form formulas for the upper bound on the information channel capacity remain unknown.

7.1 Further Thoughts and Future Work

In order to raise the practical worth of the neural communication theory evolved in the thesis, the findings shall undergo a validation using experiments on real neurons and data. This is, however, a challenging and multidisciplinary issue which requires in-vivo measurements, the use of a sophisticated set of electronics, and high precision. Afterwards, the analysis shall be extended from two perspectives: first, it shall be enhanced with mechanisms that address neglected physiological effects of signal propagation through dendrites, spontaneous spike generation, and dynamic axonal functionalities; second, is shall be expanded from the "*neural physical layer*" to the "*neural network layer*". Potential neural analysis at network layer should offer the alternative understanding and models of neuroplasticity, which is characterized as the brain's ability to reorganize clusters of neurons by forming new neural connections throughout life. Neuroplasticity allows neurons to compensate for disease and malfunctioning parts of the system, and to adjust their activities in response to new situations. This distinctive feature of neurons makes them even more intriguing, and their networking paradigm even more favorable for adaptive nano-networks.

A specific analysis at neuronal network layer has been done by the author. Nonetheless, as this analysis uses graph theoretical tools and abstractions which deviate from other theoretical tools presented in the thesis, the content is provided in appendices.

More specifically,

- Appendix A promotes basic graph theoretical modeling of neuronal system;
- Appendix B promotes a usage of specified graph theory concepts for selection of targeted neurons whose control can overcome specific problems and lead to adequate formation of a strategy assisting in the treatment and diagnosis of neuronal diseases.

In terms of information theory of neurons/synapses, it is of primary importance to determine closed-form bounds without synaptic CSI in general future research efforts, aiming to find more exact capacity bounds for neural synapses. Also, discovering the information flow achievable by the whole neuron is identified here as a future work. To this end, one must consider the capacity of several synapses constituted by two observed neurons (and the astrocyte) that lead to spiking at the post-synaptic neuron. The evaluation of the multiple-synapse capacity requests a new system model with encompassed role of the multiple-access interference that has not been considered in Chapter 6. Moreover, a verification of theoretical results derived in Chapter 6 using experimental simulations and real data should also be done in the future.

Bibliography

[1] Alzheimer's disease international. http://www.alz.co.uk/. Accessed: 1/12/2013.

[2] Dynamic connectome lab. http://www.biological-networks.org/?page_id=25. Accessed: 1/12/2013.

[3] Electrophysiological values of maximum firing rate across neuron types from literature. http://neuroelectro.org/ephys_prop/35/. Accessed: 15/07/2016.

[4] IEEE Recommended Practice for Nanoscale and Molecular Communication Framework. *IEEE Std 1906.1-2015*, pages 1–64, Jan 2016.

[5] Naveed A. Abbasi and Ozgur B. Akan. A queueing-theoretical delay analysis for intra-body nervous nanonetwork. *Nano Communication Networks*, 6(4):166–177, 2015. Bio-Nano Communications Networks and Systems.

[6] Laurence F. Abbott. Lapicque's introduction of the integrate-and-fire model neuron (1907). *Brain Research Bulletin*, 50(5-6):303–304, 1999.

[7] Ozgur B. Akan, Hamideh Ramezani, Tooba Khan, Naveed A. Abbasi, and Murat Kuscu. Fundamentals of molecular information and communication science. *Proceedings of the IEEE*, 105(2):306–318, Feb 2017.

[8] Ian F. Akyildiz, Fernando Brunetti, and Cristina Blazquez. Nanonetworks: A new communication paradigm. *Computer Networks*, 52(12):2260–2279, 2008.

[9] Ian F. Akyildiz, Faramarz Fekri, Raghupathy Sivakumar, Craig R. Forest, and Brian K. Hammer. MoNaCo: Fundamentals of molecular nano-communication networks. *IEEE Wireless Communications*, 19(5):12–18, Oct 2012.

[10] Ian F. Akyildiz, Josep Miquel Jornet, and Chong Han. Terahertz band: Next frontier for wireless communications. *Physical Communication*, 12:16–32, 2014.

[11] Baris Atakan. *Molecular Communications and Nanonetworks*. Springer, 2014.

[12] Sasitharan Balasubramaniam, Noreen T. Boyle, Andrea Della-Chiesa, Frank Walsh, Adil Mardinoglu, Dmitri Botvich, and Adriele Prina-Mello. Devel-

opment of artificial neuronal networks for molecular communication. *Nano Communication Networks*, 2(2-3):150–160, 2011. Biological Information and Communication Technology.

[13] Eren Balevi and Ozgur B. Akan. A physical channel model for nanoscale neurospike communications. *IEEE Transactions on Communications*, 61(3):1178–1187, 2013.

[14] Israel Bar-David. Communication under the Poisson regime. *IEEE Transactions on Information Theory*, 15(1):31–37, Jan 1969.

[15] Alain Barrat, Alessandro Vespignani, and Marc Barthelemy. *Dynamical processes on complex networks*. Cambridge University Press, 2008.

[16] Mark F. Bear, Barry W. Connors, and Michael A. Paradiso. *Neuroscience: Exploring the Brain*. Lippincott Williams & Wilkins, third edition, 2006.

[17] Toby Berger and William B. Levy. A mathematical theory of energy efficient neural computation and communication. *IEEE Transactions on Information Theory*, 56(2):852–874, Feb 2010.

[18] Michael J. Berridge. The AM and FM of calcium signalling. *Nature*, 386:759–760, 1997.

[19] Michael J. Berry and Markus Meister. Refractoriness and neural precision. *The Journal of Neuroscience*, 18(6):2200–2211, 1998.

[20] Richard Bertram, Arthur Sherman, and Elise F. Stanley. Single-domain/bound calcium hypothesis of transmitter release and facilitation. *Journal of Neurophysiology*, 75(5):1919–1931, 1996.

[21] Alexander Borst and Frederic E. Theunissen. Information theory and neural coding. *Nature Neuroscience*, 2(11):947–957, 1999.

[22] Tiago Branco and Kevin Staras. The probability of neurotransmitter release: variability and feedback control at single synapses. *Nature Reviews Neuroscience*, 10(5):373–383, 2009.

[23] Ed Bullmore and Olaf Sporns. Complex brain networks: graph theoretical analysis of structural and functional systems. *Nature Reviews Neuroscience*, 10:186–198, 2009.

[24] Stephen F. Bush. *Nanoscale Communication Networks*. Artech House, 2010.

[25] Angela Sara Cacciapuoti, Marcello Caleffi, and Alessandro Piras. Modeling the dynamic processing of the presynaptic terminals for intra-body nanonetworks. *IEEE Transactions on Communications*, 64(4):1636–1645, 2016.

[26] Angela Sara Cacciapuoti and Marcelloi Caleffi. Receiver design for a bionic nervous system: Modeling the dendritic processing power. *IEEE Internet of Things Journal*, 3(1):27–37, Feb 2016.

[27] Nicholas T. Carnevale and Michael L. Hines. NEURON for empirically-based simulations of neurons and networks of neurons. `http://www.neuron.yale.edu/neuron/`. Accessed: 25/2/2015.

[28] Youssef Chahibi and Ian F. Akyildiz. Molecular communication noise and capacity analysis for particulate drug delivery systems. *IEEE Transactions on Communications*, 62(11):3891–3903, Nov 2014.

[29] Kaushik Chakraborty and Prakash Narayan. The Poisson fading channel. *IEEE Transactions on Information Theory*, 53(7):2349–2364, July 2007.

[30] Francois Christophe, Vafa Andalibi, Teemu Laukkarinen, Tommi Mikkonen, and Kai Koskimies. Survey and evaluation of neural computation models for bio-integrated systems. *Nano Communication Networks*, 6(4):155–165, 2015.

[31] David E. Clapham. Calcium signaling. *Cell*, 80(2):259–268, 1995.

[32] Erik P. Cook, Jennifer A. Guest, Yong Liang, Nicholas Y. Masse, and Costa M. Colbert. Dendrite-to-soma input/output function of continuous time-varying signals in hippocampal CA1 pyramidal neurons. *Journal of Neurophysiology*, 98:2943–2955, 2007.

[33] Thomas M. Cover and Joy A. Thomas. *Elements of Information Theory*. Wiley, New York, 2006.

[34] Mark H. A. Davis. Capacity and cutoff rate for Poisson-type channels. *IEEE Transactions on Information Theory*, 26(6):710–715, Nov 1980.

[35] Peter Dayan and Laurence F. Abbott. *Theoretical Neuroscience: Computational and Mathematical Modeling of Neural Systems*. The MIT Press, Cambridge, Massachusets, London, England, 2001.

[36] Maurizio De Pittà, Mati Goldberg, Vladislav Volman, Hugues Berry, and Eshel Ben-Jacob. Glutamate regulation of calcium and IP3 oscillating and pulsating dynamics in astrocytes. *Journal of Biological Physics*, 35(4):383–411, 2009.

[37] Tim Denison, Milton Morris, and Felice Sun. Building a bionic nervous system. *IEEE Spectrum*, 52(2):32–39, February 2015.

[38] Frederick A. Dodge and Rami Rahamimoff. Co-operative action of calcium ions in transmitter release at the neuromuscular junction. *The Journal of Physiology*, 193(2):419–432, 1967.

[39] Eric K. Drexler. *Engines of Creation: The Coming Era of Nanotechnology*. Doubleday, 1986.

[40] Pinchas D. Einziger, Leonid M. Livshitz, and Joseph Mizrahi. Generalized cable equation model for myelinated nerve fiber. *IEEE Transactions on Biomedical Engineering*, 52(10):1632–1642, Oct 2005.

[41] Cornelis J. Stam et al. Small-world networks and functional connectivity in Alzheimer's disease. *Cerebral Cortex*, 17(1):92–99, 2007.

[42] Zhouyan Feng, Ying Yu, Zheshan Guo, Jiayue Cao, and Dominique M. Durand. High frequency stimulation extends the refractory period and generates axonal block in the rat hippocampus. *Brain Stimulation*, 7(5):680–689, 2014.

[43] Todd A. Fiacco and Ken D. McCarthy. Intracellular astrocyte calcium waves in situ increase the frequency of spontaneous AMPA receptor currents in CA1 pyramidal neurons. *The Journal of Neuroscience*, 24(3):722–732, 2004.

[44] Richard FitzHugh. Impulses and physiological states in theoretical models of nerve membrane. *Biophysical Journal*, 1(6):445–466, 1961.

[45] Linton C. Freeman. A set of measures of centrality based upon betweenness. *Sociometry*, 40:35–41, 1977.

[46] Michael R. Frey. Information capacity of the Poisson channel. *IEEE Transactions on Information Theory*, 37(2):244–256, March 1991.

[47] Johan H. M. Frijns, Jaap Mooij, and Jaap H. ten Kate. A quantitative approach to modeling mammalian myelinated nerve fibers for electrical prosthesis design. *IEEE Transactions on Biomedical Engineering*, 41(6):556–566, June 1994.

[48] Laura Galluccio, Ozgur B. Akan, Sasitharan Balasubramaniam, and Raghupathy Sivakumar. Wireless communications at the nanoscale [guest editorial]. *IEEE Wireless Communications*, 19(5):10–11, Oct 2012.

[49] Laura Galluccio, Sergio Palazzo, and G. Enrico Santagati. Characterization of signal propagation in neuronal systems for nanomachine-to-neurons communications. In *2011 IEEE Conference on Computer Communications Workshops (INFOCOM WKSHPS)*, pages 437–442, April 2011.

[50] Laura Galluccio, Sergio Palazzo, and G. Enrico Santagati. Modeling signal propagation in nanomachine-to-neuron communications. *Nano Communication Networks*, 2(4):213–222, 2011.

[51] Weisi Guo, Christos Mias, Nariman Farsad, and Jiang-Lun Wu. Molecular versus electromagnetic wave propagation loss in macro-scale environments. *IEEE Transactions on Molecular, Biological and Multi-Scale Communications*, 1(1):18–25, March 2015.

[52] James Hindmarsh and Malcom Rose. A model of neuronal bursting using three coupled first order differential equations. *Proceedings of the Royal Society of London B: Biological Sciences*, 221(1222):87–102, 1984.

[53] Alan L. Hodgkin and Andrew F. Huxley. A quantitative description of membrane current and its application to conduction and excitation in nerve. *Journal of Physiology*, 117(4):500–544, 1952.

[54] Steve Hranilovic and Frank R. Kschischang. Capacity bounds for power- and band-limited optical intensity channels corrupted by Gaussian noise. *IEEE Transactions on Information Theory*, 50(5):784–795, May 2004.

[55] Ian W. Hunter and Michael J. Korenberg. The identification of nonlinear biological systems: Wiener and Hammerstein cascade models. *Biological Cybernetics*, 55:135–144, 1986.

[56] Shiro Ikeda and Jonathan H. Manton. Spiking neuron channel. In *Proceedings of the IEEE International Symposium on Information Theory, ISIT 2009.*, pages 1589–1593, June 2009.

[57] NanoNetworking Center in Catalunya. N3Sim: a simulation framework for diffusion-based molecular communication. `http://www.n3cat.upc.edu/n3sim`. Accessed: 6/2/2015.

[58] Eugene M. Izhikevich. Simple model of spiking neurons. *IEEE Transactions on Neural Networks*, 14(6):1569–1572, 2003.

[59] Bob Jacobs, Lori Driscoll, and Matthew Schall. Life-span dendritic and spine changes in areas 10 and 18 of human cortex: A quantitative Golgi study. *The Journal of Comparative Neurology*, 386(4):661–680, 1997.

[60] Josep Miquel Jornet and Ian F. Akyildiz. Graphene-based nano-antennas for electromagnetic nanocommunications in the terahertz band. In *Proceedings of the Fourth European Conference on Antennas and Propagation (EuCAP)*, pages 1–5, April 2010.

[61] Josep Miquel Jornet and Ian F Akyildiz. Channel modeling and capacity analysis for electromagnetic wireless nanonetworks in the terahertz band. *IEEE Transactions on Wireless Communications*, 10(10):3211–3221, October 2011.

[62] Josep Miquel Jornet and Ian F. Akyildiz. Graphene-based plasmonic nano-antenna for terahertz band communication in nanonetworks. *IEEE Journal on Selected Areas in Communications*, 31(12):685–694, December 2013.

[63] Josep Miquel Jornet and Ian F. Akyildiz. Graphene-based plasmonic nano-transceiver for terahertz band communication. In *Proceedings of The 8th European Conference on Antennas and Propagation (EuCAP 2014)*, pages 492–496, April 2014.

[64] Yurii M. Kabanov. The capacity of a channel of the Poisson type. *Theory of Probability & Its Applications*, 23(1):143–147, 1978.

[65] Marcus Kaiser and Claus C. Hilgetag. Nonoptimal component placement, but short processing paths, due to long-distance projections in neural systems. *PLoS Computational Biology*, 2(7):e95, 2006.

[66] Maurice G. Kendall and Alan Stuart. *The Advanced Theory of Statistics, Vol. 1.* London: Griffin, 1963.

[67] Tooba Khan, Bilgesu A. Bilgin, and Ozgur B. Akan. Diffusion-based model for synaptic molecular communication channel. *IEEE Transactions on NanoBioscience*, PP(99):1–1, 2017.

[68] Christof Koch. *Biophysics of computation: Information processing in single neurons*. New York: Oxford University Press, 1999.

[69] Rie Komuro and Ilangko Balasingham. Effects of ion channel currents on induced action potentials. In *Proceedings of the IEEE EMBS Conference on Neural Engineering (NER)*, pages 601–604, 2013.

[70] Broadband Wireless Networking Lab. Molecular nano-communication networks. `http://bwn.ece.gatech.edu/monaco/`. Accessed: 16/11/2016.

[71] Simon B. Laughlin. Energy as a constraint on the coding and processing of sensory information. *Current Opinion in Neurobiology*, 11(4):475–480, 2001.

[72] Yue-Xian Li and John Rinzel. Equations for InsP3 receptor-mediated $[Ca^{2+}]_i$ oscillations derived from a detailed kinetic model: A Hodgkin-Huxley like formalism. *Journal of Theoretical Biology*, 166(4):461–473, 1994.

[73] Qiang Liu, Peng He, Kun Yang, and Supeng Leng. Inter-symbol interference analysis of synaptic channel in molecular communications. In *Proceedings of the IEEE International Conference on Communications (ICC)*, pages 4424–4429, June 2014.

[74] Ignacio Llatser, Christian Kremers, Albert Cabellos-Aparicio, Josep Miquel Jornet, Eduard Alarcón, and Dmitry N. Chigrin. Graphene-based nano-patch antenna for terahertz radiation. *Photonics and Nanostructures - Fundamentals and Applications*, 10(4):353–358, 2012. TaCoNa-Photonics 2011.

[75] Derya Malak and Ozgur B. Akan. A communication theoretical analysis of synaptic multiple-access channel in hippocampal-cortical neurons. *IEEE Transactions on Communications*, 61(6):2457–2467, June 2013.

[76] Derya Malak and Ozgur B. Akan. Synaptic interference channel. In *Proceedings of the IEEE International Conference on Communications Workshops (ICC)*, pages 771–775, June 2013.

[77] Derya Malak and Ozgur B. Akan. Communication theoretical understanding of intra-body nervous nanonetworks. *IEEE Communications Magazine*, 52(4):129–135, April 2014.

[78] Derya Malak, Murat Kocaoglu, and Ozgur B. Akan. Communication theoretic analysis of the synaptic channel for cortical neurons. *Nano Communication Networks*, 4(3):131–141, 2013.

[79] Amit Manwani and Christof Koch. Detecting and estimating signals over noisy and unreliable synapses: information-theoretic analysis. *Neural computation*, 13(1):1–33, January 2001.

[80] Fabio Mesiti and Ilangko Balasingham. Correlated neuronal activity in networks of neurons stimulated with nanomachines. In *Proceedings of ACM The First Annual International Conference on Nanoscale Computing and Communication*, NANOCOM' 14, pages 11:1–11:5, 2007.

[81] Fabio Mesiti and Ilangko Balasingham. Nanomachine-to-neuron communication interfaces for neuronal stimulation at nanoscale. *IEEE Journal on Selected Areas in Communications*, 31(12):695–704, December 2013.

[82] Fabio Mesiti, Pål Anders Floor, Anna Na Kim, and Ilangko Balasingham. On the modeling and analysis of the RF exposure on biological systems: A potential treatment strategy for neurodegenerative diseases. *Elsevier Nano Communication Networks*, 3:103–115, 2012.

[83] Fabio Mesiti, Mladen Veletić, Pål Anders Floor, and Ilangko Balasingham. Astrocyte-neuron communication as cascade of equivalent circuits. *Nano Communication Networks*, 6(4):183–197, 2015. Bio-Nano Communications Networks and Systems.

[84] Catherine Morris and Harold Lecar. Voltage oscillations in the barnacle giant muscle fiber. *Biophysical Journal*, 35(1):193–213, 1981.

[85] Saizalmursidi Md Mustam, Sharifah Kamilah Syed Yusof, and Samad Nejatian. Multilayer diffusion-based molecular communication. *Transactions on Emerging Telecommunications Technologies*, 28(1):e2935:1–10, 2015.

[86] Suhita Nadkarni and Peter Jung. Dressed neurons: modeling neural-glial interactions. *Physical Biology*, 1(1-2):35–41, 2004.

[87] Suhita Nadkarni and Peter Jung. Modeling synaptic transmission of the tripartite synapse. *Physical Biology*, 4(1):1–9, 2007.

[88] Suhita Nadkarni, Peter Jung, and Herbert Levine. Astrocytes optimize the synaptic transmission of information. *PLoS Computational Biology*, 4:e1000088, May 2008.

[89] Jin-Ichi Nagumo, Suguru Arimoto, and Shuji Yoshizawa. An active pulse transmission line simulating nerve axon. *Proceedings of the IRE*, 50(10):2061–2070, Oct 1962.

[90] Tadashi Nakano, Andrew W. Eckford, and Tokuko Haraguchi. *Molecular Communication*. Cambridge University Press, 2013.

[91] Tadashi Nakano and Jian-Qin Liu. chapter Information Transfer through Calcium Signaling, pages 29–33. Springer Berlin Heidelberg, 2009.

[92] Tadashi Nakano, Tatsuya Suda, Takako Koujin, Tokuko Haraguchi, and Yasushi Hiraoka. Molecular communication through gap junction channels: System design, experiments and modeling. In *Proceedings of the 2nd Bio-Inspired*

Models of Network, Information and Computing Systems, Bionetics, pages 139–146, Dec 2007.

[93] Erwin Neher. Vesicle pools and Ca^{2+} microdomains: New tools for understanding their roles in neurotransmitter release. *Neuron*, 20:389–399, March 1998.

[94] Konstantin S. Novoselov and Andre K. Geim et al. Electric field effect in atomically thin carbon films. *Science*, 306(5696):666–669, 2004.

[95] Project NumFocus. Julia: an open-source programing language. `http://www.julialang.org/`. Accessed: 20/6/2016.

[96] Yusuke Ota, Alexander T. Zanetti, and Robert M. Hallock. The role of astrocytes in the regulation of synaptic plasticity and memory formation. *Neural Plasticity*, 2013:1–11, 2013.

[97] Karim G. Oweiss. *Statistical Signal Processing for Neuroscience and Neurotechnology*. Elsevier, 2010.

[98] Sonia Paixao and Rudiger Klein. Neuron-astrocyte communication and synaptic plasticity. *Current Opinion in Neurobiology*, 20(4):466–473, August 2010.

[99] Tomas Palacios, Allen Hsu, and Han Wang. Applications of graphene devices in RF communications. *Communications Magazine, IEEE*, 48(6):122–128, June 2010.

[100] Vladimir Parpura, Trent A. Basarsky, Fang Liu, Ksenija Jeftinija, Srdija Jeftinija, and Philip G. Haydon. Glutamate-mediated astrocyte-neuron signalling. *Nature*, 369(6483):744–747, 1994.

[101] Fernando Patolsky, Brian P. Timko, Guihua Yu, Ying Fang, Andrew B. Greytak, Gengfeng Zheng, and Charles M. Lieber. Detection, stimulation, and inhibition of neuronal signals with high-density nanowire transistor arrays. *Science*, 313:1100–1104, 2006.

[102] Jean Philibert. One and a half century of diffusion: Fick, Einstein, before and beyond. *Diffusion Fundamentals*, 2:1.1–1.10, 2005.

[103] Massimiliano Pierobon and Ian F. Akyildiz. A physical end-to-end model for molecular communication in nanonetworks. *IEEE Journal on Selected Areas in Communications*, 28(4):602–611, May 2010.

[104] Massimiliano Pierobon and Ian F. Akyildiz. Noise analysis in ligand-binding reception for molecular communication in nanonetworks. *IEEE Transactions on Signal Processing*, 59(9):4168–4182, Sept 2011.

[105] Massimiliano Pierobon and Ian F. Akyildiz. *Fundamentals of Diffusion-Based Molecular Communication in Nanonetworks*, volume 8. Foundations and Trends® in Networking, 2013.

[106] Victor Pikov, Xianghong Arakaki, Michael Harrington, Scott Fraser, and Peter Siegel. Modulation of neuronal activity and plasma membrane properties with low-power millimeter waves in organotypic cortical slices. *Journal of Neural Engineering*, 7:1–9, 2010.

[107] Paul F. Pinsky and John Rinzel. Intrinsic and network rhythmogenesis in a reduced Traub model for CA3 neurons. *Journal of Computational Neuroscience*, (1):39–40, 1994.

[108] Morten Raastad and Gordon M. G. Shepherd. Single-axon action potentials in the rat hippocampal cortex. *The Journal of Physiology*, 548:745–752, 2003.

[109] Hamideh Ramezani and Ozgur B. Akan. Synaptic channel model including effects of spike width variation. In *Proceedings of ACM The Second Annual International Conference on Nanoscale Computing and Communication*, NANOCOM' 15, pages 11:1–11:6. ACM, 2015.

[110] Hamideh Ramezani and Ozgur B. Akan. A communication theoretical modeling of axonal propagation in hippocampal pyramidal neurons. *IEEE Transactions on NanoBioscience*, PP(99):1–1, 2017.

[111] Claire Ribrault, Ken Sekimoto, and Antoine Triller. From the stochasticity of molecular processes to the variability of synaptic transmission. *Nature Reviews Neuroscience*, (12):375–387, July 2011.

[112] Magnus Richardson, Nicolas Brunel, and Vincent Hakim. From subthreshold to firing-rate resonance. *Journal of Neurophysiology*, 89:2538–2554, 2003.

[113] Takuya Sasaki. The axon as a unique computational unit in neurons. *Neuroscience Research*, 75(2):83–88, 2013.

[114] Alan Schoen, Ali Salehiomran, Matthew E. Larkum, and Erik P. Cook. A compartmental model of linear resonance and signal transfer in dendrites. *Neural Computation*, 24(12):3126–3144, Dec 2012.

[115] Shlomo Shamai and Amos Lapidoth. Bounds on the capacity of a spectrally constrained poisson channel. *IEEE Transactions on Information Theory*, 39(1):19–29, Jan 1993.

[116] James Sneyd, Andrew C. Charles, and Michael J. Sanderson. A model for the propagation of intercellular calcium waves. *American Journal of Physiology - Cell Physiology*, 266(1):C293–C302, 1994.

[117] Olaf Sporns. *Neuroscience database*, chapter Graph Theory Methods for the Analysis of Neural Connectivity Patterns, pages 171–185. Springer US, 2003.

[118] Richard B. Stein. The information capacity of nerve cells using a frequency code. *Biophysical Journal*, 6(7):797–826, 1967.

[119] Prapun Suksompong and Toby Berger. Capacity analysis for integrate-and-fire neurons with descending action potential thresholds. *IEEE Transactions on Information Theory*, 56(2):838–851, Feb 2010.

[120] Junichi Suzuki, Sasitharan Balasubramaniam, Sophie Pautot, Victor Didier Perez Meza, and Yevgeni Koucheryavy. A service-oriented architecture for body area nanonetworks with neuron-based molecular communication. *Mobile Networks and Applications*, 19(6):707–717, 2014.

[121] Junuchi Suzuki, Pruet Boonma, and Dung H. Phan. Neuronal signaling optimization for intrabody nanonetworks. In *Proceedings of the Fourth International Conference on Digital Information and Communication Technology and it's Applications (DICTAP)*, pages 69–74, 2014.

[122] Norio Taniguchi. On the basic concept of 'nanotechnology'. In *Proceedings of the International Conference on Production Engineering*, pages 18–23, 1974.

[123] Roger D. Traub, Robert K. Wong, Richard Miles, and Hillary Michelson. A model of a CA3 hippocampal pyramidal neuron incorporating voltage-clamp data on intrinsic conductances. *Journal of Neurophysiology*, 2(66):635–650, 1991.

[124] Mladen Veletić and Ilangko Balasingham. The neural communication network: A brief review on neuromodeling and neuroengineering. In *Proceedings of the 24th IEEE Telecommunications Forum (TELFOR 2016)*, pages 1–4, November 2016.

[125] Mladen Veletić, Ilangko Balasingham, and Zdenka Babić. On spectrum analysis for nanomachine-to-neuron communications. In *Proceedings of the IEEE International Black Sea Conference on Communications and Networking (BlackSeaCom)*, pages 64–68, July 2013.

[126] Mladen Veletić, Pål Anders Floor, Zdenka Babić, and Ilangko Balasingham. Peer-to-peer communication in neuronal nano-network. *IEEE Transactions on Communications*, 64(3):1153–1166, March 2016.

[127] Mladen Veletić, Pål Anders Floor, and Ilangko Balasingham. From nanoscale neural excitability to long term synaptic modification. In *Proceedings of ACM The First Annual International Conference on Nanoscale Computing and Communication*, NANOCOM' 14, pages 22:1–22:9. ACM, 2014.

[128] Mladen Veletić, Pål Anders Floor, Youssef Chahibi, and Ilangko Balasingham. On the upper bound of the information capacity in neuronal synapses. *IEEE Transactions on Communications*, 64(12):5025–5036, December 2016.

[129] Mladen Veletić, Fabio Mesiti, Pål Anders Floor, and Ilangko Balasingham. Communication theory aspects of synaptic transmission. In *Proceedings of the IEEE International Conference on Communications (IEEE ICC 2015)*, pages 2719–2724, June 2015.

[130] Sergio Verdu. Poisson communication theory. In *The International Technion Communication Day in honor of Israel Bar-David*, March 1999. Invited talk.

[131] Samuel S. Wang, Adawia A. Alousi, and Stuart H. Thompson. The lifetime of inositol 1,4,5-trisphosphate in single cells. *The Journal of General Physiology*, 105(1):149–171, 1995.

[132] Xiao-Jing Wang and György Buzsaki. Gamma oscillation by synaptic inhibition in a hippocampal interneuronal network model. *The Journal of Neuroscience*, (16):6402–6413, 1996.

[133] Duncan J. Watts and Steven H. Strogatz. Collective dynamics of 'small-world' networks. *Nature (London)*, 393:440–442, 1998.

[134] Yunlei Yang, Wooping Ge, Yiren Chen, Zhijun Zhang, Wanhua Shen, Chienping Wu, Muming Poo, and Shumin Duan. Contribution of astrocytes to hippocampal long-term potentiation through release of D-serine. In *Proceedings of the National Academy of Sciences of the United States of America*, volume 100(25), pages 15194–15199, 2003.

[135] Yunguo Yu, Marshall Crumiller, Bruce Knight, and Ehud Kaplan. Estimating the amount of information carried by a neuronal population. *Frontiers in Computational Neuroscience*, 4:1–10, 2010.

[136] Kaiyu Zheng, Leonid P. Savtchenko, and Dmitri A. Rusakov. Diffusion of glutamate in the synaptic cleft. *Proceedings of The Physiological Society*, (3):PC171, August 2006.

Appendix A

Graph Theoretical Modeling of Neuronal System

A significant number of neuroscience databases provides researchers with comprehensive data sets of connectional relationships between individual neurons or brain areas. The availability of such data sets necessitates the development of appropriate computational tools for their analysis. One avenue for such an analysis is provided by graph theory [117].

The anatomical configuration of brain networks can quantitatively been characterized by a graph representing either inter-neuronal- or inter-regional connectivity. If inter-neuronal connectivity is analyzed, structural networks can be described as graphs which are composed of vertices (nodes) denoting neurons, that are linked by edges representing their physical connections, i.e., synapses. Conversely, if inter-regional connectivity is analyzed, graph theory describes structural networks as graphs which are composed of nodes denoting brain regions, that are further linked by edges representing axonal projections. The former approach is the subject of this appendix. Thereby, graph G representing neuronal network that consists of V set of vertices and E set of edges, denoted as $G(V, E)$, is analyzed here.

Quantitative characterization of anatomical patterns can be mathematically described through matrices, such as the Adjacency Matrix (AM), also called the connection matrix. The AM is with non-zero entries a_{ij} if a connection/synapse is present between neurons i and j; otherwise, a_{ij} is zero. For any given synapse, the synaptic weight, w_{ij}, is found as a function of $[Ca^{2+}]_e$ and $[Mg^{2+}]_e$, where index e denotes the extra-cellular concentration [38]:

$$w_{ij} \sim \left(\frac{[Ca^{2+}]_e/K_c}{[Ca^{2+}]_e/K_c + [Mg^{2+}]_e/K_m + 1} \right)^y . \tag{A.1}$$

K_c and K_m are equilibrium constants of calcium and magnesium, respectively, and y is the number of independent sites Ca^{2+} must bind to in order to release neu-

rotransmitters. Depending on the nature of ion flows, the synapses representing connections can have either an excitatory, depolarizing, or inhibitory, hyperpolarizing, effect on the post-synaptic neuron. Hence, excitatory and inhibitory synaptic connections correspond to positive and negative a_{ij} values in AM, respectively.

Anatomically, many compartments (e.g., dendrites) of single pre-synaptic neuron i can be connected to post-synaptic neuron j, making a numerous synaptic connections. In the presented analysis, it is assumed that the weights of all the connections are superimposed resulting a_{ij}. Furthermore, each two neurons can both be the pre- and post-synaptic ones to each other, in which case they mutually share two connections represented by different values of a_{ij} and a_{ji} in AM. Additionally, the graph $G(V, E)$ representing neuronal network is directed due to the one-way axonal transmission. This ultimately makes the $G(V, E)$ being directed, weighted, and signed. Excluding the self-connections, all diagonal elements of AM are zero.

With the neuronal network mapped (usually by means of functional Magnetic Resonance Imaging (fMRI) or electrophysiological techniques, such as Electroencephalography (EEG) and Magnetoencephalography (MEG)), the connectivity patterns and structure formed of densely connected clusters linked together in a small-world network [23] can be revealed. Small-worldness combines high levels of local clustering among neurons, associated with high efficiency of information transfer and robustness, and short paths, that link all neurons of the regional network. Small-world organization is intermediate between that of random networks, characterized with short overall path length and low level of local clustering, and that of regular networks, characterized with long path length accompanied by high level of clustering. Such a structure is essential not only for regions of specialized neurons, but also for the brain in general, since it combines two fundamental functioning aspects: *segregation*, where the similar specialized neuronal units are organized in densely connected groups that are inter-connected, and the functional *integration*, which allows the collaboration of a large number of neurons to build cognitive states [15].

Appendix B

The Strategy of Diagnosis and Treatment of Neural Disorders

The objective of this appendix is to promote a possible graph-based[1] strategy of driving the neuronal communication through controlled concentration of Ca^{2+}, since findings from the thesis have proved that they play a crucial role in neural communication performance. It is believed that any disruption in the processes that regulate calcium concentration levels (referred as *calcium dysregulation*), leads to dramatic changes in neural functioning. A possible treatment in brains with calcium dysregulation is, therefore, through techniques that re-establish proper calcium regulation.

As shown in Appendix A, graph interpretation of neuronal connectivity at network layer provides researchers with connectional relationships between individual neurons and ability to computationally analyze the connectivity patterns. Although this appendix is mostly confined to formation of adequate strategy assisting in diagnosis and treatment of neurons struck by mental disorders, e.g., hippocampal neurons, two-dimensional spatial representations of a local subnetwork of 131 neurons with 764 unidirectional connections within *Caenorhabditis elegans* rostral ganglia (available in [65] and [2]), can be used for analysis without any loss of generality.

In terms of network quantification, the first parameter that can be easily computed is the average connection density, k. Value of k represents the number of all non-zero entries in AM, divided by the maximal possible number of connections, i.e., $n^2 - n$ (n stands for a number of vertices in V set) for a directed graph, excluding self-connections. The sparser the $G(V, E)$, the lower its average connection density. The average connection densities vary depending on the particular anatomical structure. For instance, connected cells across the entire cerebral cortex typically produce k values ranging from 10^{-7} to 10^{-6} [117]. Conversely, local connection densities are

[1] As graph theory has recently started being utilized in neuroscience, the most appropriate graph theory measures for the analysis of brain have not been selected. Nonetheless, a set of those that might have certain relevance for neural communication performance analysis and neuroscience applications are deployed here.

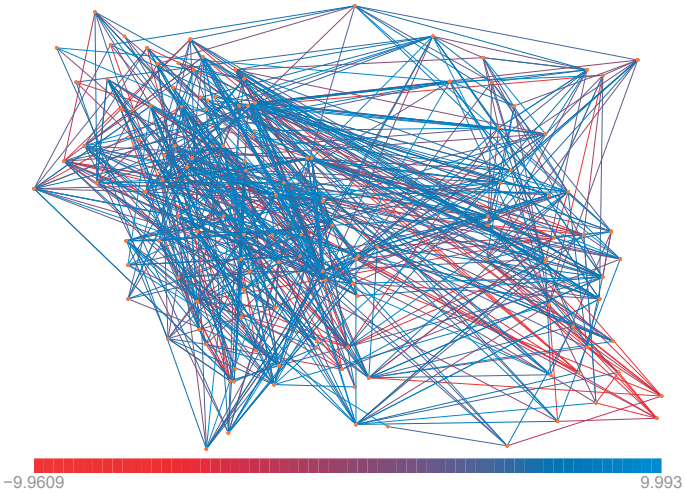

Figure B.1: Two-dimensional spatio-temporal pattern of weighted excitatory and inhibitory synapses. Red lines denote the inhibitory connections; blue lines denote excitatory connections.

significantly higher, as shown for analyzed *Caenorhabditis elegans* network where $k = 0.0449$. Although the result suggests a dense property of network, k value in addition to binary, unweighted, and, at this point still unsigned AM, does not provide a detailed insight into the functional organization of the region. Nonetheless, potential application of average connection density is in diagnosis: decreased k value of monitored brain sub-network can mark disorder producing increased failures in neuronal links.

To keep the reasoning as realistic as possible, a modification of 20% of the number of synapses in AM is introduced giving them negative weights (considering inhibitory synapses). Modified $G(V, E)$ is visualized as shown in Fig B.1, where spatial two-dimensional positions represent the position of the soma of individual neurons. The x-axis colormap ranging from -10 to 10 is used to differentiate between inhibitory and excitatory synapses; the distribution of inhibitory and excitatory cells is not temporal, unlike the time-variable synaptic weight values. Different synaptic patterns are known to be beyond the LTP and LTD processes. The LTP refers to strengthening of the connection between neurons, and is usually initiated when the activity of connected neurons is synchronized (or highly correlated). The LTD refers to weakening of the connection between neurons, and is usually initiated when the activity of neurons is non-synchronized (or have low correlation). Synchronized and non-synchronized neuronal activities in the hippocampus are crucial for memory formation. During learning, the LTP and LTD processes will create memory as certain

connection patterns in the (hippocampal) neuron network.

Presented spatial and temporal visualization can also be used in neuroscience as one possible way of diagnosis. For instance, significant reduction of clustering and loss of small-worldness might provide a *clinically useful diagnostic marker* indicating an Alzheimer's disease [1, 23]. Moreover, graph theory measures can be used to create a certain *visualization tool* that might lead to an efficient and effective process of human regulation of $[Ca^{2+}]$. In what follows, the concepts built upon the outdegree-, clustering coefficient-, node- and edge centrality criteria are presented.

B.0.1 Centrality Criterion

In graph theory and network analysis, centrality of a vertex measures its importance within a graph. Although centrality concepts were first developed in social networks, they can provide general answers to questions like "How influential a person is within a social network?", "How important a room is within a building?", and "How well-used a road is within an urban network?". Here, centrality is applied to examine *"How involved a cell is in neural communication system?"* in order to identify those to be monitored, "guided", and controlled in terms of $[Ca^{2+}]$. There are variety of measures of centrality that focus on different concepts and definitions, such as degree, betweenness, closeness, and eigenvector. As historically first, conceptually simplest, and very useful measure of centrality, degree is first applied to find neurons with the most numerous synaptic connections. Additionally, betweenness centrality is also deployed in what follows since that criterion is introduced as a measure for quantifying the control of a human on the communication between other humans in a social network [45]. Conversely, closeness and eigenvector centrality do not qualify themselves as usable criteria in this study due to the unmatched physical interpretations. For instance, closeness can be regarded as a measure of how long it will take to spread information from analyzed vertex to all other vertices sequentially, thereby being completely irrelevant in $[Ca^{2+}]$ regulation strategy.

Outdegree Centrality

The degree of a vertex in a network is the number of edges attached to it. Computationally, degree is the sum of vertex's indegree and outdegree values defined as the number of incoming (afferent) or outgoing (efferent) edges, respectively. In many cases, vertices with the highest degrees in a network play important roles in functioning of the system. Hence, degree can be a useful guide for focusing attention on the system's most crucial elements. In particular, outdegrees, $od(v)$, are of interest here due to the obvious functional interpretation: high outdegree of analyzed neuron indicates a large number of potential functional targets, i.e., receivers. Although the corresponding values are subject to constraints due to the growth, tissue volume, or metabolic limitations [117], the criterion satisfactorily qualifies an adequate neurons

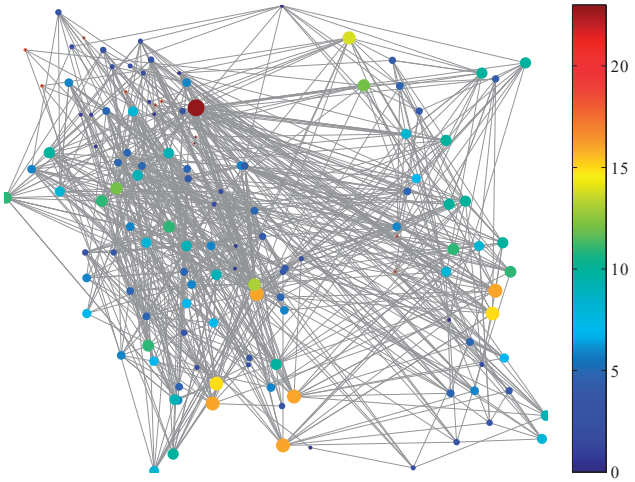

Figure B.2: Representation of neurons according to the outdegree criterion. Blue color indicates cells with no importance communication-wise. Important and potentially treated neurons are orange and red colored.

whose $[Ca^{2+}]$ is to be regulated. In such a way, any message sent from identified and treated neuron will be effectively spread throughout the network reaching the maximum number of recipients. Outdegree centrality criterion visualizes the $G(V, E)$ in a way shown in Fig. B.2.

Betweenness Centrality

Betweenness centrality also measures a vertex's or edge's importance in a network. If σ_{hj} is the total number of shortest paths from h to j, and $\sigma_{hj}(i)$ is the number of these shortest paths that pass through the vertex i, the betweenness of vertex i is defined as [15]

$$b_i = \sum_{h \neq j \neq i} \frac{\sigma_{hj}(i)}{\sigma_{hj}}. \tag{B.1}$$

The calculated value may be normalized by dividing through the number of pairs of vertices not including v, i.e., $(n-1)(n-2)$ for directed graphs. Analogous to the vertex betweenness, the betweenness centrality of edges is calculated as the number of shortest paths among all the possible vertex couples that pass through the given edge. Vertices and edges with high centrality values are assumed to be crucial for the graph connectivity and, thereby, shall be monitored in potentially malfunctioning brains. Neurodegenerative disease removing important neurons and synaptic connections leads to both anatomically and functionally disconnected clusters. The

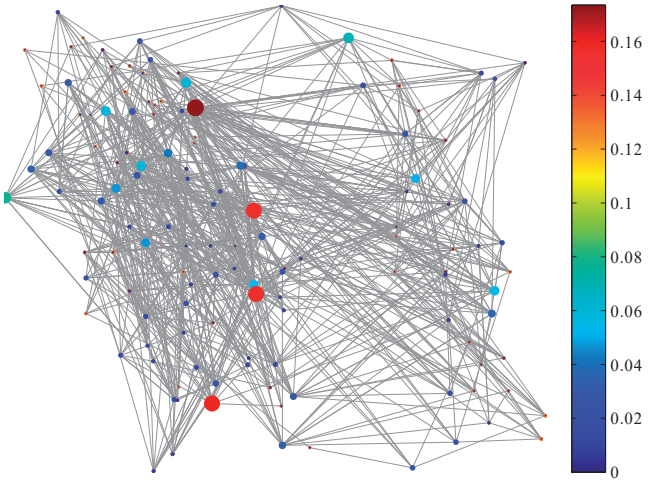

Figure B.3: Representation of neurons according to the node betweenness centrality criterion. Red markers identify the most influential cells in the region. Disease of these cells would produce two weakly connected- or even disconnected clusters.

most important edges, called bridges, are particularly important for decreasing the average path length among neurons in a network, and for speeding up the information transmission.

Computationally, betweenness centrality of all vertices in $G(V, E)$ requires calculation of the shortest paths between all pairs of vertices. Inhibitory and excitatory cells, as well as synaptic weights that change versus time depending on LTP and LTD, should not be taken into account when calculating neurons' betweenness. Thus, for finding shortest paths of a binary directed graph with positive edge (but with no cycles), Floyd-Warshall algorithm (also known as Floyd's algorithm, Roy-Warshall algorithm, Roy-Floyd algorithm) is deployed. The algorithm compares all possible paths through the graph between each pair of vertices. An execution finds the lengths of the shortest paths between all pairs of vertices, though it does not return details of the paths themselves. When applied to local *Caenorhabditis elegans* subnetwork, Floyd-Warshall algorithm visualizes the network as shown in Fig. B.3. Most important neurons are again colored in red as ones that are either to be monitored, in order to prevent disorders producing malfunctioning network, or whose $[Ca^{2+}]$ is to be regulated, in case disorder has already took place. For analyzed network consisting of 131 frontal neurons, 4 cells are identified as essential in preserving the proper communication. In general, *the higher the number of important neurons, the lower the network robustness.*

The distance matrix that results the Floyd-Warshall algorithm execution provides

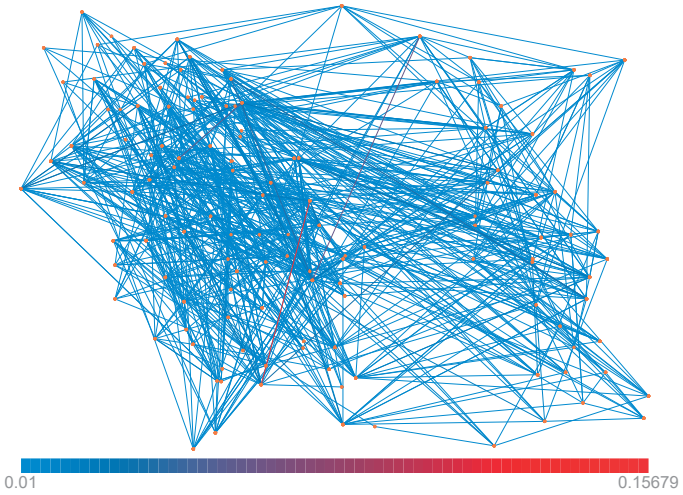

Figure B.4: Representation of neurons according to the edge betweenness centrality criterion. Similarly, red lines denote crucial synaptic junctions which disunity produce harmful effects.

calculation of average path length, l_{avg}, also one of the most important and basic graph theory measures. Short average path length is basically what makes the brain efficient in information transfer from one part to the other. It is also a function of degree (e.g., for a random network $l_{avg} \approx \log(n)/\log(< k >)$; $< k >$ is the average degree). In brains with Alzheimer's disease, one can typically observe an increase of average path length, as described in [41]. The average path length is calculated as

$$l_{avg} = \frac{1}{N(N-1)} \sum_{i \neq j} d(i,j),$$

where $d(i,j)$ denotes the shortest distance between i and j, and $d(i,j) = 0$ if j cannot be reached from i. For network analyzed here $l_{avg} = 3.1277$.

The Girvan-Newman algorithm extends the definition of node betweenness to the case of edges, defining the edge betweenness as the number of shortest paths between pairs of nodes that run along it. Edge betweenness may be interested in this study as a way of detecting important synapses. However, preserving those synapses is not trivial since execution of Girvan-Newman algorithm does not return details on the source and sink vertices, or equivalently the pre- and post-synaptic neurons. Therefore, information about the specified cell, whose $[Ca^{2+}]$ should be regularly kept, is missing. Nonetheless, it would not be superfluous if important synapses are visualized (see Fig. B.4).

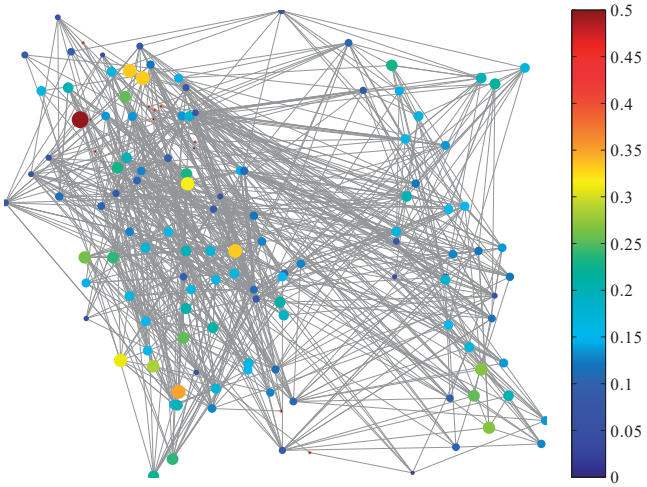

Figure B.5: Representation of neurons according to the clustering coefficient criterion. Red colored cell points to a region consisting of neurons that mutually share structural connections and function in a closely related manner.

B.0.2 Clustering Criterion

The cluster coefficient of a vertex, $\gamma(v)$, is defined in [133]. As a measure of degree to which vertices in a $G(V, E)$ tend to cluster together, it indicates how many connections are maintained between a vertex's neighbors. In particular scenario with directed graph on board, neighbors are all those neurons that are connected through an incoming or outgoing synaptic connections to the central neuron v. The ratio of actually existing connections between the neighboring neurons and the maximal number of such connections possible defines the neuron's cluster coefficient. If neuron does not have any neighbors, then $\gamma(v) = 0$, by convention. The average of the cluster coefficients determines the cluster coefficient of the $G(V, E)$.

Albeit $\gamma(v)$ does not provide the information about the number or size of clustering groups, and only captures local connectivity patterns involving the direct neighbors of the central vertex [117], high $\gamma(v)$ points to a neuronal region consisting of groups of units that mutually share structural connections and function in a closely related manner. Accordingly, high γs set candidates whose controlled $[Ca^{2+}]$ properly regulates communication within the entire cluster (see Fig. B.5). Note that cluster-based strategy might be destructive communication-wise, since $\gamma(v)$ can candidate an inhibitory cell which calcium is to be controlled.